Non-Covalent DNA-Binding Ruthenium Anticancer Drugs

Anna Łęczkowska

A thesis submitted to the University of Birmingham for the degree of Doctor of Philosophy

School of Chemistry
College of Engineering and Physical Sciences
The University of Birmingham
June 2011

ACKNOWLEDGMENTS

I would like to express my deep gratitude to all the people who provided me with their help and support during my PhD.

I would like to acknowledge Prof. Mike Hannon for having me in his group and giving me many great opportunities to participate in a number of conferences and scientific events. Prof. Kevin Chipman, Dr. Chris Bunce and Dr. Nik Hodges and their groups and all those with whom I shared time in Biosciences laboratories are very gratefully acknowledged, especially Dr. Farhat Khanim for giving me much useful advice for cell tests and biological studies.

Many thanks are also due to Dr. Louise Male who solved the crystal structures of my compounds, Dr. Neil Spencer for his help with NMR experiments and Peter Ashton for mass spectrometry.

The work presented in this thesis was financially supported by the European Union (Marie Curie Fellowship, COST D39) and the University of Birmingham and to these institutions I would like to express my gratitude for the generous funding I obtained.

Finally, I would like to thank to my family and friends. *Without your love and support I would not be even half way through this journey.* In particular, I am grateful to Jean-Louis. *Thank you for everything you have done for me.*

TABLE OF CONTENTS

ABBREVIATIONS

General abbreviations

Å	Angstrom
aq.	aqueous
bpy	2,2'-bipyridine
CH_3CN	acetonitrile
$CHCl_3$	chloroform
DCM	dichloromethane
DSC	Differential Scanning Calorimetry
DMSO	dimethyl sulphoxide
DNA	2'-deoxyribonucleic acid
EA	Elemental Analysis
EtOH	ethanol
ICP-MS	Inductively Coupled Plasma Mass Spectrometry
ITC	Isothermal Titration Calorimetry
M	molar
Me	methyl
MeOH	methanol
MTT	3-(4,5-dimethylthiazol-2-yl)-2,5-diphenyltetrazolium bromide
NH_4PF_6	ammonium hexafluorophosphate
t-Bu_4NCl	tetrabutylammonium chloride
µM	micromolar
µmol	micromole
mmol	millimole

mp.	melting point
m/z	mass/charge
nm	nanometer
P	partition coefficient
Ph	phenyl
phen	1,10-phenanthroline
RNA	ribonucleic acid
T_m	melting temperature (ct-DNA)
terpy	2,2':6',2'-terpyridine

Spectroscopic terms

CD	Circular Dichroism
LD	Linear Dichroism
ICD	Induced Circular Dichroism
IR	Infra-Red
NMR	Nuclear Magnetic Resonance
UV-Vis	Ultra-Violet - Visible
ES	Electrospray
MS	Mass Spectrometry

NMR terms

$CDCl_3$	deuterated chloroform
CD_3CN	deuterated acetonitrile
COSY	Correlated Spectroscopy
D_2O	deuterium oxide

δ	chemical shift
d	doublet
dd	doublet of doublets
MHz	megahertz
ppm	parts per million
q	quartet
s	singlet
t	triplet

UV-Vis terms

MLCT	Metal to Ligand Charge Transfer
ε	extinction coefficient
hν	light energy
λ	wavelength

Fluorescence terms

λ_{ex}	Wavelength of excitation
λ_{em}	Wavelength of emission

Thermodynamic terms

ΔC_p	heat capacity change
ΔG	free energy change
ΔH	enthalpy change
ΔS	entropy change
ΔT	temperature change

K	equilibrium binding constant
R	gas constant (8.314 J K^{-1} mol^{-1})

DNA terms

ct-DNA	calf-thymus DNA
ds-DNA	double-stranded DNA
ss-DNA	single-stranded DNA
A	adenine
C	cytosine
G	guanine
T	thymine
3WJ	DNA three-way junction

Gel electrophoresis terms

ϕ	unwinding angle
σ	superhelicity
r_b	coalescence point

ABSTRACT

The research work described in this thesis concerns metal-based anticancer drugs with an emphasis on non-covalent DNA-binding supramolecular assemblies.

The project involves the preparation of a series of mono- and bi-metallic ruthenium complexes with a primary focus on fluorescent dinuclear triple-stranded helicates with different structural topographies. Emphasis is then directed towards an investigation of the DNA binding characteristics of these molecules and an evaluation of their anticancer properties in human cancer cell lines. Attention is brought to the significance that the cylinder-building moieties and their structural characteristics have to these features.

The studies also include an examination of the effects of chirality of the investigated supramolecular systems and the impact they have on molecular recognition. This is addressed via studies of the interaction of optical isomers of ruthenium triple-stranded helicates with DNA as a biomolecular target system and with Δ-TRISPHAT as a representative small chiral molecule.

Non-Covalent DNA-Binding Ruthenium Anticancer Drugs

1

Introduction

1.1 DNA structures and properties

DNA is a key biomolecule, which encodes genetic information essential to create and control living systems. This code begins to be processed when unwinding of the DNA helix is promoted and the DNA strands serve as templates to construct complementary molecules of messenger RNA in the process of transcription. The information contained in RNA is then ‘decoded’ and used for the synthesis of particular combinations of amino-acids to further manufacture proteins. The gene expression is mostly regulated by particular proteins, which bind non-covalently and reversibly to the DNA mainly through specific subunits like helix-turn-helix, leucine zippers or zinc finger motifs.[1] DNA is a very attractive medicinal target for small molecules, because interfering with DNA transactions such as replication or transcription or with DNA-protein interactions can lead to control of gene expression and thus potentially control diseases.

1.1.1 B-DNA structure

B-DNA is built of two inter-twined polynucleotide strands (Fig. 1.1). These strands consist of nucleobases (adenine A, guanine G, cytosine, C and thymine, T) bound to 2’-deoxyribose sugars, which in turn are held together by phosphodiester bonds.[1, 2]

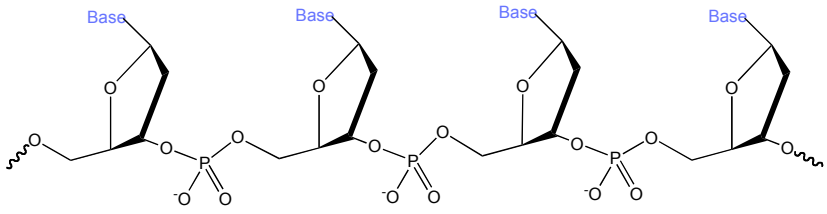

Fig. 1.1 Chemical structure of polynucleotide

The two anionic polynucleotide strands assemble into a helix spontaneously in a self-assembly process, which is assisted by hydrophobic interactions, hydrogen bonding between the complementary bases from the opposite, antiparallel strands (A -T and G-C) (Fig. 1.2) and π-π stacking between the adjacent base pairs.

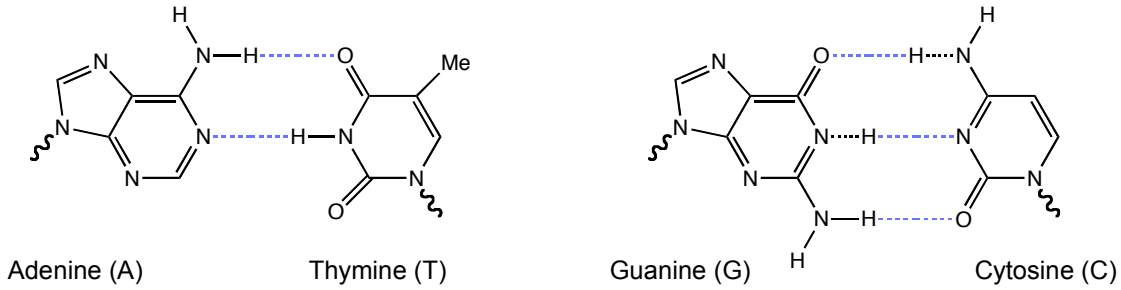

Fig. 1.2 Hydrogen bonding between the complementary DNA bases

This in turn results in the formation of a helical arrangement, where the two strands are coiled around each other with the hydrophilic sugars placed outside the helix and hydrophobic bases inside (Fig. 1.3).

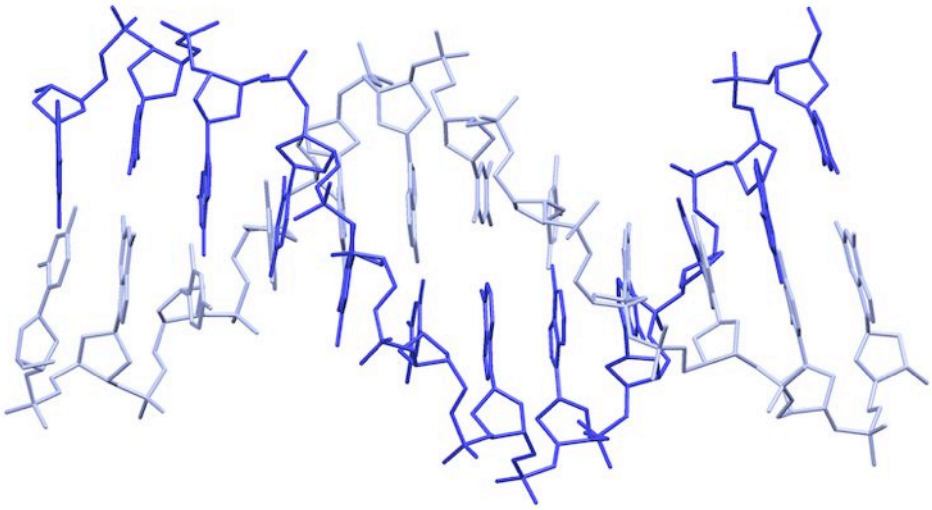

Fig. 1.3 Structure of Watson-Crick DNA double helix

There are two different grooves in the B-DNA structure, named major and minor groove, which differ in size and depth. The B form of DNA is the main form found in cells, however under different conditions DNA may exist in a wide variety of different possible topologies such as left handed and multiple-stranded helices.[3] This includes Z-DNA (left handed DNA), the dehydrated A-DNA, but also multiplexes and branched structures such as three-[4] or four-way junctions (Fig. 1.4),[5-7] which are key intermediates in principal cellular processes such as transcription or replication.

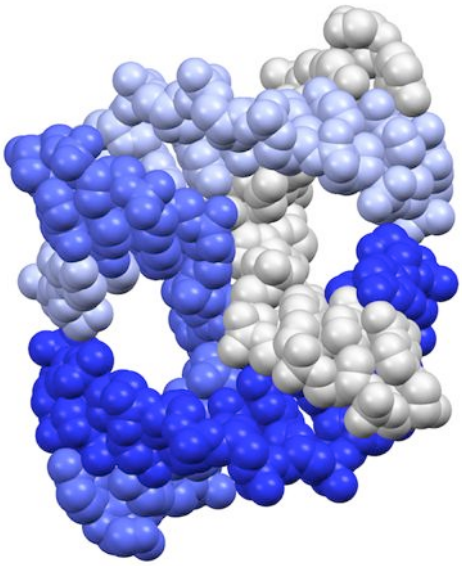

Fig.1.4 Structure of DNA Holiday junction (PDB ref. 1ZF2)[7]

1.2 Metallo-anticancer drugs

Metal complexes have a great potential for pharmaceutical use due to their wide range of coordination geometries, electronic properties and a variety of oxidation states. They have been investigated for clinical applications in a broad range of medicinal disciplines as MRI contrast agents,

radiopharmaceuticals, antibacterial agents, superoxide dismutase mimics, antidiabetic or anticancer drugs.[8-10]

1.2.1 Cisplatin and its derivatives

Interest in using metal complexes as anticancer agents has been increasing since the discovery of the antibacterial and anticancer properties of cis-diaminedichloroplatinum(II), cisplatin (Fig. 1.5),[11, 12] which now alone and in combination with other drugs, *e.g.* topoisomerase II inhibitors, antimetabolites or mustards, is effectively used in the treatment of several different solid tumors such as bladder cancer, small cell lung cancer, head and neck cancers and being particularly potent against testicular cancer.[13]

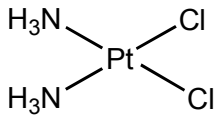

Fig. 1.5 Chemical structure of cis-diaminedichloroplatinum(II), cisplatin

Although in living cells cisplatin can interact with a number of biomolecules,[14] DNA is believed to be its primary cellular target. The mechanism of action of cisplatin involves several stages.[15] Once it is administered, it binds to blood plasma proteins, mostly to albumin,[16] and is transported in the blood stream. Early research suggested that cellular uptake and efflux of cisplatin occurs through passive diffusion,[17, 18] however recent studies show that these processes can also be linked to copper transport proteins[19, 20] or cation transporters.[21] After the compound crosses the cell membrane cisplatin undergoes hydrolysis to $[Pt(NH_3)_2Cl(H_2O)]^+$ and $[Pt(NH_3)_2(H_2O)_2]^{2+}$, which then

can interact with DNA bases forming covalent bonds to N^7 positions of purine bases, affording primarily formation of 1,2- or 1,3-intrastrand cross-links. This results in distortions in the DNA helical structure[22, 23] and its kinking by ~45° towards the major groove (Fig. 1.6).[24] The new, induced DNA structure is then recognised by cellular proteins such as HMG-domain (High Mobility Group) proteins, which have been proposed to inhibit the nucleotide excision repair, leading to cell apoptosis.[25]

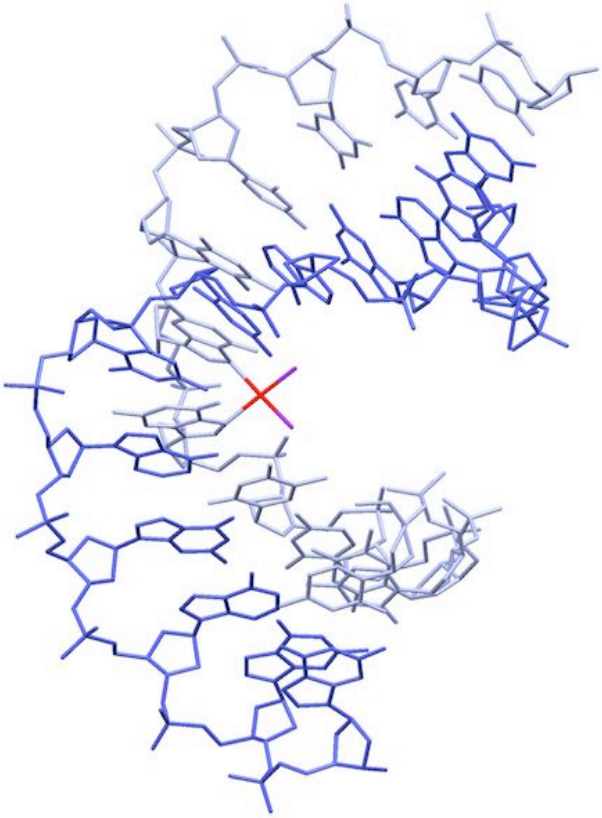

Fig. 1.6 The crystal structure of duplex DNA containing a cisplatin 1,2-d(GpG) intrastrand cross-link (PDB ref. 3LPV)[24]

However, the chemotherapeutic application of cisplatin is limited by multiple side effects such as neuro-, hepato- or nefrotoxicity,[13] resulting from its lack of specificity, and often also by acquired or inherent resistance of tumor cells to

this drug.[27, 28] This has led to the development of other alkylating agents, which were designed to overcome or, to some extent, diminish the side effects. Five of them, carboplatin, oxaliplatin, nedaplatin, lobaplatin and heptaplatin (Fig. 1.7) have been approved for clinical use.

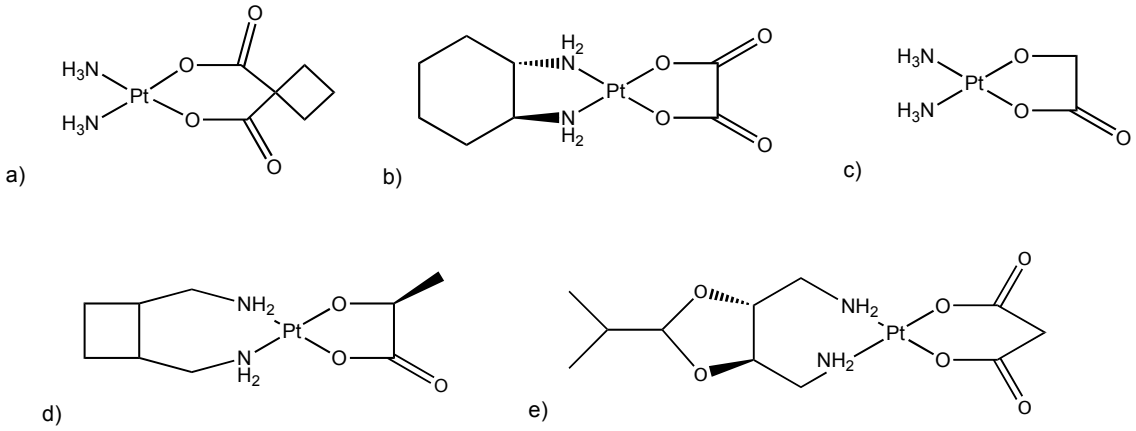

Fig. 1.7 Clinically used platinum-based chemotherapeutics: a) carboplatin, b) oxaliplatin, c) nedaplatin, d) lobaplatin, e) heptaplatin

Carboplatin (Fig. 1.7a) is less antitumor active than cisplatin. This is due to the substitution of the chloride ligands with 1,1-cyclobutanedicarboxylate, which aquates slowly, thus reduces the reactivity of this compound and consequently lowers its cytotoxicity and side effects. Carboplatin is used clinically to treat several types of cancer such as ovarian carcinoma, lung, head and neck cancer. However, it shows cross-resistance with cisplatin, which indicates the same cellular resistance mechanisms to both drugs.[23] Oxaliplatin (Fig. 1.7b) is particularly effective against colorectal cancer, where it can also be used in combination with 5-fluorouracil, and against cancers that have developed resistance towards cisplatin.[29] Nedaplatin (Fig. 1.7c) (approved for clinical use in Japan) has been used for treatment of lung carcinoma, head and neck

cancers and shows also promising effects in combination therapy.[30] Approved in China lobaplatin (Fig. 1.7d) is a mixture of *S,S* and *R,R* diastereomers and has been approved for treatment of chronic myelogenous leukaemia, metastatic breast cancer and small cell lung cancer.[30]

The above-mentioned platinum drugs fulfil the initially formulated structural requirements for metallo-anticancer agents (neutral species with *cis*- geometry, two ammine ligands and two labile ligands that can hydrolyze), however other, non-traditional platinum drugs have also been developed.[31] Four of them, picoplatin, satraplatin, ProLindac and lipoplatin (Fig. 1.8) are currently in clinical trials.[30]

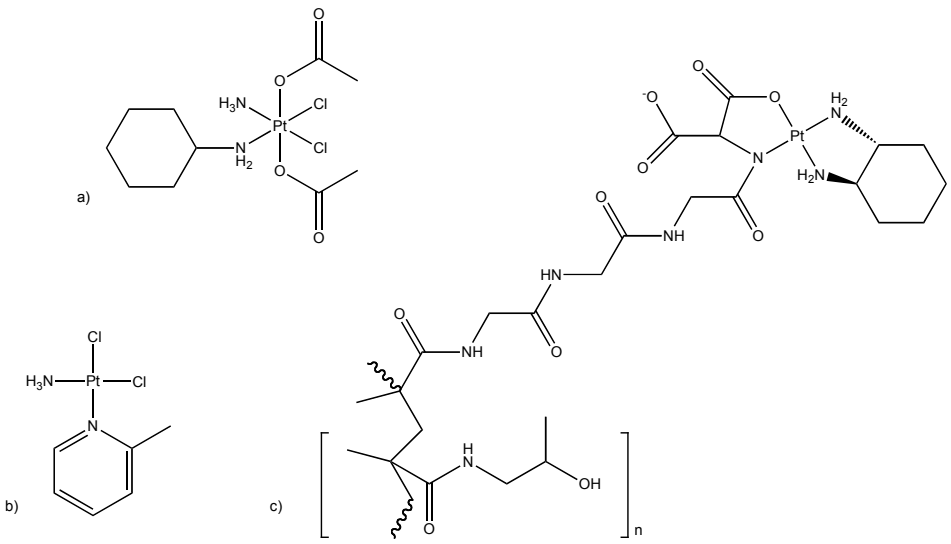

Fig. 1.8 Platinum-based anticancer drugs currently under clinical evaluation; a) satraplatin, b) picoplatin, c) ProLindac

1.2.2 Non-platinum antitumor agents

Platinum based complexes are currently the most successful metallo-anticancer drugs used clinically for solid tumors,[32] nevertheless using other metal ions, with different coordination preferences and physicochemical characteristics has been one of the new strategies in the design of new generation of anticancer drugs. This approach has been the subject of many investigations in recent years[33, 34] and, among others, complexes of iron,[35] gold,[36] titanium,[37] gallium,[38, 39] osmium[40] or ruthenium[41] have been widely explored for their anticancer properties.

1.2.3 Ruthenium anticancer drugs

Ruthenium has a number of properties that may make its compounds particularly good alternatives to platinum drugs.[42] These are: octahedral coordination geometries, slow ligand exchange kinetics, a range of oxidation states reachable in physiological environment (Ru^{II}, Ru^{III}, Ru^{IV}) and 'the ability to mimic iron in the binding to biomolecules', such as transferrin or albumin.[42] Furthermore, the photophysical properties of some ruthenium complexes, particularly Ru polypyridyl complexes, can offer many advantages when studying the distribution and action of the potential drug in living cells[43] or to probe DNA structures.[44] As a result of above there has been an increased interest in using ruthenium as a metal center for the design of potential anticancer drugs.[41, 45, 46]

Early investigations of the antitumor properties of Ru complexes demonstrated that Ru(III) ammine-based compounds such as *cis*-$[Ru(NH_3)_4Cl_2]Cl$ and *fac*-$[Ru(NH_3)_3Cl_3]$ show promising antiproliferative effects in leukemia cancer

cells.[47, 48] Since then a number of Ru-based complexes have been synthesized and tested *in vitro* and *in vivo* for their anticancer properties. Three classes of such compounds are described below.

NAMI-A, $[RuCl_4(Im)(S\text{-}dmso)](ImH^+)$,[49] and KP-1019, $[RuCl_4(Ind)_2](IndH^+)$[50] (Fig. 1.9) are the Ru-based complexes, which are currently under clinical investigations.

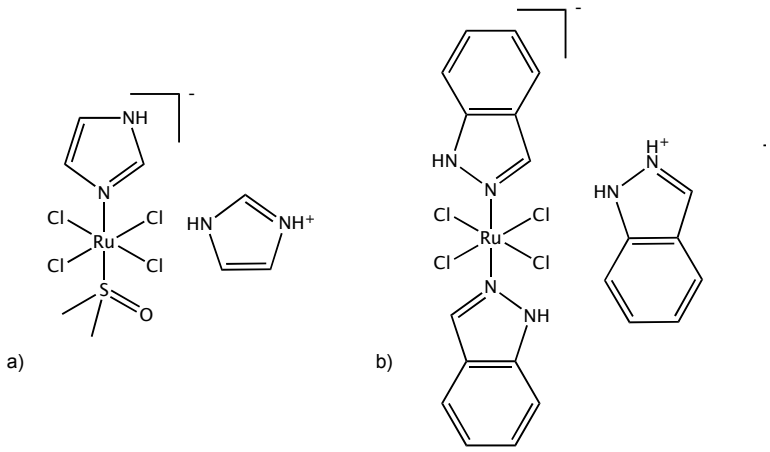

Fig. 1.9 Ruthenium anticancer drug candidates a) NAMI-A, b) KP1019

NAMI-A, developed by Alessio, has antimetastatic properties and only little effect on primary cancers.[51] The exact mechanism of action of this drug is still under investigation, nevertheless it is suggested that the antiangiogenic and antiinvasive properties of NAMI-A arise from its binding to collagens or to actin-type proteins.[52-54]

Developed by Keppler KP1019 exhibits a high level of cytotoxicity *in vitro* against cisplatin resistant colorectal cancer.[49] The activity of this drug is believed to be mediated by a mitochondrial pathway.[55] Furthermore, it has been shown that KP1019 can bind to iron pockets in transferrin, which has been suggested to play a significant role in the mechanism of action of KP1019.[56]

Organometallic anticancer complexes have attracted much attention in the field of modern medicinal chemistry.[57] Particularly, ruthenium-arene complexes with the characteristic 'piano-stool' geometry have been extensively studied as anticancer drugs.[58-60] Sadler and co-workers developed Ru-based complexes of a general formula $[Ru(\eta^6\text{-arene})(XY)(Z)]^+$, where XY is a neutral chelating ligand such as ethylenediamine and Z is monoanionic labile ligand *e.g.* Cl^- (Fig.1.10a).

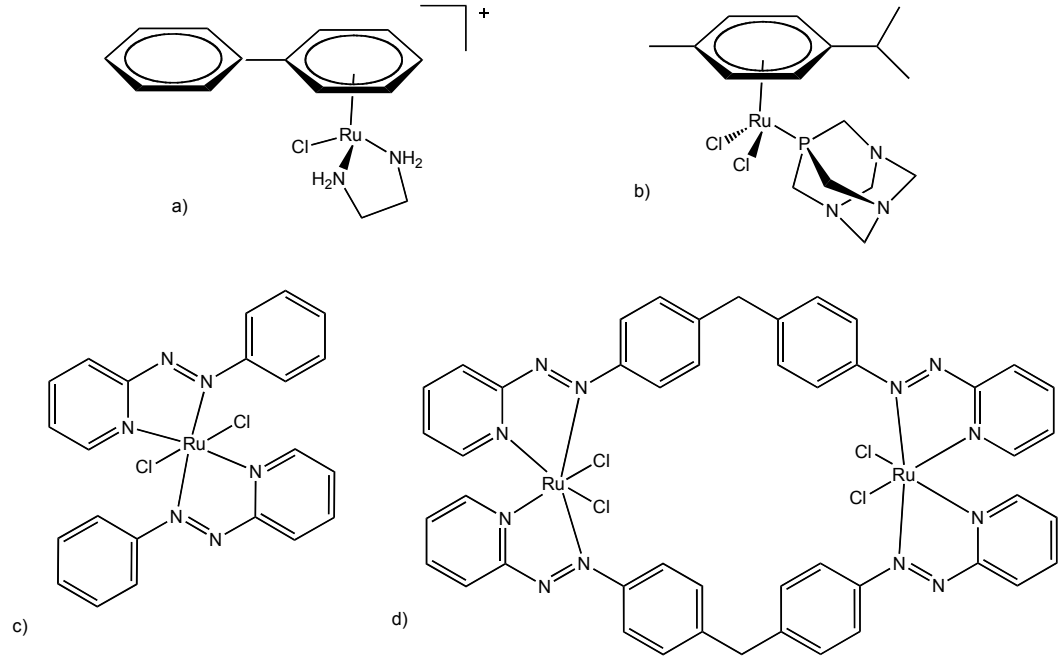

Fig. 1.10 Representative Ru-based complexes tested for anticancer activities:
a) $[(\eta^6\text{-arene})Ru(en)(Cl)]^+$, b) RAPTA-C, c) $[RuL^{azpy}{}_2Cl_2]$, d) $[Ru_2L^a{}_2Cl_4]$

These compounds possess very promising cytotoxic activities *in vitro* against a range of tumors and are particularly active against ovarian cancer cell lines (A2780).[59, 61] The activation of these complexes is believed to take place via hydrolysis to $[Ru(\eta^6\text{-arene})(XY)(H_2O)]^{2+}$, and thus it relies on the lability of the monoanionic ligand.[62] The aquated species can then interact with biomolecules, however it has been proposed that DNA is a cellular target of

these compounds.[63] It was shown that they bind to DNA helix with strong preference towards N^7 of guanine residues.[64] These interactions can be assisted by intercalation of the arene moiety between the base stack and also by hydrogen bonding of chelating ligand with guanine residues.[65] Moreover, studies on structure-activity relationships of these drugs showed that their anticancer activity increases with the increased size of the arene ligand (*e.g.* benzene < biphenyl < dihydroanthracene < tetrahydroanthracene),[66] while the nature of the chelating ligand does not have a significant influence on the cytotoxicity of these compounds.[67]

Dyson and co-workers have developed another type of Ru-organometallic complexes, commonly known as RAPTA compounds (Fig. 1.10b). These are based on arene moieties and pta ligands where pta is 1,3,5-triaza-7-phosphatricyclo[3.3.1.1.]decane.[68] Similarly to NAMI-A, RAPTA compounds exhibit only little effect on malignant growth, but have been shown to selectively target metastases *in vivo* and display a very low general toxicity.[69, 70] Although these compounds can bind to DNA,[71] proteins have been proposed to be the biological targets of RAPTA family. It was shown that the activity of RAPTA compounds can be mediated by mitochondrial and p53-JNK pathways[72] and they act as effective inhibitors of Catepsin B.[73]

Ruthenium azopyridyl complexes, $[RuL^{azpy}{}_2Cl_2]$ where L^{azpy} is azopyridyl ligand $(C_5H_4N)N{=}N(C_6H_5)$ (Fig. 1.10c), are another interesting class of ruthenium anticancer drugs. These complexes, due to an asymmetric character of the azopyridine ligand, can exist in five different isomeric forms, four of which (α-, β-, γ- and δ-) have been structurally characterised.[74] The ruthenium azopyridine complexes were found to exhibit cytotoxicity in a wide panel of

cancer cells, however it was found that the structural features of these compounds remarkably influence their antitumor activities.[75] It was shown that the α-[RuL$^{azpy}_2$Cl$_2$] has significantly higher cytototoxicity than the corresponding β- or γ- analogues. Moreover, further studies on these systems showed that functionalisation of the azopyridine ligand with methyl groups, does not alter the general trend in the cytotoxic activity of these compounds.[76] More recently Hotze reported a set of isomeric dinuclear analogues of these complexes, [Ru$_2$L$^a_2$Cl$_4$], where L^a is a bisazopyridine bridging ligand (Fig. 1.10d).[76] Three isomers, αα-, αγ-, γγ-, have been isolated and tested *in vitro* for their antiproliferative properties. Interestingly, these compounds showed much greater cytotoxic activities than cisplatin and similarly to the mononuclear complexes the anticancer properties of the [Ru$_2$L$^a_2$Cl$_4$] were associated with their isomeric differences.[77] However, due to their poor solubility in aqueous solution further studies on these systems have not been undertaken.

The remarkable anticancer effects of Ru-azopyridine complexes might be associated with their redox properties.[78] Sadler and co-workers, based on the studies on [Ru(η^6-arene)L^{azpy}I]$^+$ (Fig.1.11), showed that these complexes can be activated by reduction in A549 cancer cells, which results in an increase of the level of reactive oxygen species.[79]

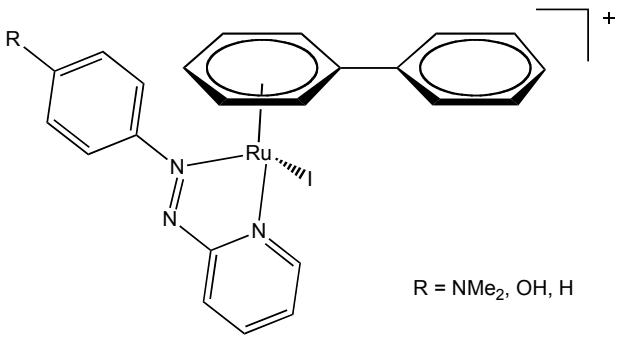

Fig.1.11 Molecular structure of [Ru(η^6-arene)L^{azpy}I]$^+$

Indeed, using azopyridine moiety as a chelating ligand in piano-stool ruthenium arene complexes leads also to an increase of inertness of these compounds towards hydrolysis. Nevertheless, the studied complexes show remarkable effect on human ovarian and lung cancer cell lines (A2780, A549), which may imply a different mode of action of these species to that proposed for 'classical' $[Ru(\eta^6\text{-arene})(XY)(Z)]^+$ compounds.[79]

1.3 Supramolecular DNA-binding anticancer drugs

Over the last few years much attention in modern medicine has been focused on the development of novel strategies to target cancer, which could potentially allow for the creation of new drugs with unconventional modes of action and a new range of cellular activities.[80] Numerous approaches have been developed in order to improve bioavailability and specificity of the potential drugs and consequently enhance their effectiveness and minimize side effects. These innovative strategies include development of drug carriers for improved specificity,[81, 82] development of prodrugs that could be, for example, photo-[83] or redox activated,[84] but also targeting biomolecules other than DNA *i.e.* proteins or enzymes. Nevertheless, DNA as a 'blueprint of life' is still being an attractive target for cancer and gene therapy.[85]

While a metal centre in cisplatin and many other related anticancer metallo-drugs plays a role as an active centre that binds covalently to DNA and induces its structural changes, targeting biomolecules can also be achieved by constructing larger, three-dimensional structures, where the metal ion acts as a

scaffold for supramolecular frameworks and is not directly involved in the interactions with biomolecule.[80] From this aspect supramolecular chemistry offers many avenues towards the assembly of 'small' molecules that can mimic or interfere with biologically important protein or enzyme moieties. As a consequence of this such molecules could, much like the natural progenitors, selectively target other, larger biomolecules like nucleic acids. This approach, followed by rational drug design and comprehensive studies of the intermolecular interactions between the drug and its biological target, has a great potential for the development of superior alternatives to classical drugs not only for gene or cancer therapy but also for wider medicinal applications.

1.3.1 Thermodynamics of drug-DNA interactions

Understanding the molecular insights of drug-DNA interactions can be a great facilitator for the sensible design and development of new successful therapeutics. Hence, it is important to thoroughly understand the factors responsible for drug to biomolecule binding affinity, drug specificity and/or its selectivity and have a comprehensive picture of the nature and character of drug – DNA complex formation. From this aspect it is essential to fully understand the molecular principals of the binding events.

Thermodynamic analysis of the drug-DNA interactions is an important accompaniment to structural data. The energetics of the drug – biomolecule binding give information about the forces that drive the recognition processes

and therefore can be a very useful tool for optimization of current drugs but also for the design and development of new therapeutics.

The initial step of the thermodynamic analysis of drug-DNA binding involves the determination of the equilibrium binding constant (K) and deriving from it binding free energy (ΔG)[1]. ΔG is a function of enthalpy (ΔH) and entropy change (ΔS),[2] hence its magnitude depends on a number of factors such as pH, ionic strength, temperature, concentration *etc.*. Although the binding free energy is a principal parameter in the thermodynamic analysis, since it is a measure of the location of the molecular equilibrium, the thermodynamic analysis of the drug-DNA interactions includes determination of binding free energy (ΔG), enthalpy (ΔH) and entropy change (ΔS) and heat capacity change (ΔC_p). The enthalpy change of the binding process can be determined either from the van't Hoff equation based on the relationship between the temperature and equilibrium binding constant or using calorimetric methods such as isothermal titration calorimetry (ITC) or differential scanning calorimetry (DSC).[86-89] These two techniques are the primary methods used for thermodynamic studies of the drug-DNA interactions.

The energetics of drug-DNA recognition (ΔG) is a function of a number of events that take place until the system reaches equilibrium. These events, among others, include shift of the drug towards the DNA binding site, DNA structural changes associated with allocation of the drug, solvation effects as well as intermolecular interactions between the drug and the DNA moieties. All these events are related to certain energy benefits or penalties. However, if the

[1] $\Delta G^o = -RT\ln K$, where ΔG^o – Gibbs free energy change, R – gas constant (8.314 J K^{-1} mol^{-1}), T – temperature (K), K – equilibrium binding constant

[2] $\Delta G = \Delta H - T\Delta S$ where ΔG – free energy change, ΔH – enthalpy change, T – temperature, ΔS – entropy change

recognition is to take place, the magnitude(s) of favorable energetics needs to be greater than that of energy costs.[89]

The thermodynamics of the drug-DNA complex formation (ΔG) is postulated to be predominantly a function of five Gibbs free energy components: 'conformational changes in the DNA and drug' (ΔG_{conf}), 'losses in translational and rotational degrees of freedom upon complex formation' (ΔG_{r+t}), 'hydrophobic transfer of the drug from solution to the DNA binding site' (ΔG_{hyd}), 'polyelectrolyte effects' (ΔG_{pe}) and finally 'non-covalent interactions between the drug and the DNA' (ΔG_{mol}).[90, 91]

The binding of the drug to the DNA may induce the DNA structural alterations. These include *i.e.* formation of an intercalation cavity, unwinding and/or lengthening of the helix but also its kinking, bending and conformational changes. These events cost the system energy and thus have an unfavorable contribution to the overall energetics. Early investigations of the thermodynamics of the formation of an intercalation pocket for actinomycin D in B- and Z-DNA showed that this process is associated with the free energy (ΔG_{conf}) of ~ 10 kcal mol^{-1}.[92] More recently, Trieb and co-workers, using computational studies on the intercalation of daunomycin and bisdaunomycin, showed that the introduction of one single intercalation site in the DNA for daunomycin costs the system 32 kcal mol^{-1}, while for double intercalation of bisdaunomycin the respective values decreases to 27 kcal mol^{-1} for the first intercalation cavity and 24 kcal mol^{-1} for the second cavity.[93] These studies suggest that binding of one ligand can have an effect on the second binding site.

The formation of the drug-DNA molecular complex leads to losses in translational and rotational degrees of freedom for both DNA and drug. This results in an entropic penalty and corresponding adverse free energy contribution to overall energetics of the molecular complex formation ($\Delta G_{r+t} > 0$). The hydrophobic transfer of the drug to the DNA binding site is an energetically favorable process and consists of two components: enthalpic contribution arising from the stabilization of water molecules released from the DNA binding site by interaction with these from the bulk solvent, and entropic contribution, which is associated with disruptions of the solvent structure.[94, 95] An approximate magnitude of the energetics corresponding to the hydrophobic transfer (ΔG_{hyd}) of the drug to DNA can be determined from changes in solvent accessible surface areas (ΔSASA) or from heat capacity changes (ΔC_p).[96, 97] The free energy corresponding to the hydrophobic shift of the binding molecule to the DNA binding site seems to have a major favorable contribution to the energetics of the drug-DNA binding event.[90]

Since DNA is a highly charged polyanion, in the buffer the counterions (*e.g.* Na^+) are condensed around the biomolecule.[98, 99] The recognition by the positively charged drug results in a release of these counterions (polyelectrolyte effect) and this gives a substantial favorable entropic contribution to the binding free energy. Consequently, the magnitude of ΔG_{pe} depends on the ionic strength of the buffer and also on the charge of the binding molecule.[3]

The intermolecular interactions between the host molecule and the binding drug also contribute to the thermodynamic profile of the binding process. Hydrogen bonding, van der Waals interactions *etc.* result in favorable enthalpy

[3] $\delta \ln K / \delta \ln M^+ = -Z\varphi$, where: K- ligand binding constant, M^+ - monovalent cation concentration, Z – charge on the ligand, φ - fraction of monovalent cation associated per DNA phosphate, $\varphi_{B\text{-}DNA} = 0.88$

contributions,[100] however assignment of the energetic contributions to the constituent non-covalent interactions is not trivial and requires consideration of a number of factors.[101]

As described above, the energetics of drug-DNA binding is a function of several thermodynamic components, which can have an additive and cooperative contribution to the overall free energy of the recognition process. For example, hydrophobic shift of the drug towards the DNA binding site can result in variations in the DNA hydration, which in turn can induce substantial distortions in DNA structures like conformational changes or helix unwinding.[102] All these effects are associated with certain energy gains and losses, some of which can balance or compensate each other thus determining the affinity of drug to biomolecule.

1.3.2 Metallointercalators and metalloinsertors

Intercalators are poly(hetero)cyclic aromatic compounds often with a large planar surface that bind reversibly to DNA by inserting their extended ligands in between the stacked base pairs and forming with them face-face π-π interactions. The intercalation ordinarily results in local alterations in the DNA structure, which may include helix lengthening and/or unwinding. Intercalators can be considered to be the largest and most investigated group of non-covalent DNA binders with anticancer activity.[103-105] Many organic intercalators such as acridine or anthracene derivatives have been widely explored for their antitumor properties and some of them, such as doxorubicin or daunorubicin (Fig. 1.12), are already in clinical use for chemotherapeutic treatment of different cancers.

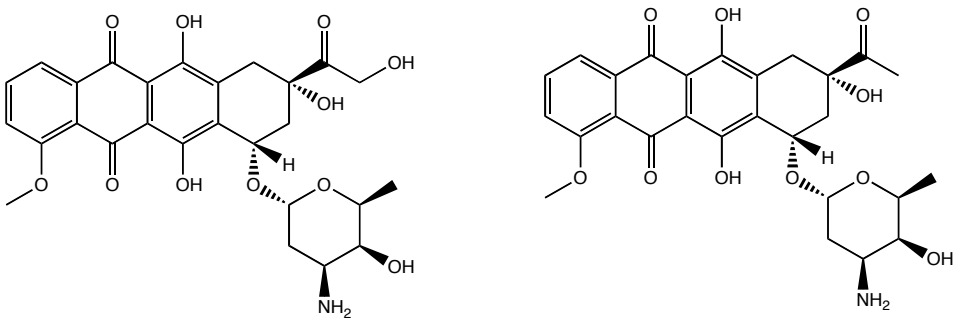

Fig. 1.12 Clinically used DNA intercalating anticancer drugs; (left) doxorubicin, (right) daunorubicin

However, metallo-intercalators represent a different category of DNA-binding antitumor agents. The introduction of metal centers gives, in addition to the potential for hydrophobic effects and π-π interactions, an electronic contribution to the overall binding efficiency of a drug. Furthermore, the binding characteristics and therefore biological effects of the metallointercalators may be fine tuned through judicious selections of the ancillary ligands.

The first metallointercalator, $[Pt(terpy)(SCH_2CH_2OH)]^+$ reported by Lippard and co-workers consisted of a terpyridine unit bound to Pt center (Fig. 1.13) and was shown to reversibly bind to polymeric DNA, which results in the DNA lengthening.[106, 107]

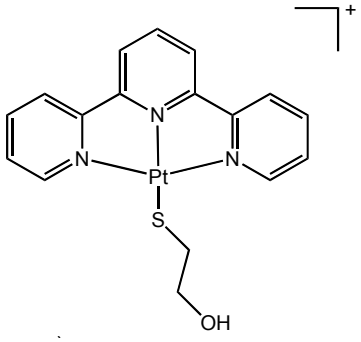

Fig. 1.13 Molecular structure of $[Pt(terpy)(SCH_2CH_2OH)]^+$

A number of other square-planar complexes with different extended aromatic moieties such as terpyridine, phenanthroline, bipyridyne or DPPZ have been investigated for their intercalative properties and, in addition to their DNA binding characteristics, the structure-activity relationships (SAR) of such complexes have also been investigated. For example, based on the studies on platinum methyl-substituted phenanthroline systems, Aldrich-Wright showed that the cytotoxic activities of these complexes depend not only on the amount of methyl groups and their location in the phenantroline moiety but also on the character and configuration of the ancillary ligands.[108-111]

Octahedral metal-based metallointercalators, mainly of Ru(II) and Rh(III), have been extensively studied by Barton and co-workers.[112] An example of such a complex is Δ-$[Rh(phi)(R,R\text{-}Me_2trien)]^{3+}$ (phi - 9,10-phenanthrenequinone diimine and *R,R*-Me_2trien - 2R,9R-2,9-diamino-4,7-diazadecane) (Fig. 1.14), which stereospecifically recognizes 5'-TGCA-3' DNA sequences.[113]

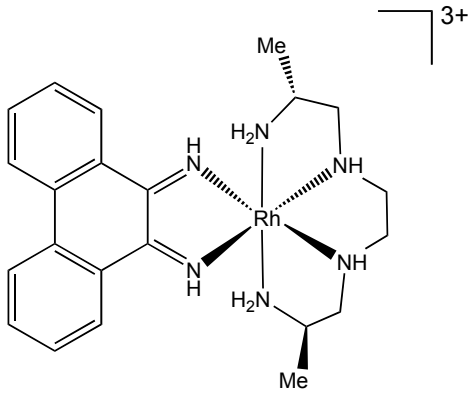

Fig. 1.14 Molecular structure of [Rh(phi)(Me_2trien)]$^{3+}$

The crystal structure of Δ-[Rh(phi)(*R,R*-Me_2trien)]$^{3+}$ bound to DNA oligonucleotide, 5'-G-dIU-TGCAAC-3', shows that the compound targets DNA duplex from the major groove, where the aromatic moiety of the complex intercalates deeply between GC base stacks, whilst the ancillary ammine ligands form hydrogen bonds with the guanine edges (Fig. 1.15).[114]

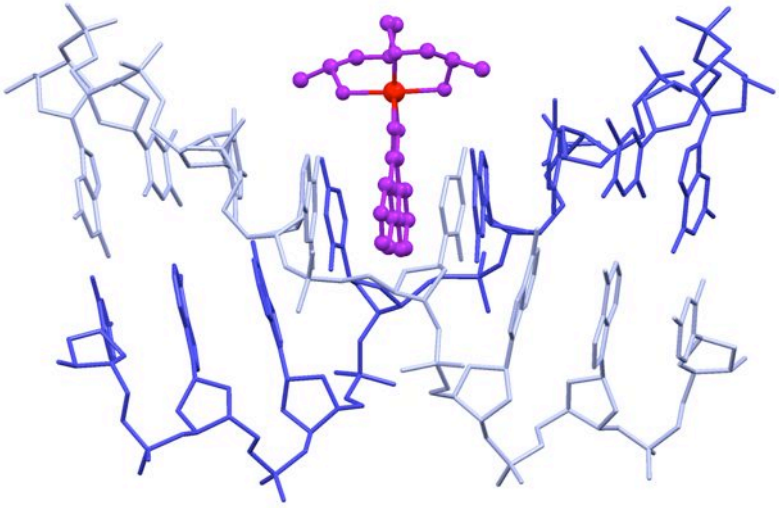

Fig. 1.15 Intercalation of [Rh(phi)(Me_2trien)]$^{3+}$ (PDB ref. 454D) [114]

Important examples of metal complexes that bind stereoselectively to DNA are Δ-[Rh(bpy)$_2$chrysi]$^{3+}$, and Δ-[Rh(bpy)$_2$phzi]$^{3+}$, where bpy - 2,2'-bipyridine, chrysi - chrysene-5,6-dione, phzi - benzo[a]-phenazine-5,6-quinone diimine (Fig. 1.16).

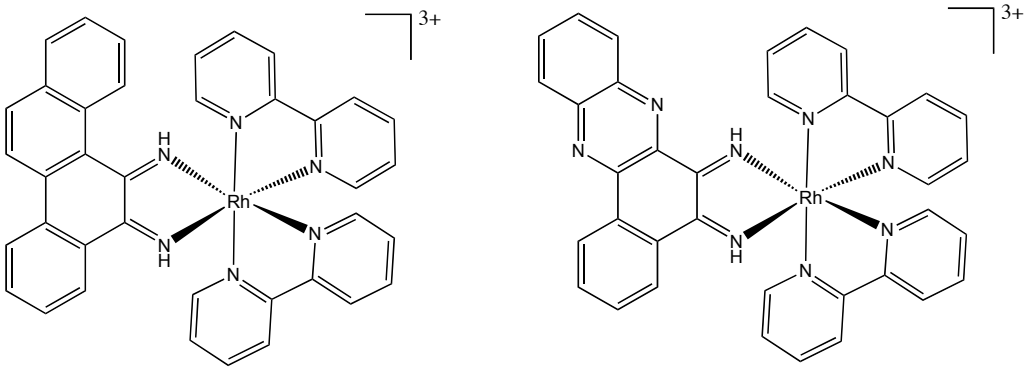

Fig. 1.16 Mismatch specific metallo-insertors: (left) Δ-[Rh(bpy)$_2$chrysi]$^{3+}$, (right) Δ-[Rh(bpy)$_2$phzi]$^{3+}$.

These two complexes, due to the extended aromatic surfaces of their diimine moieties, chrysi and phzi, do not intercalate into the ordinary DNA duplex, but instead show a high specificity towards mismatched DNA structures. NMR solution studies with a *CC* mismatched DNA sequence and further X-ray analysis of the complex Δ-[Rh(bpy)$_2$(chrysi)]$^{3+}$ with the *AA* mismatched oligonucleotide duplex, 5'-CGG*A*AATT*A*CCG-3', reveal that the complex recognizes DNA from its minor groove side.[115, 116] It subsequently inserts its chrysi ligand between the base pairs, 'ejecting the mismatched nucleobase into the major groove', and interacts with DNA bases via π-π stacking. Interestingly, upon photoactivation, these complexes induce the DNA strand breaks in the position opposite to the mismatch site[117, 118] and furthermore exhibit antiproliferative properties in cancer cells.[119] These effects were shown to be associated with the chiral nature of the binding complexes and thus their ability

to recognize the DNA mismatches.[119] The Δ-enantiomers of $[Rh(bpy)_2\ chrysi]^{3+}$ and $[Rh(bpy)_2phzi]^{3+}$, which can bind to DNA mismatched sequences were found to exhibit antiproliferative properties in cancer cells, while the Λ-isomers did not display such features. Studies on the chrysi family of compounds, $[RhL_2chrysi]^{3+}$, where L is NH_3, DIP, HDPA, 2,2'-bipyridine and 1,10-phenanthroline, confirm the correlation between the DNA mismatch recognition and the antiproliferative activity of these compounds.[120] Moreover, these studies also demonstrate that the ancillary ligands can alter the mismatch binding affinity of the rhodium metalloinsertors.

Bisintercalators are another interesting class of non-covalently DNA-binding drugs. They consist of two linked intercalating moieties, however the DNA binding properties of such molecules depend predominantly on the character of the linking ligand.

Interesting DNA binding properties are shown by bisintercalators based on hairpin-shaped platinum motifs linked via lanthanide moiety (Fig. 1.17). These complexes can act as luminescent probes for DNA structures,[121] but also, as shown by Crossley, can selectively target tumor cells, accumulating particularly in cell nuclei.[122]

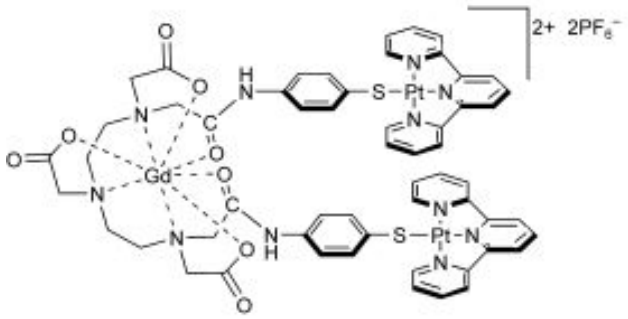

Fig. 1.17 Gadolinium bisintercalator; Figure adapted from ref. [122]

Lowe and co-workers developed a series of potential DNA bisintercalators with substituted terpyridine ligands linked via rigid spacer groups.[123] Studies on the cytotoxic activities in glioma cell lines showed that these systems exhibit promising anticancer activities, but they were also shown to inhibit human thioredoxin reductase.[124]

Bisintercalators studied by Lincoln are structurally different from these described above. Here the two metallointercalators *e.g.* $[Ru(phen)_2dppz]^{2+}$ are linked via dppz moiety (Fig. 1.18), hence classical intercalation can not occur.[125] These compounds present unusual DNA binding modes, in which the bridging ligand is inserted between base pairs with the two Ru centers located in opposite DNA grooves *i.e.* threading effect.

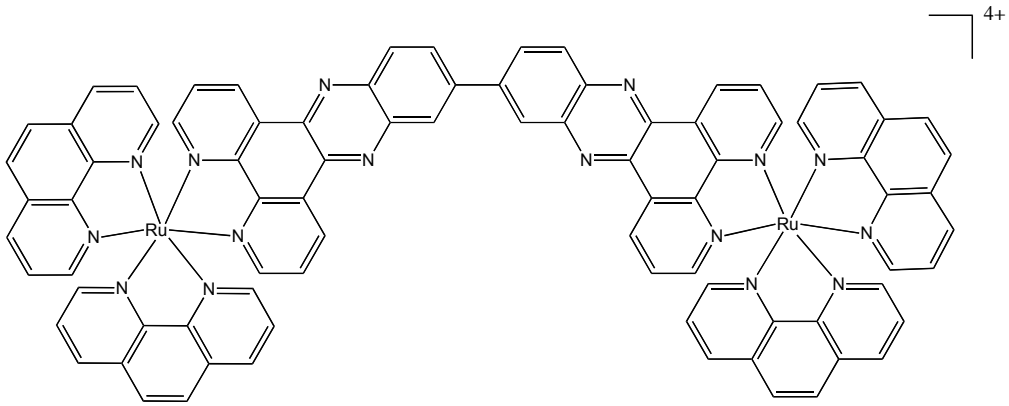

Fig. 1.18 The threading bis-intercalator $[\mu(bidppz)(phen)_4Ru_2]^{4+}$.

Studies on the effect of the bridging ligand on the threading properties of this kind of compound showed that their threading efficiency is determined by length and flexibility or rigidity of the bridging ligand.[126] Nevertheless, these complexes, particularly $[\mu(bidppz)(phen)_4Ru_2]^{4+}$, have been found to selectively target alternating AT base pairs.[127]

1.3.3 Binding to sugar-phosphate backbone

Polynuclear metal complexes can be a promising alternative to the mononuclear supramolecular DNA-binding metallo-drugs.[128]

TriplatinNC and TriplatinNC-A (Fig. 1.19), the non-covalent DNA-binding analogues of the clinically investigated BBR3464, within DNA interact exclusively with the DNA phosphate backbone.[129]

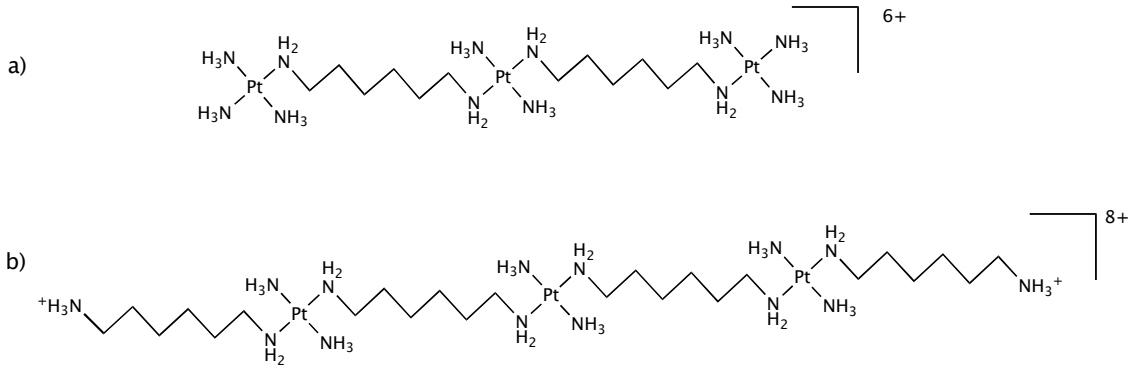

Fig. 1.19 The chemical structures of trinuclear phosphate clamps: a) TriplatinNC-A, b) TriplatinNC

The crystal structure of TriplatinNC with the Dickerson-Drew Dodecamer (5'-CGCGAATTCGCG-3') shows the selective interactions of the platinum complex with oxygen-rich polyanionic sugar-phosphate backbone (Fig. 1.20).[129] This recognition takes place mainly through electrostatic interactions and formation of amine(NH)···phosphate(O)···ammine(HN) hydrogen bonds with the phosphate oxygens.

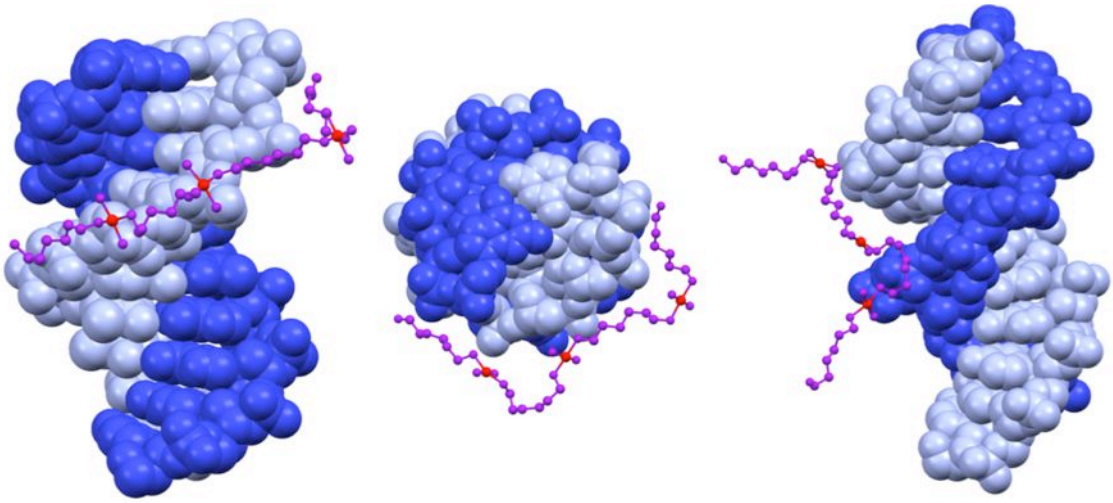

Fig. 1.20 Recognition of phosphate backbone by trinuclear platinum complex (left) side view, (middle) top view (right) spanning of two phosphate backbones, (PDB ref. 2DYW).[129]

In vitro testing of TriplatinNC and TriplatinNC-A for their anticancer properties shows that both complexes, exhibit micromolar cytotoxicity against certain ovarian cancer cell lines.[130] However, the TriplatinNC seems to be remarkably more active than TriplatinNC-A. This was suggested to be attributed to the cellular uptake of both compounds.

1.3.4 Beyond the canonical right-handed double helix

The research on DNA binding drugs for a long time was focused on the recognition of B-DNA structures. However, over the past few years much attention has been drawn to targeting non-classical structures and conformations of nucleic acids such as branched DNA structures, DNA hairpins, triplexes or quadruplex DNA topologies.

1.3.4.1 DNA junction structures recognition

Hannon and co-workers developed a series of metallo-supramolecular dinuclear triple-stranded helicates, which have a size and shape similar to helix-turn-helix protein DNA recognition units (~2 nm in length and ~1 nm in diameter). These compounds were found to bind strongly to the major groove of the DNA, promoting bending and intramolecular DNA coiling,[131] but were also shown to target the core cavity of DNA Y-shaped junctions without causing alterations in the DNA structure (Fig. 1.21).[132-135]

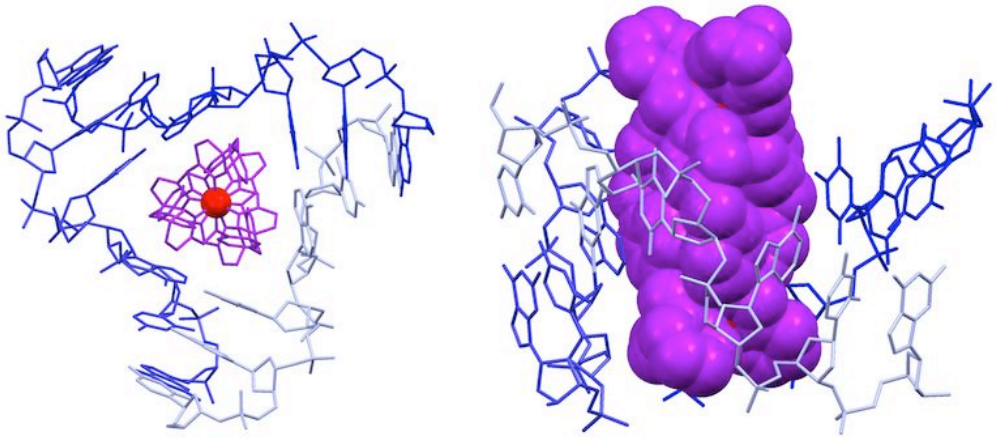

Fig.1.21 Recognition of DNA three way junction by metallo-supramolecular helicate. Left (top view), right (side view) (PDB ref. 2ET0).[132]

The crystal structure of the Fe helicate with the palindromic DNA sequence (5'-CGTACG-3') showed the complex DNA-helicate to be stabilized by a number of supramolecular interactions: π-π stacking between base pairs and phenyl rings of the cylinder (Fig. 1.22), CH…N hydrogen bonding, hydrophobic effects, as well as sandwiching interactions on the minor groove side.[132] However, this kind of recognition is not limited to the palindromic DNA

sequences, yet the cylinders can recognize different DNA three-way junction topologies.[136]

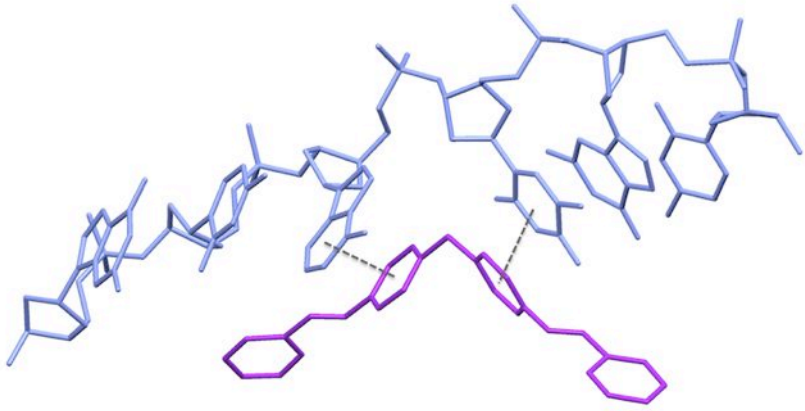

Fig. 1.22 The stacking of the DNA bases with the phenyl rings of one strand of the triple-helicate (PDB ref. 2ET0).[132]

In vitro supramolecular helicates exhibit cytotoxicity only 2-5 fold lower than cisplatin,[137] but unlike the latter drug they were found to be non-genotoxic.[138] They cause arrest of the G_o/G_1 phase of cell cycle[138] and were also found to inhibit DNA transactions by interfering with *Taq* polymerase binding to DNA.[139] This can be a strong indication that the non-covalent DNA binding supramolecular cylinders may be able to influence the processing of the genetic code by proteins.

1.3.4.2 G-quadruplex DNA recognition

Quadruplex nucleic acids are four-stranded DNA structures based on hydrogen-bonded guanine quartets (Fig. 1.23).[140, 141] They are found in *e.g.* chromosomal DNA, especially in telomeres, ribosomal DNA and in the promoters of genes. The formation of quadruplex structures inhibits the telomerase enzyme from maintaining telomere length,[142] which prevents the

cell senescence and further apoptosis.[143] Therefore, molecules that selectively target or induce formation of quadruplex DNA can be a new class of anticancer drugs.[144, 145]

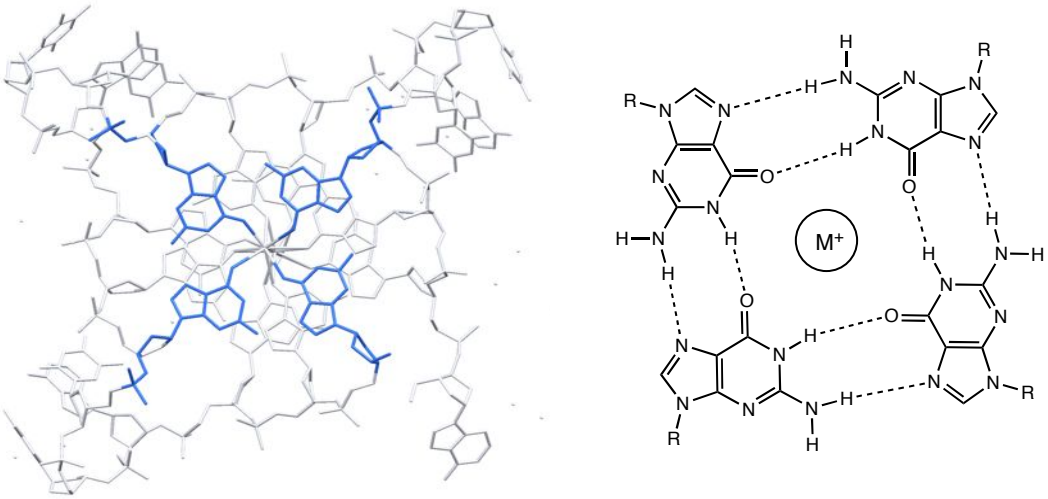

Fig. 1.23 Structure of G-quadruplex (PDB ref. 1KF1)[141]

The general properties of G-quadruplex DNA recognizing agents include cationic charge and an extended, planar aromatic core suited for π-π stacking with the G4 ‘surface’. Numerous metal-based compounds have been shown to selectively recognize G-rich DNA sequences.[146] For example, piperidine functionalised, square-planar nickel(II) complex (Fig. 1.24a) was found to be >50 fold more effective in stabilizing G-quadruplex structures over duplex DNA, and was shown to inhibit telomerase activity at concentrations of 0.1 μM.[147] More recently, it was reported that a terpyridine-based bimetallic complex binds even more strongly to quadruplex DNA with around 100 fold better selectivity towards these structures versus duplex DNA.[148] It has been proposed that the binding properties of this dinuclear compound arise from its dual mode of

action, which involves π-π stacking of the terpyridine unit with G-quartets and the interaction of the metal-dipicolyl moiety with the DNA backbone.

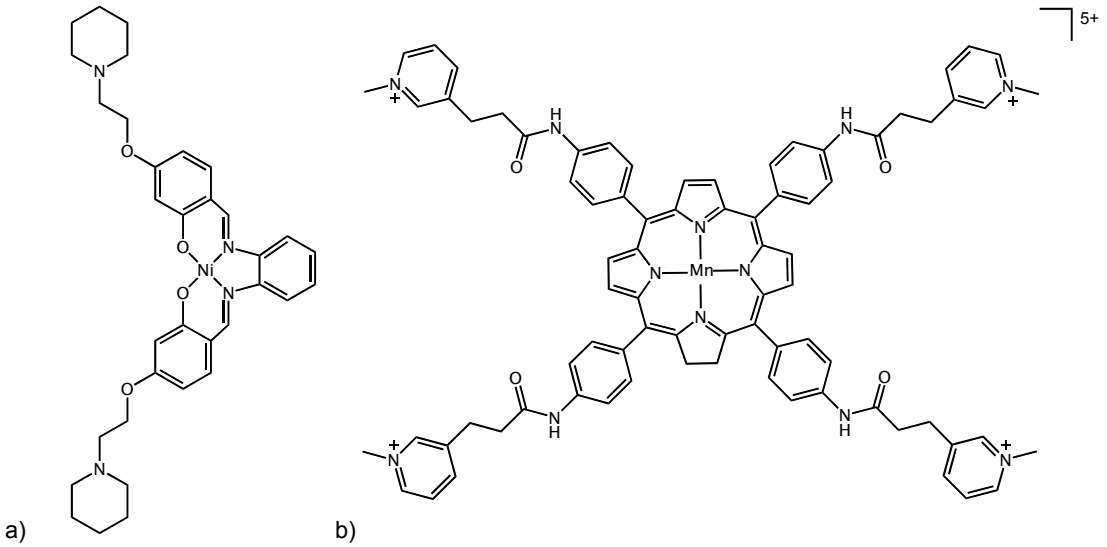

Fig. 1.24 Chemical structures of G-quadruplex recognizing agents; a) Nickel-salphen complex, b) Manganese porphyrin complex.

The functionalisation of the terminal regions of the planar moiety with flexible 'arms' appears to be a favoured strategy for improving the selectivity of the G-quadruplex binding agents. One of the leading examples of this type of drug is a manganese-porphyrin complex (Fig. 1.24b), consisting of a flat aromatic core and four flexible arms suited to non-covalent interactions with the grooves and loops of the G-quadruplex structures. This compound was found to be >10 000 times more selective towards G-quadruplex sequences compared to duplex DNA.[149] Nevertheless, the high cationic charge of this complex also makes a substantial contribution to the energetics and stabilization of the system. Guanidiniozinc phtalocyanines (Fig. 1.25), reported by Luedtke[150] are further intriguing compounds of this genre.

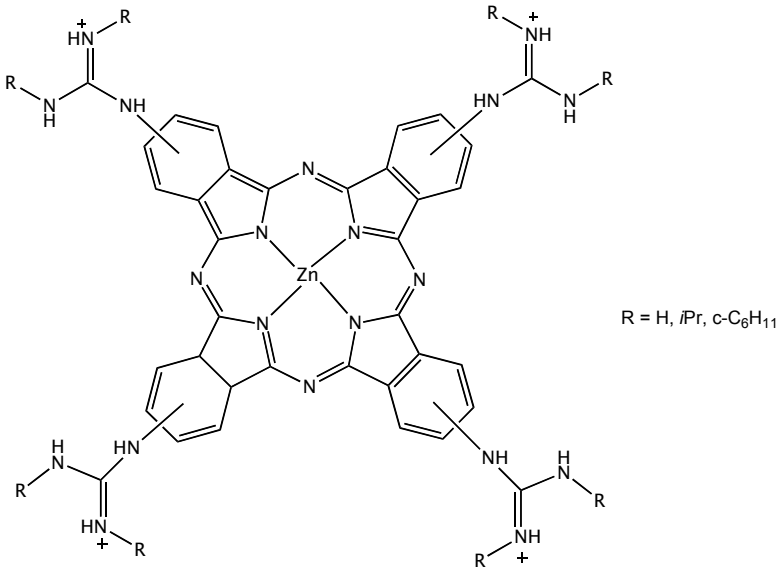

Fig. 1.25 Molecular structure of guanidiniozinc phtalocyanines

Zn-DIGP (shown in Fig. 1.25, where R = *i*Pr), not only extremely strongly and selectively binds to the c-myc DNA, but also exhibits 'turn-on' luminescence upon binding to this structure.[150] Interestingly, this complex was shown to be able to reduce mRNA expression.

Breaking old, cisplatin rules and finding novel strategies for the development of new drugs can be a crucial step to obtain new selective and targeted drugs with novel mechanisms of action and a wide range of cellular activities. Supramolecular chemistry can have a great input into this new approach. Creating new drugs, where the metal ion can act as a scaffold for the assembly of three-dimensional structures for the selective recognition of the biologically important molecules, can draw a line between traditional metallo-drugs and future therapeutics.

1.4 Aim and outline of this thesis

In this work the supramolecular approach is used for the design and preparation of new kinetically stable dinuclear cylinder-shaped metal complexes that can interact with biomolecules exclusively via non-covalent interactions.

The aim of the research described in this work is to synthesize new derivatives of the rare, stable, fluorescent ruthenium triple-stranded helicates and to investigate the factors that influence their biomolecule binding properties and biological activities. The second objective is to understand the effect of chirality on the DNA binding properties of the above systems.

Chapter 2 addresses the improved methodologies applied to the synthesis and purification of ruthenium(II) triple stranded helicates with imine-based ligands as well as the synthesis and characterisation of three new Ru cylinders. The new compounds were studied for their DNA binding properties. All complexes were found to interact with ct-DNA and coil/bend DNA. Complexes also extensively unwind negatively supercoiled DNA and possess promising micromolar cytotoxicities against human breast cancer cell lines.

Chapter 3 presents the enantiomeric resolution of left and right-handed Ru triple-helicate and DNA binding studies of these enantiopure isomers using a number of spectroscopic techniques. Both enantiomers were found to have different DNA binding properties but were individually similar to their previously reported Fe analogues.

In Chapter 4 the interaction of racemic mixture and enantiopure optical isomers of the Ru(II) cylinder with a chiral shift reagent (Δ-TRISPHAT) is investigated using ^{1}H NMR spectroscopy.

Chapter 5 describes the synthesis and characterisation of ammine and azopyridyl based mono and dinuclear Ru(II) complexes. DNA binding studies of these compounds using a number of spectroscopic techniques are also presented.

In Chapter 6 detailed experimental synthetic procedures and characterisation of new compounds are presented. The details of the biological studies are also provided.

1.5 References

[1] J. M. Berg, J. L. Tymoczko, L. Stryer, *Biochemistry*, 5th ed., Spektrum, New York, **2002**; M. J. Hannon, *Chem. Soc. Rev.* **2007**, *36*, 280.

[2] C. R. Calladine, H. R. Drew, *Understanding DNA: The molecule and how it works*, 2nd ed., Academic Press: New York, **1997**.

[3] A. Ghosh, M. Bansal, *Acta Crystallogr. D* **2003**, *59*, 620.

[4] K. C. Woods, S. S. Martin, V. C. Chu, E. P. Baldwin, *J. Mol. Biol.* **2001**, *313*, 49.

[5] D. M. J. Lilley, *Q. Rev. Biophys.* **2000**, *33*, 109.

[6] S. S. Martin, E. Pulido, V. C. Chu, T. S. Lechner, E. P. Baldwin, *J. Mol. Biol.* **2002**, *319*, 107.

[7] F. A. Hays, A. Teegarden, Z. J. Jones, M. Harms, D. Raup, J. Watson, E. Cavaliere, P. S. Ho, *Proc. Natl. Acad. Sci. USA* **2005**, *102*, 7157.

[8] Z. J. Guo, P. J. Sadler, *Angew. Chem. Int. Ed.* **1999**, *38*, 1513.

[9] C. X. Zhang, S. J. Lippard, *Curr. Opin. Chem. Biol.* **2003**, *7*, 481.

[10] T. Storr, K. H. Thompson, C. Orvig, *Chem. Soc. Rev.* **2006**, *35*, 534.

[11] B. Rosenberg, L. Van Camp, T. Krigas, *Nature* **1965**, *205*, 698.

[12] B. Rosenberg, L. Van Camp, E. B. Grimley, A. J. Thomson, *J. Biol. Chem.* **1967**, *242*, 1347.

[13] B. Lippert, in *Cisplatin, Chemistry and Biochemistry of a Leading Anticancer Drug*, Wiley-VCH, Weinheim, **1999**.

[14] J. Reedijk, *Chem. Rev.* **1999**, *99*, 2499.

[15] D. Wang, S. J. Lippard, *Nat. Rev. Drug Discov.* **2005**, *4*, 307.

[16] M. Sooriyaarachchi, A. Narendran, J. Gailer, *Metallomics* **2011**, *3*, 49.

[17] R. A. Hromas, J. A. North, C. P. Burns, *Cancer Letters* **1987**, *36*, 197.

[18] S. P. Binks, M. Dobrota, *Biochem. Pharmacol.* **1990**, *40*, 1329.

[19] S. Ishida, J. Lee, D. J. Thiele, I. Herskowitz, *Proc. Natl. Acad. Sci. USA* **2002**, *99*, 14298.

[20] K. Ohashi, K. Kajiya, S. Inaba, T. Hasegawa, Y. Seko, T. Furuchi, A. Naganuma, *Biochem. Biophys. Res. Commun.* **2003**, *310*, 148.

[21] C. A. Puckett, *Dalton Trans.* **2010**, *30*, 1159.

[22] M. J. Hannon, *Pure Appl. Chem.* **2007**, *79*, 2243.

[23] E. R. Jamieson, S. J. Lippard, *Chem. Rev.* **1999**, *99*, 2467.

[24] P. M. Takahara, A. C. Rosenzweig, C. A. Frederick, S. J. Lippard, *Nature* **1995**, *377*, 649.

[25] J.-S. Hoffmann, D. Locker, G. Villani, M. Leng, *J. Mol. Biol.* **1997**, *270*, 539.

[26] R. C. Todd, S. J. Lippard, *J. Inorg. Biochem.* ***2010***, *104*, 902.

[27] P. Heffeter, U. Jungwirth, M. Jakupec, C. Hartinger, M. Galanski, L. Elbling, M. Micksche, B. Keppler, W. Berger, *Drug Resistance Updates*, **2008**, *11*, 1.

[28] D. J. Stewart, *Crit. Rev. Oncol. Hemat.* **2007**, *63*, 12.

[29] O. Rixe, W. Ortuzar, M. Alvarez, R. Parker, E. Reed, K. Paull, T. Fojo, *Biochem. Pharmacol.* **1996**, *52*, 1855.

[30] N. J. Wheate, S. Walker, G. E. Craig, R. Oun, *Dalton Trans.* **2010**, *39*, 8113.

[31] K. S. Lovejoy, S. J. Lippard, *Dalton Trans.* **2009**, 10651.

[32] L. Kelland, *Nat. Rev. Cancer* **2007**, *7*, 573.

[33] I. Ott, R. Gust, *Archiv der Pharmazie* **2007**, *340*, 117.

[34] T. Gianferrara, I. Bratsos, E. Alessio, *Dalton Trans.* **2009**, 7588.

[35] E. Hillard, A. Vessieres, L. Thouin, G. Jaouen, C. Amatore, *Angew. Chem. Int. Ed.* **2006**, *45*, 285.

[36] S. Nobili, E. Mini, I. Landini, C. Gabbiani, A. Casini, L. Messori, *Med. Res. Rev.* **2010**, *30*, 550.

[37] P. M. Abeysinghe, M. M. Harding, *Dalton Trans.* **2007**, 3474.

[38] P. Collery, B. Keppler, C. Madoulet, B. Desoize, *Crit. Rev. Oncol. Hemat.* **2002**, *42*, 283.

[39] M. A. Jakupec, B. K. Keppler, *Curr. Top. Med. Chem.* **2004**, *4*, 1575.

[40] S. H. van Rijt, A. Mukherjee, A. M. Pizarro, P. J. Sadler, *J. Med. Chem.* **2010**, *53*, 840.

[41] A. Levina, A. Mitra, P. A. Lay, *Metallomics* **2009**, *1*, 458.

[42] C. S. Allardyce, P. J. Dyson, *Platinum Met. Rev.* **2001**, *45*, 62.

[43] V. Fernandez-Moreira, F. L. Thorp-Greenwood, M. P. Coogan, *Chem. Commun.* **2010**, *46*, 186.

[44] M. R. Gill, J. Garcia-Lara, S. J. Foster, C. Smythe, G. Battaglia, J. A. Thomas, *Nat. Chem.* **2009**, *1*, 662.

[45] M. J. Clarke, *Coord. Chem. Rev.* **2002**, *232*, 69.

[46] W. H. Ang, P. J. Dyson, *Eur. J. Inorg. Chem.* **2006**, 4003.

[47] M. J. Clarke, *Met. Ions Biol. Syst.* **1980**, *11*, 231.

[48] M. J. Clarke, F. Zhu, D. R. Frasca, *Chem. Rev.* **1999**, *99*, 2511.

[49] E. Alessio, G. Mestroni, A. Bergamo, G. Sava, *Curr. Top. Med. Chem.* **2004**, *4*, 1525.

[50] C. G. Hartinger, S. Zorbas-Seifried, M. A. Jakupec, B. Kynast, H. Zorbas, B. K. Keppler, *J. Inorg. Biochem.* **2006**, *100*, 891.

[51] M. Cocchietto, S. Zorzet, A. Sorc, G. Sava, *Investig. New Drugs* **2003**, *21*, 55.

[52] A. Vacca, M. Bruno, A. Boccarelli, M. Coluccia, D. Ribatti, A. Bergamo, S. Garbisa, L. Sartor, G. Sava, *Br. J. Cancer* **2002**, *86*, 993.

[53] G. Sava, S. Zorzet, C. Turrin, F. Vita, M. Soranzo, G. Zabucchi, M. Cocchietto, A. Bergamo, S. DiGiovine, G. Pezzoni, L. Sartor, S. Garbisa, *Clin. Cancer Res.* **2003**, *9*, 1898.

[54] G. Sava, F. Frausin, M. Cocchietto, F. Vita, E. Podda, P. Spessotto, A. Furlani, V. Scarcia, G. Zabucchi, *Eur. J. Cancer* **2004**, *40*, 1383.

[55] S. Kapitza, M. Pongratz, M. A. Jakupec, P. Heffeter, W. Berger, L. Lackinger, B. K. Keppler, B. Marian, *J. Cancer Res. Clin. Oncol.* **2005**, *131*, 101.

[56] A. R. Timerbaev, C. G. Hartinger, S. S. Aleksenko, B. K. Keppler, *Chem. Rev.* **2006**, *106*, 2224.

[57] G. Gasser, I. Ott, N. Metzler-Nolte, *J. Med. Chem.* **2011**, *54*, 3

[58] C. S. Allardyce, A. Dorcier, C. Scolaro, P. J. Dyson, *Appl. Organomet. Chem.* **2005**, *19*, 1.

[59] Y. K. Yan, M. Melchart, A. Habtemariam, P. J. Sadler, *Chem. Commun.* **2005**, 4764.

[60] C. G. Hartinger, P. J. Dyson, *Chem. Soc. Rev.* **2009**, *38*, 391.

[61] R. E. Morris, R. E. Aird, P. del Socorro Murdoch, H. Chen, J. Cummings, N. D. Hughes, S. Parsons, A. Parkin, G. Boyd, D. I. Jodrell, P. J. Sadler, *J. Med. Chem.* **2001**, *44*, 3616.

[62] F. Wang, A. Habtemariam, E. P. L. van der Geer, R. Fernandez, M. Melchart, R. J. Deeth, R. Aird, S. Guichard, F. P. A. Fabbiani, P. Lozano-Casal, I. D. H. Oswald, D. I. Jodrell, S. Parsons, P. J. Sadler, *Proc. Natl. Acad. Sci. USA* **2005**, *102*, 18269.

[63] H. Chen, J. A. Parkinson, O. Novakova, J. Bella, F. Wang, A. Dawson, R. Gould, S. Parsons, V. Brabec, P. J. Sadler, *Proc. Natl. Acad. Sci. USA* **2003**, *100*, 14623.

[64] H. Chen, J. A. Parkinson, R. E. Morris, P. J. Sadler, *J. Am. Chem. Soc.* **2002**, *125*, 173.

[65] H. Chen, J. A. Parkinson, S. Parsons, R. A. Coxall, R. O. Gould, P. J. Sadler, *J. Am. Chem. Soc.* **2002**, *124*, 3064.

[66] A. Habtemariam, M. Melchart, R. Fernandez, S. Parsons, I. D. H. Oswald, A. Parkin, F. P. A. Fabbiani, J. E. Davidson, A. Dawson, R. E. Aird, D. I. Jodrell, P. J. Sadler, *J. Med. Chem.* **2006**, *49*, 6858.

[67] R. E. Aird, J. Cummings, A. A. Ritchie, M. Muir, R. E. Morris, H. Chen, P. J. Sadler, D. I. Jodrell, *Br. J. Cancer* **2002**, *86*, 1652.

[68] W. Han Ang, P. J. Dyson, *Eur. J. Inorg. Chem.* **2006**, *2006*, 4003.

[69] A. Bergamo, A. Masi, P. J. Dyson, G. Sava, *Int. J. Oncol.* **2008**, *33*, 1281.

[70] C. Scolaro, A. Bergamo, L. Brescacin, R. Delfino, M. Cocchietto, G. b. Laurenczy, T. J. Geldbach, G. Sava, P. J. Dyson, *J. Med. Chem.* **2005**, *48*, 4161.

[71] C. S. Allardyce, P. J. Dyson, D. J. Ellis, S. L. Heath, *Chem. Commun.* **2001**, 1396.

[72] S. Chatterjee, S. Kundu, A. Bhattacharya, C. G. Hartinger, P. J. Dyson, *J. Biol. Inorg. Chem.* **2008**, *13*, 1149.

[73] A. Casini, C. Gabbiani, F. Sorrentino, M. P. Rigobello, A. Bindoli, T. J. Geldbach, A. Marrone, R. Nazzareno, C. G. Hartinger, P. J. Dyson, L. Messori, *J. Med. Chem.* **2008**, *51*, 6773.

[74] A. H. Velders, K. van der Schilden, A. C. G. Hotze, J. Reedijk, H. Kooijman, A. L. Spek, *J. Chem. Soc. Dalton Trans.* **2004**, 448.

[75] A. H. Velders, H. Kooijman, A. L. Spek, J. G. Haasnoot, D. de Vos, J. Reedijk, *Inorg. Chem.* **2000**, *39*, 2966.

[76] A. Hotze, S. Caspers, D. Vos, H. Kooijman, A. Spek, A. Flamigni, M. Bacac, G. Sava, J. Haasnoot, J. Reedijk, *J. Biol. Inorg. Chem.* **2004**, *9*, 354.

[77] A. C. G. Hotze, B. M. Kariuki, M. J. Hannon, *Angew. Chem. Int. Ed.* **2006**, *45*, 4839.

[78] A. E. M. Boelrijk, A. M. Jorna, J. Reedijk, *J. Mol. Cat. A Chem.* **1995**, *103*, 73.

[79] S. J. Dougan, A. Habtemariam, S. E. McHale, S. Parsons, P. J. Sadler, *Proc. Natl. Acad. Sci. U S A* **2008**, *105*, 11628.

[80] P. C. Bruijnincx, P. J. Sadler, *Curr. Opin. Chem. Biol.* **2008**, *12*, 197.

[81] C. Sanchez-Cano, M. J. Hannon, *Dalton Trans.* **2009**, 10702.

[82] V. P. Torchilin, *Nat. Rev. Drug. Discov.* **2005**, *4*, 145.

[83] N. J. Farrer, P. J. Sadler, *Aust. J. Chem.* **2008**, *61*, 669.

[84] T. W. Failes, C. Cullinane, C. I. Diakos, N. Yamamoto, G. Lyons, T. W. Hambley, *Chem. Eur. J.* **2007**, *13*, 2974.

[85] A. M. Pizarro, P. J. Sadler, *Biochimie* **2009**, *91*, 1198.

[86] I. Jelesarov, H. R. Bosshard, *J. Mol. Recognit.* **1999**, *12*, 3.

[87] P. C. Weber, F. R. Salemme, *Curr. Opin. Struct. Biol.* **2003**, *13*, 115.

[88] I. Haq, B. Z. Chowdhry, T. C. Jenkins, M. J. W. Jonathan B. Chaires, in *Methods Enzymol., Vol. 340*, Academic Press, **2001**.

[89] J. B. Chaires, *Arch. Biochem. Biophys.* **2006**, *453*, 26.

[90] J. B. Chaires, *Biopolymers* **1998**, *44*, 201.

[91] I. Haq, J. Ladbury, *J. Mol. Recognit.* **2000**, *13*, 188.

[92] M. Prabhakaran, S. C. Harvey, *Biopolymers* **1988**, *27*, 1239.

[93] M. Trieb, C. Rauch, F. R. Wibowo, B. Wellenzohn, K. R. Liedl, *Nucleic Acids Res.* **2004**, *32*, 4696.

[94] D. B. Smithrud, E. M. Sanford, I. Chao, S. B. Ferguson, D. R. Carcangue, J. D. Evanseck, K. N. Houk, F. Dietrich, *Pure Appl. Chem.* **1990**, *62*, 2227

[95] B. Jayaram, J. Tarun, *Annu. Rev. Biophys. Biomol. Struct.* **2004**, *33*, 343

[96] I. Haq, *Arch. Biochem. Biophys.* **2002**, *403*, 1.

[97] R. S. Spolar, M. T. Record, Jr., *Science* **1994**, *263*, 777

[98] G. S. Manning, *Quart. Rev. Biophys.* **1978**, *11*, 179

[99] M. T. Record, Jr., C. F. Anderson, T. M. Lohman, *Quart. Rev. Biophys.* **1978**, *11*, 103

[100] I. Haq, T. C. Jenkins, B. Z. Chowdhry, J. Ren, J. B. Chaires, G. K. A. Michael L. Johnson, in *Methods Enzymol., Vol. Volume 323*, Academic Press, **2000**, pp. 373.

[101] A. Cooper, *Curr. Opin. Chem. Biol.* **1999**, *3*, 557

[102] C.-H. Lee, H. Mizusawa, T. Kakefuda, *Proc. Natl. Acad. Sci. USA* **1981**, *78*, 2838

[103] R. Martinez, L. Chacon-Garcia, *Curr. Med. Chem.* **2005**, *12*, 127.

[104] N. J. Wheate, C. R. Brodie, J. G. Collins, S. Kemp, J. R. Aldrich-Wright, *Mini-Rev. Med. Chem.* **2007**, *7*, 627.

[105] H.-K. Liu, P. J. Sadler, *Acc. Chem. Res.* **2011**, *44*, 349.

[106] K. W. Jennette, S. J. Lippard, G. A. Vassiliades, W. R. Bauer, *Proc. Natl. Acad. Sci. USA* **1974**, *71*, 3839.

[107] P. J. Bond, R. Langridge, K. W. Jennette, S. J. Lippard, *Proc. Natl. Acad. Sci. USA* **1975**, *72*, 4825.

[108] J. G. Collins, R. M. Rixon, J. R. Aldrich-Wright, *Inorg. Chem.* **2000**, *39*, 4377.

[109] C. R. Brodie, J. G. Collins, J. R. Aldrich-Wright, *Dalton Trans.* **2004**, 1145.

[110] D. Jaramillo, D. P. Buck, J. G. Collins, R. R. Fenton, F. H. Stootman, N. J. Wheate, J. R. Aldrich-Wright, *Eur. J. Inorg. Chem.* **2006**, *2006*, 839.

[111] D. M. Fisher, P. J. Bednarski, R. Grünert, P. Turner, R. R. Fenton, J. R. Aldrich-Wright, *Chem. Med. Chem.* **2007**, *2*, 488.

[112] B. M. Zeglis, V. C. Pierre, J. K. Barton, *Chem. Commun.* **2007**, 4565.

[113] A. H. Krotz, B. P. Hudson, J. K. Barton, *J. Am. Chem. Soc.* **1993**, *115*, 12577.

[114] K. E. Erkkila, B. P. Hudson, J. K. Barton, D. C. Rees, *Nat. Struct. Biol.* **2000**, *7*, 117.

[115] C. Cordier, V. C. Pierre, J. K. Barton, *J. Am. Chem. Soc.* **2007**, *129*, 12287.

[116] B. M. Zeglis, V. C. Pierre, J. T. Kaiser, J. K. Barton, *Biochemistry* **2009**, *48*, 4247

[117] B. A. Jackson, J. K. Barton, *J. Am. Chem. Soc.* **1997**, *119*, 12986.

[118] H. Junicke, J. R. Hart, J. Kisko, O. Glebov, I. R. Kirsch, J. K. Barton, *Proc. Natl. Acad. Sci. USA* **2003**, *100*, 3737.

[119] J. R. Hart, O. Glebov, R. J. Ernst, I. R. Kirsch, J. K. Barton, *Proc. Natl. Acad. Sci.* **2006**, *103*, 15359.

[120] R. J. Ernst, H. Song, J. K. Barton, *J. Am. Chem. Soc.* **2009**, *131*, 2359.

[121] P. B. Glover, P. R. Ashton, L. J. Childs, A. Rodger, M. Kercher, R. M. Williams, L. De Cola, Z. Pikramenou, *J. Am. Chem. Soc.* **2003**, *125*, 9918.

[122] E. L. Crossley, J. B. Aitken, S. Vogt, H. H. Harris, L. M. Rendina, *Angew. Chem. Int. Ed.* **2010**, *49*, 1231.

[123] G. Lowe, S. A. Ross, M. Probert, *Chem. Commun.* **2001**, 1288.

[124] K. Becker, C. Herold-Mende, J. J. Park, G. Lowe, R. H. J. Schirmer, *J. Med. Chem.* **2001**, 2784.

[125] F. Westerlund, L. M. Wilhelmsson, B. Norden, P. Lincoln, *J. Phys. Chem.* **2005**, *B*, 21140.

[126] J. Andersson, M. Li, P. Lincoln, *Chem. Eur. J.* **2010**, *16*, 11037.

[127] P. Nordell, F. Westerlund, L. M. Wilhelmsson, B. Nordén, P. Lincoln, *Angew. Chem. Int. Ed.* **2007**, *46*, 2203.

[128] J. B. Mangrum, N. P. Farrell, *Chem. Commun. (Camb)* **2010**, *46*, 6640.

[129] S. Komeda, T. Moulaei, K. K. Woods, M. Chikuma, N. P. Farrell, L. D. Williams, *J. Am. Chem. Soc.* **2006**, *128*, 16092.

[130] A. L. Harris, X. H. Yang, A. Hegmans, L. Povirk, J. J. Ryan, L. Kelland, N. P. Farrell, *Inorg. Chem.* **2005**, *44*, 9598.

[131] I. Meistermann, V. Moreno, M. J. Prieto, E. Moldrheim, E. Sletten, S. Khalid, P. M. Rodger, J. C. Peberdy, C. J. Isaac, A. Rodger, M. J. Hannon, *Proc. Natl. Acad. Sci. USA* **2002**, *99*, 5069.

[132] A. Oleksy, A. G. Blanco, R. Boer, I. Uson, J. Aymami, A. Rodger, M. J. Hannon, M. Coll, *Angew. Chem. Int. Ed.* **2006**, *45*, 1227.

[133] J. Malina, M. J. Hannon, V. Brabec, *Chemistry* **2007**, *13*, 3871.

[134] L. Cerasino, M. J. Hannon, E. Sletten, *Inorg. Chem.* **2007**, *46*, 6245.

[135] D. R. Boer, J. M. C. A. Kerckhoffs, Y. Parajo, M. Pascu, I. Usón, P. Lincoln, M. J. Hannon, M. Coll, *Angew. Chem. Int. Ed.* **2010**, *49*, 2336.

[136] J. Malina, M. J. Hannon, V. Brabec, *Chem. Eur. J.* **2007**, *13*, 3871.

[137] G. I. Pascu, A. C. Hotze, C. Sanchez-Cano, B. M. Kariuki, M. J. Hannon, *Angew. Chem. Int. Ed.* **2007**, *46*, 4374.

[138] A. C. G. Hotze, N. J. Hodges, R. E. Hayden, C. Sanchez-Cano, C. Paines, N. Male, M.-K. Tse, C. M. Bunce, J. K. Chipman, M. J. Hannon, *Chem. Biol.* **2008**, *15*, 1258.

[139] C. Ducani, A. Leczkowska, N. J. Hodges, M. J. Hannon, *Angew. Chem. Int. Ed.* **2010**, *49*, 8942.

[140] S. Burge, G. N. Parkinson, P. Hazel, A. K. Todd, S. Neidle, *Nucleic Acids Res.* **2010**, *34*, 5402.

[141] G. N. Parkinson, M. P. Lee, S. Neidle, *Nature* **2002**, *417*, 876;

[142] D. Sun, B. Thompson, B. E. Cathers, M. Salazar, S. M. Kerwin, J. O. Trent, T. C. Jenkins, S. Neidle, L. H. Hurley, *J. Med. Chem.* **1997**, *40*, 2113.

[143] N. W. Kim, M. A. Piatyszek, K. R. Prowse, C. B. Harley, M. D. West, P. L. Ho, G. M. Coviello, W. E. Wright, S. L. Weinrich, J. W. Shay, *Science* **1994**, *266*, 2011.

[144] S. Neidle, G. Parkinson, *Nat. Rev. Drug Discov.* **2002**, *1*, 383.

[145] S. Balasubramanian, S. Neidle, *Curr. Opin. Chem. Biol.* **2009**, *13*, 345.

[146] S. N. Georgiades, N. H. Abd Karim, K. Suntharalingam, R. Vilar, *Angew. Chem. Int. Ed.* **2010**, *49*, 4020.

[147] J. E. Reed, A. A. Arnal, S. Neidle, R. Vilar, *J. Am. Chem. Soc.* **2006**, *128*, 5992.

[148] K. Suntharalingam, A. J. P. White, R. Vilar, *Inorg. Chem.* **2010**, *49*, 8371.

[149] I. M. Dixon, F. Lopez, A. M. Tejera, J.-P. Esteve, M. A. Blasco, G. Pratviel, B. Meunier, *J. Am. Chem. Soc.* **2007**, *129*, 1502.

[150] J. Alzeer, B. R. Vummidi, P. J. C. Roth, N. W. Luedtke, *Angew. Chem. Int. Ed.* **2009**, *48*, 9362.

2

Dinuclear Ru(II) Triple-Stranded Helicates

Synthesis, DNA Binding and Cytotoxic Activities

Abstract

In this chapter improved methodologies for the synthesis and purification of rare Ru(II) triple-stranded helicates with different structural topologies are described. Three new ruthenium cylinders have been synthesized and characterised and the molecular structures of $[Ru_2L^{o}_3](PF_6)_4$ and $[Ru_2L^{2\text{-}im}_3](PF_6)_4$ where L^{o} is an oxygen bridged bispyridylimine ligand $(C_6H_4N)C=N(C_6H_5)O(C_6H_5)N=C(C_6H_4N)$ and $L^{2\text{-}im}$ is 2-substituted bisimidazoleimine ligand $(C_3H_4N_2)C=N(C_6H_5)CH_2(C_6H_5)N=C(C_3H_4N_2)$ have been determined by X-ray diffraction analysis. The DNA binding of all three new complexes has been investigated using UV-Vis, circular and linear dichroism spectroscopy and an agarose gel electrophoretic mobility shift assay. The compounds have also been investigated for their cytotoxic activities against human ovarian cancer cell lines.

2.1 Introduction to supramolecular cylinders

In nature, sequence-specific DNA recognition relies primarily upon the formation of hydrogen bonds between DNA nucleobases and protein subunits *e.g.* helix-turn-helix, zinc fingers, or alternatively on 'indirect readout', which principally involves the sequence-dependent structural deformability of the DNA helix. This discrete DNA recognition is a distinctive feature of cellular regulatory processes such as regulation of gene expression. Indeed, uncontrolled cellular reproduction events *i.e.* DNA transactions such as replication or transcription may result in diseased conditions, which then may lead to cancer or viral infections. Developing small molecules that can selectively and specifically interact with nucleic acid structures or sequences has been of great interest in modern medicinal chemistry. Such molecules could restrict or moderately affect processing of genetic code and thereby act to regulate cellular processes. From this aspect there has been much effort devoted to creating synthetic molecules that could interact with DNA in a protein-like fashion.[1]

Research in Hannon group led to the development of metallo-supramolecular assemblies, which have a size and shape similar to natural protein DNA recognition subunits (Fig. 2.1).[2]

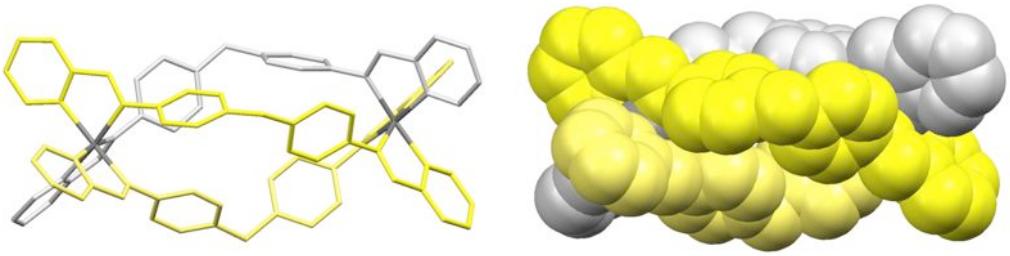

Fig. 2.1 Structure of the iron triple-stranded helicate, $[Fe_2L_3]^{4+}$

These compounds are cationic, dinuclear triple-stranded helicates built of three bisbidentate ligands wrapped around two metal centers in a helical fashion. The cylinders were found to recognize the major groove of the DNA spanning five base pairs and causing substantial intramolecular coiling of polymeric DNA.[3, 4] It was also found that the specific dimensions of metallo-supramolecular cylinders (2 nm in length and 1 nm in diameter) are crucial for their distinctive DNA binding properties.[5, 6] More recently, an iron helicate was shown to target the core cavity of DNA three-way junctions (Fig. 2.2) without causing alterations in the DNA structure.[7-9]

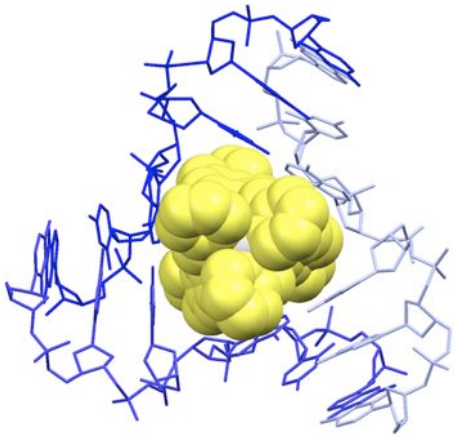

Fig. 2.2 Crystal structure of an iron(II) triple-helicate bound to the junction point of a DNA three-way junction (PDB ref. 2ETO).[7]

Gel electrophoresis studies showed that a cylinder can recognize a variety of different Y-shaped junction topologies.[10] In fact DNA three-way junction structures are present during DNA replication and these structures have also been found to be involved in several human diseases such as Huntington's disease.[11] Therefore, this new mode of DNA recognition opens up the opportunity to approach new biological targets and can also be a very powerful

tool in studies of DNA replication or transcription processes, for instance by interfering with or monitoring them.

The biological studies show that the iron(II) cylinder binds to the bacterial DNA and exhibits antimicrobial properties against *B. subtilis* and *E. coli*.[12] Further biological evaluation of metallo-supramolecular helicates showed that the cylinders exhibit antiproliferative properties in a wide range of human cancer cell lines without causing genotoxic or mutagenic effects.[13] It was also found that the level of cytotoxicity of supramolecular cylinders depends on both the incubation time and the total amount of drug applied.[14]

Several different helical systems have been developed to study their effects on DNA structures. These include copper helicates, which were shown to be able to act as synthetic nucleases[15] and a ruthenium triple-stranded helicate, which has similar structural characteristics to its previously synthesized iron(II) analogue (Fig. 2.3).[16, 17]

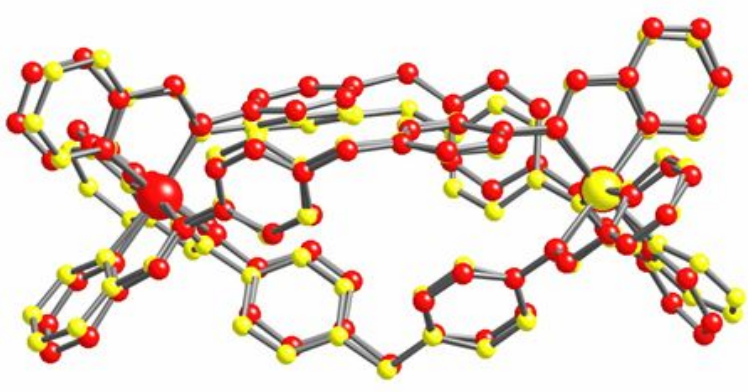

Fig. 2.3 Overlay of crystal structures of ruthenium (II) triple-stranded helicate (red) and its iron (II) analogue (yellow); Figure taken from [17].

Although the DNA binding and coiling properties of the ruthenium cylinder were found to be comparable to these of iron cylinder, unlike the latter complex, this compound causes DNA strand breaks upon irradiation with UV-Vis light thus cleaving DNA in a sequence-dependent fashion, mostly at guanine bases.[18] There were also found to be some differences in the cytotoxic activities of the ruthenium and iron helicates. While iron cylinder exhibits micromolar cytotoxicity in breast and ovarian cancer cell lines, ruthenium analogue was found to be active only in breast cancer cells (T47D and HBL100).[16]

The above-mentioned biological effects of the cylinders were believed to be a consequence of their binding to the DNA. However, further studies on these complex-DNA systems had to be undertaken in order to access more detailed information on the mechanism of action and to better understand the possible relationship between their DNA binding properties and cellular effects.

Although in the Hannon group DNA binding studies focused primarily on Fe(II) supramolecular cylinders, the lack of stabilities of these systems in aqueous solution limited the scope of experiments that could be performed. Since the ruthenium analogue proved to be very stable in aqueous solution and biological mediums,[17] and the structural properties of the cylinders were believed to be crucial for cylinder-like activities, the $[Ru_2L_3]^{4+}$ was chosen as an alternative model compound for our systems. The fluorescent properties of this compound are also useful for probing DNA binding and, most importantly, investigating and monitoring of the action of the drug in living cells.

Formation of dinuclear triple-stranded helicates is ordinarily a spontaneous self-assembly process. An example of this can be the preparation of an iron cylinder, where the pure compound can be obtained within 2 hours in a high yield.[2] However, using inert metal ions, such as Ru(II), as building units for the helicate may disrupt or hinder the assembly of such systems. Indeed the synthesis and purification of the ruthenium analogue of the iron triple-stranded helicate initially proved to be very challenging, giving an analytically pure compound in ~ 1 % yield.[16] Thus, having established that the ruthenium compound can be a valuable probe for our systems the first aim of the work presented in this chapter was to find new, improved strategies towards synthesis and/or purification of the Ru-based triple-stranded helicates, which would allow further, detailed biological studies on these systems.

2.2 Results and discussion

2.2.1 Synthesis of $[Ru_2L_3]Cl_4$

A few reports on the formation of the heterometallic helicates containing Ru(II) are found in the literature.[19-22] However, as yet there are only two literature examples of the homometallic ruthenium triple-stranded complexes.[16, 23]

Synthesis of the very first Ru(II) triple-stranded cylinder with bispyridylimine ligands was reported in 2007 by Pascu.[16] Later, in 2008, Glasson and co-workers showed that microwave irradiation could also be employed for the successful synthesis of this class of Ru compounds.[23] Using quaterpyridine ligands as building blocks for the cylinder and the microwave radiation based synthetic methodology allowed to obtain an analytically pure product in 36 % yield.

To initiate the project on ruthenium triple-stranded helicates it was first decided to repeat the original synthesis of Pascu, but to explore other ways of purification. Following this, alternative methods of synthesis were also explored.

Ligand L (Fig. 2.4) was synthesized following a previously published method.[2]

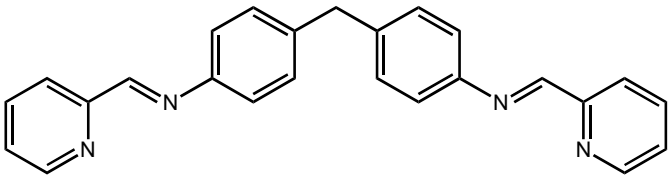

Fig. 2.4 Molecular structure of L

The synthesis of $[Ru_2L_3]Cl_4$ was performed by reacting *cis*-$[Ru(DMSO)_4Cl_2]$ and ligand L under argon atmosphere for 7 days. This was followed by silica gel column chromatography to obtain a pure material in a final yield of 11 %. The ^1H NMR spectrum of the purified compound is shown in Fig. 2.5.

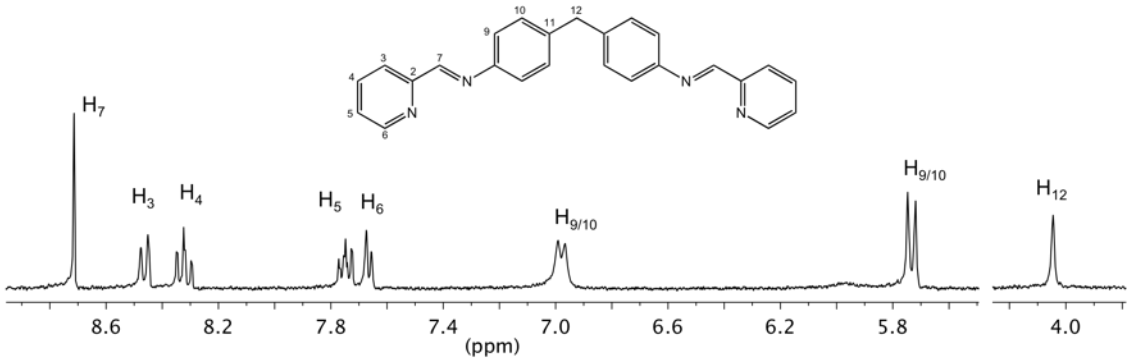

Fig. 2.5 ^1H NMR spectrum of $[Ru_2L_3](PF_6)_4$ in CD_3CN

The mass spectrum of the chloride form of the compound reveals peaks corresponding to $[Ru_2L_3]^{4+}$ (*m/z* 333.1), $[Ru_2L_3]^{3+}$ (*m/z* 444.0), $[Ru_2L_3]Cl^{2+}$

(*m/z* 683.7) and $[Ru_2L_3]Cl_2^{2+}$ (*m/z* 701.2) and analytical purity of the obtained compound was confirmed by elemental analyses.

The purification of the Ru triple-stranded helicate on the silica gel seems to be more efficient than the original purification technique on an alumina column (neutral alumina with CH_3CN/H_2O/sat. KNO_3, 20:1:1) where, during the purification process, a part of the compound remains on the column and this subsequently lowers the final yield. Although the multiple columning necessary for the purification using the silica gel also leads to the loss of some of the product, the amount lost is less than using the alumina. However, to try to minimize the loss of the compound at this stage alternative purification routes were pursued.

A superior technique for purification of ruthenium triple-stranded helicate was found to be positive ion exchange chromatography on Sephadex C-50 resin with a gradient of aq. NaCl (0.05 – 0.8 M). This involved using the water-soluble chloride salt of the crude. Nevertheless, using this method an analytically pure compound was obtained in 16 % yield, which was improved by a factor of 60 over the original yield reported by Pascu.

This method was found to be moderately more efficient in terms of yield than the silica gel approach, and unlike the previously discussed technique it does not necessitate multiple columning, which shortens the total required time for the purification and avoids the possibility of losing part of the product on the next column or in the analyses of the multi-step purification process. However, alternative avenues towards the synthesis of $[Ru_2L_3]Cl_4$ were also investigated.

Following Glasson strategy, it was found that ruthenium bispyridylimine ligand-based cylinder could also be effectively obtained using microwave irradiation. Exposing the mixture of *cis*-$[Ru(DMSO)_4Cl_2]$ and ligand L in ethylene glycol to microwave energy for 4 sequential 1h long cycles at 180^{o}C, followed by silica gel or cation exchange chromatography, gives the desired product in yield of 12-18 %. This is comparable to the yield obtained in the reflux-based methodology.

One of the important factors in the formation of the desired compound appears to be the need for a rapid increase in the energy for the reaction mixture. Due to the ease of formation of a number of kinetic by-products it is necessary to drive the reaction towards the desired, thermodynamically controlled, metallo-assemblies. That factor notwithstanding, the formation of the presumed polymeric impurities still appears to be unavoidable in these systems.

Although all the above-described strategies for the synthesis and purification of ruthenium triple-stranded helicate give similar yields, considering the overall timescale of the reaction and the purification efficiency, it can be concluded that the most satisfactory results were obtained when using the microwave reaction approach combined with purification by cation exchange chromatography. In summary, both, reaction yield and time requirements were substantially improved compared to the previously reported results.

These results demonstrated the viability of making ruthenium triple-helicates and allowed for the greatly expanded research and utility of this family of compounds in DNA-binding studies and in cells.

2.2.2 Towards a library of ruthenium triple-stranded helicates

It was found that the Ru cylinder, similarly to its iron analogue, can recognize and stabilize DNA and RNA three way-junction structures.[24] Further *in vitro* studies of the action of the Ru cylinder on the DNA showed that this compound 'can affect the ability of proteins to process the DNA code' by affecting Tag polymerase binding to ds-DNA.[25] Explicit research on the action of the Ru compound in living cells has also been undertaken.[26] For instance, studies on the cellular uptake and distribution of the Ru cylinder using ICP-MS showed that the compound can cross the cell membrane and reach the nucleus within a relatively short time (3h). It was found that only 3 hours after treatment already 60% of the total uptaken cylinder was accumulated in the cell nucleus.[26] These findings were further confirmed by confocal microscopy.

These and previous interesting results obtained for the ruthenium parent cylinder led to the initiation of a project for developing other, kinetically stable, fluorescent Ru cylinders. This entitled creating a library of Ru cylinders and screening them for their biomolecule binding properties and their action in cells with an ultimate goal to investigate the structure – function or structure - cytotoxicity relationship in these systems. From this aspect three other Ru triple- stranded cylinders have been prepared.

2.2.3 Synthesis and characterisation of $[Ru_2L^o_3]Cl_4$

Ligand L^o (Fig. 2.6) is analogous to the ligand L but the $-CH_2-$ group in the centre of the ligand has been replaced by an oxygen atom. The ligand L^o was prepared by reacting two equivalents of 2-pyridine carboxaldehyde with

one equivalent of 4,4'-diaminodiphenyl ether in methanol.[27] The characterisation of this compound was in agreement with the literature data.

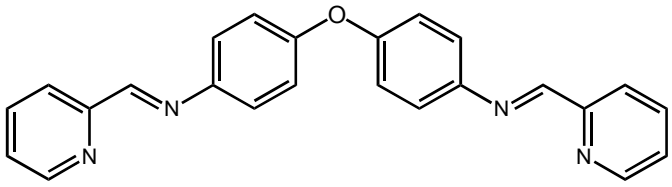

Fig. 2.6 Molecular structure of L^o

The newly developed synthetic and purification procedure for the parent $[Ru_2L_3]Cl_4$ was proved to be successful also for the new pyridine system with oxygen bridged ligand L^o. $[Ru_2L^o_3]Cl_4$ was synthesized by reacting the two equivalents of *cis*-$[Ru(DMSO)_4Cl_2]$ with three equivalents of ligand L^O in ethylene glycol at 200°C for 7 days. Analogously to the previously described method, successful purification was performed on the silica gel column with aqueous 5-15 mM NH_4PF_6/CH_3CN as an eluent. This was followed by anion metathesis with t-Bu_4NCl yielding the pure compound in a 8 % yield. The ^1H NMR spectrum reveals one set of aromatic proton resonances (Fig. 2.7), confirming the high symmetry of the isolated compound.

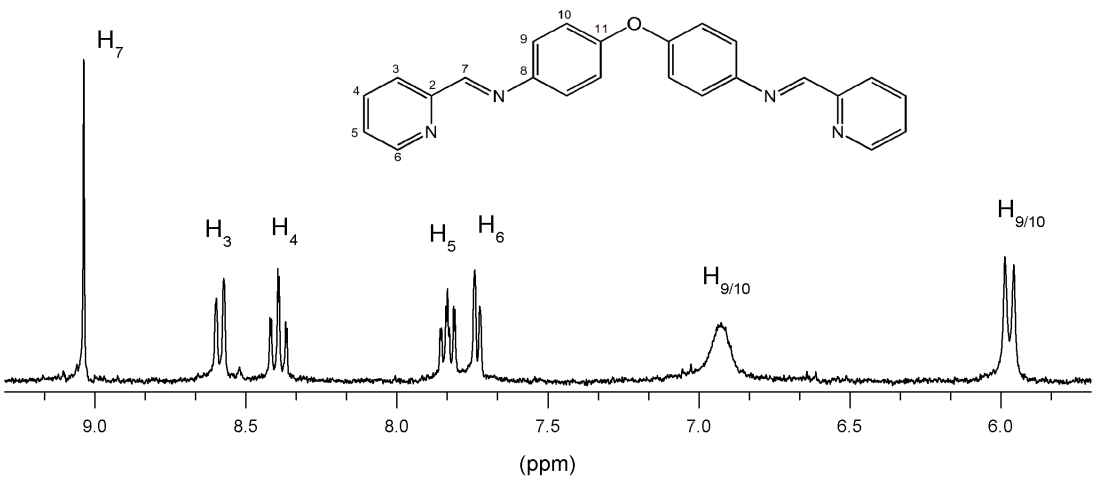

Fig. 2.7 ^1H NMR spectrum of $[Ru_2L^o_3]Cl_4$ in MeOD.

The electrospray mass spectrum (of the chloride salt of the compound) shows peaks with the isotopic distribution corresponding to $[Ru_2L^o_3]^{4+}$ (*m/z* 334.6) and $[Ru_2L^o_3]Cl^{3+}$ (*m/z* 457.5) cations. Elemental analysis data were consistent with $[Ru_2L^o_3]Cl_4$ formulation. Dark orange crystals suitable for X-ray analysis were obtained by slow diffusion of diethyl ether into an acetonitrile solution of the hexafluorophosphate salt of the compound at 4°C. The compound crystallized in an orthorhombic crystal system with the space group Pbca. The crystal structure confirms the formation of the dinuclear cation with three bis-bidentate ligands wrapped around two metal centers in a helical fashion. The Ru-N distances are in the range of 2.03 – 2.11 Å and the Ru centers are separated by 11.3 Å (Fig. 2.8).

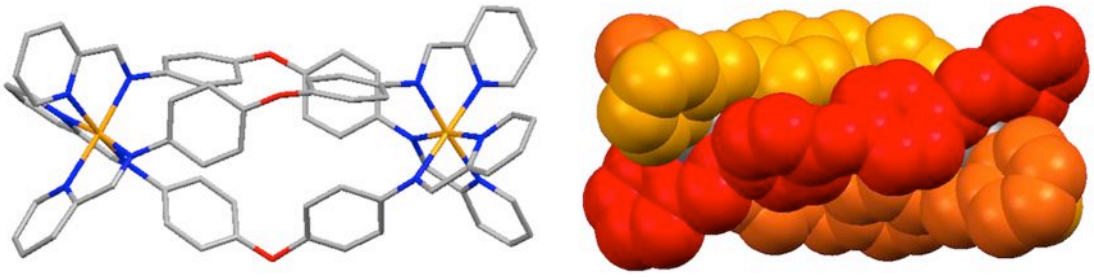

Fig. 2.8 Crystal structure of cation in $[Ru_2L^o_3](PF_6)_4$. Hydrogen atoms, counterions and solvent molecules are omitted for clarity, red-O, blue-N, grey-C, orange-Ru

This structure is highly similar to the structure of the corresponding Ru(II) cylinder with ligand L reported by G. Pascu (Fig. 2.9) and further, to the Fe(II) analogue of the latter complex.

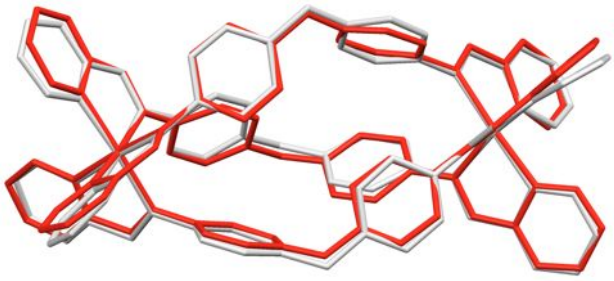

Fig. 2.9 Overlay of structures of cations in $[Ru_2L_3](PF_6)_4$ (grey) and $[Ru_2L^o_3](PF_6)_4$ (red)

The deep orange colour of the complex is typical for RuN_6 chromophores.[16] The UV-Vis spectrum shows the MLCT band with the maximum at 485 nm (ε = 21 500 M^{-1} cm^{-1} in H_2O) and inter-ligand transition bands centered at 322 and 270 nm (Fig. 2.10). Similarly to the ruthenium parent cylinder, as it has the same coordination sphere, the compound is fluorescent and excitation in the MLCT region (λ_{ex} = 485 nm) gives rise to the emission band centered at 705 nm (Fig. 2.10).

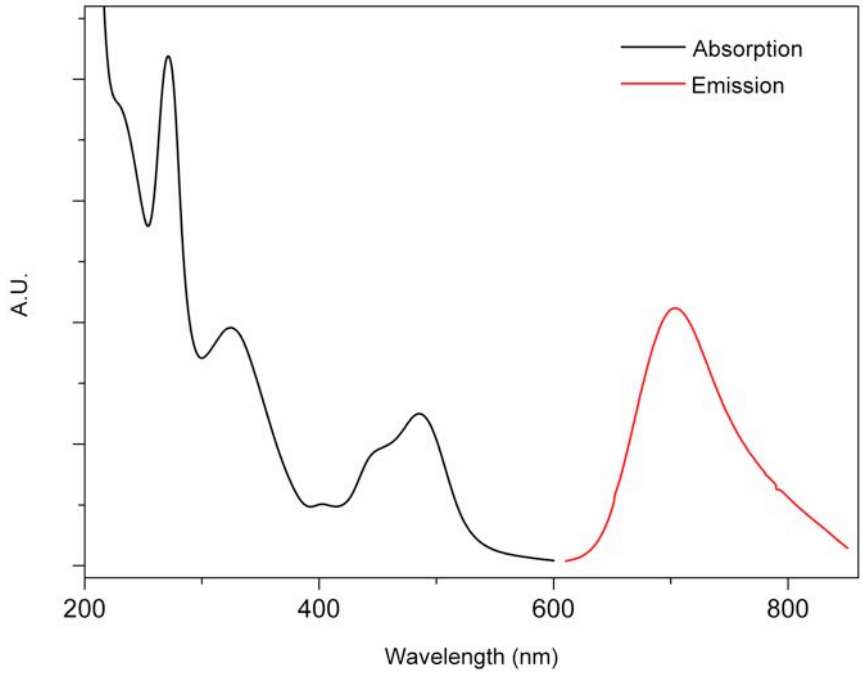

Fig. 2.10 Absorption (black) and emission (red) spectra of $[Ru_2L^o_3]Cl_4$ recorded in water (λ_{ex} = 485 nm). Spectra are not on the same scale.

2.2.4 Synthesis and characterisation of $[Ru_2L^{2\text{-im}}{}_3]Cl_4$

To investigate whether changing the coordination sphere of ruthenium, while maintaining the spacer group, can influence the DNA binding properties of the cylinder, helicates with modified ligand structure at the metal binding unit were explored.

Ligand $L^{2\text{-im}}$ (Fig. 2.11) was prepared from commercially available 4,4'-methylenediamine and 2-imidazolecarboxaldehyde following the synthetic procedure detailed by M. Pascu.[28]

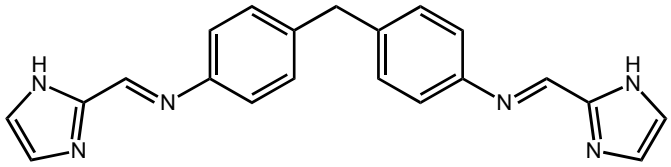

Fig. 2.11 Molecular structure of $L^{2\text{-im}}$

The coordination of the ligand to the ruthenium center was performed by method analogous to that for pyridine complexes, by stirring under reflux two equivalents of *cis*-$[Ru(DMSO)_4Cl_2]$ and three equivalents of ligand $L^{2\text{-im}}$ in ethylene glycol at high temperature (200^{o}C) for 6 to 7 days. Initial purification was performed simply by extraction of the compound from the crude product using ethanol. This was further followed by silica gel column chromatography and anion metathesis to obtain the analytically pure $[Ru_2L^{2\text{-im}}{}_3]Cl_4$ in 1 % yield. The ^{1}H NMR spectrum shows a single set of peaks, which indicates that a single, symmetrical species have been isolated (Fig. 2.12). The mass spectrum shows two peaks with the isotopic distribution corresponding to dinuclear Ru(II) complex, a peak at 632.5 m/z, $[Ru_2L^{2\text{-im}}{}_3]^{2+}$ and peak at 316.5 m/z, which corresponds to $[Ru_2L^{2\text{-im}}{}_3]^{4+}$.

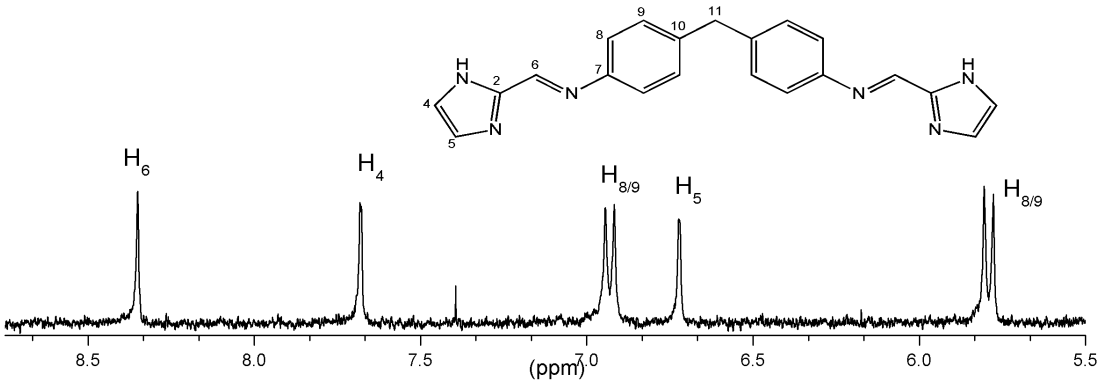

Fig. 2.12 The aromatic region of the ^{1}H NMR spectrum of $[Ru_2L^{2\text{-im}}{}_3]Cl_4$ in MeOD.

Orange crystals suitable for X-ray analysis were obtained by slow diffusion of diethyl ether into an acetonitrile solution of the compound at 4^{o}C. The compound crystallized in the monoclinic crystal system with the space group C2/c. The crystal structure shows the complex to be dinuclear with two metal centers linked by three ligands in a helical arrangement (Fig. 2.13).

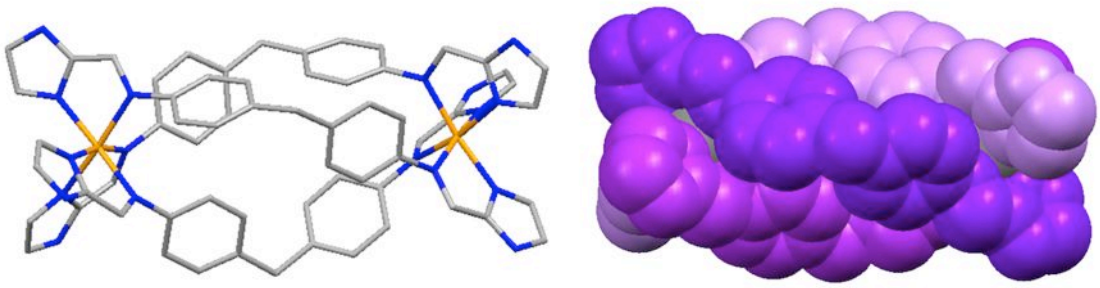

Fig. 2.13 Crystal structure of cation in $[Ru_2L_3](PF_6)_4$. Hydrogen atoms, solvent molecules and counter ions are omitted for clarity, blue-N, grey-C, orange – Ru.

The two metal centers are separated by 11.4 Å, and the Ru-N distances are in the range of 2.05 - 2.09 Å. The structure overlay of the cations $[Ru_2L_3]^{4+}$ and $[Ru_2L^{2\text{-im}}{}_3]^{4+}$ show that the imidazole-based complex is somewhat shorter (~2 Å)

than that of pyridine-based compound. However, due to the same spacer group in both ligands, the central part of the complex is relatively of the same size, therefore Ru atoms overlay perfectly in both structures (Fig. 2.14).

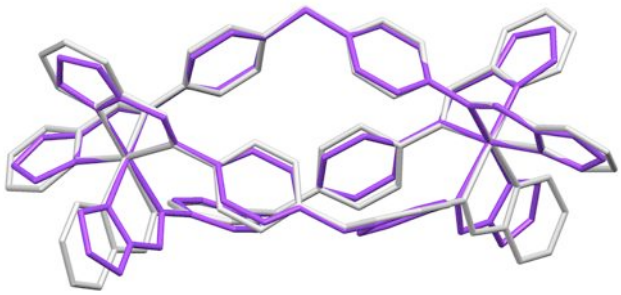

Fig. 2.14 Overlay of crystal structures of $[Ru_2L_3]^{4+}$ (grey) and $[Ru_2L^{2\text{-im}}{}_3]^{4+}$ (purple)

The UV-Vis absorption spectrum of the helicate reveals MLCT band centered at 475 nm (ε = 23 000 M^{-1} cm^{-1} in H_2O) and excitation at this wavelength (λ_{ex} = 475 nm) results in an emission band centered at 710 nm (Fig. 2.15).

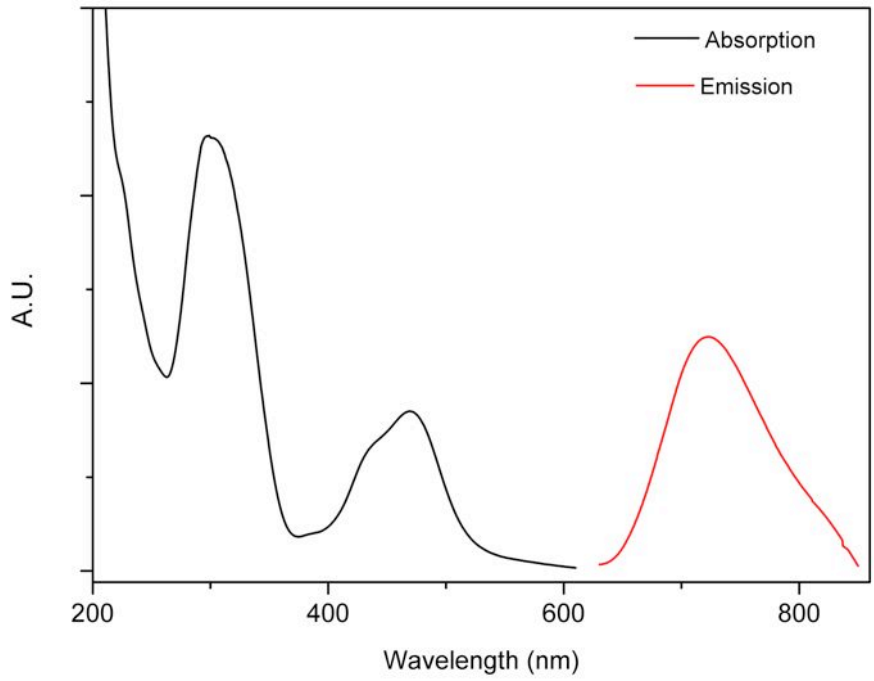

Fig. 2.15 Absorption (black) and emission spectrum (red) of $[Ru_2L^{2\text{-im}}{}_3]Cl_4$ recorded in water (λ_{ex} = 475 nm). Spectra are not on the same scale.

Undertaking the reaction for shorter durations of time led to the formation of a second symmetrical product with very similar physicochemical properties to the triple-stranded helicate and with the same mass spectrum. The ^{1}H NMR spectrum of the purified two co-existing compound(s) from the reaction (3 days of reflux) is shown in Fig. 2.16. When the duration of the reaction was shortened to one day only instead of three days the two products were obtained in a 1:2 ratio of the unidentified compound to helicate. Although multiple trials to separate the two compounds were undertaken using different stationary phases and solvent systems the full separation of the two compounds was unsuccessful. However, it was observed that extending the time of the reaction to 6-7 days results in the formation of helicate only (no second set of peaks was observed in the ^{1}H NMR spectrum).

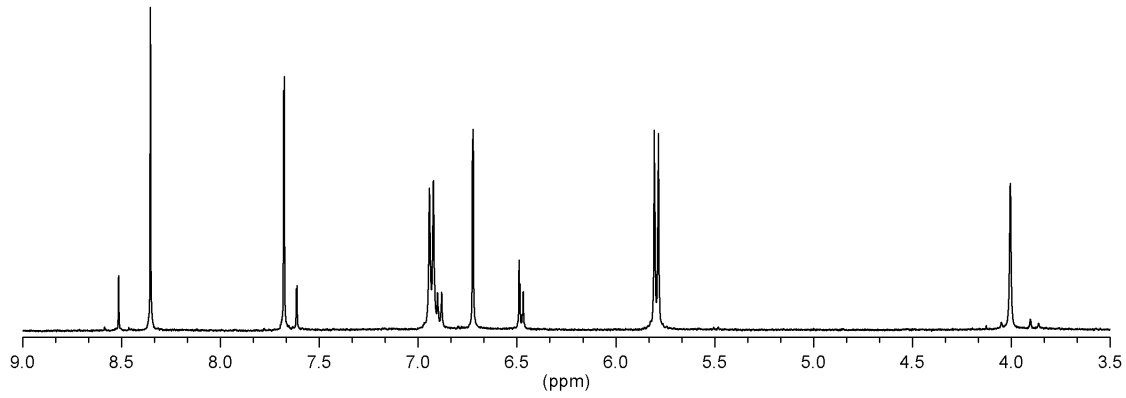

Fig. 2.16 ^{1}H NMR spectrum of $[Ru_2L^{2\text{-im}}{}_3](PF_6)_4$ (main peaks) with the second symmetrical product of the reaction.

This might be an indication that the longer duration of the reaction leads to the degradation of the second, unidentified, product or its conversion into helicate. Given that the mass spectral data indicates an $M_2L_3^{4+}$ formulation and that the NMR indicates a highly symmetrical species, but its CH_2 group appears as two

doublets, it would appear that a triple-stranded box, a mesocate,[29, 30] forms during the reaction. Moreover, if so then the triple-stranded mesocate may be a non-dissociative intermediate on the pathway to the triple-helicate, converting into a helicate by a Bailar or Ray–Dutt twist.[31] Due to the inert character of the Ru center the conversion would need very drastic conditions, like very high temperature and/or long duration of the reaction.

2.2.5 Synthesis and characterisation of $[Ru_2L^{4(5)\text{-im}}{}_3]Cl_4$

To explore whether the isomerism of the imidazole building unit can influence DNA-binding properties and cytotoxic activities of the cylinder the ligand $L^{4(5)\text{-im}}$ (Fig. 2.17) was used to prepare the second imidazole-based Ru cylinder.

The ligand was synthesized using the procedure previously detailed by Pascu.[28]

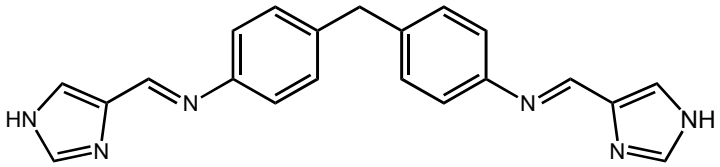

Fig. 2.17 Molecular structure of $L^{4(5)\text{-im}}$.

The ligand was prepared using the same diamine spacer moiety as in the ligand $L^{2\text{-im}}$ but the 2-imH aldehyde was replaced by 4(5)-imidazolecarboxaldehyde. The coordination of the $L^{4(5)\text{-im}}$ to Ru(II) centre was performed by a method analogous to that described for the $[Ru_2L^{2\text{-im}}{}_3]Cl_4$. The reaction between *cis*-$[Ru(DMSO)_4Cl_2]$ and $L^{4(5)\text{-im}}$ was carried out at high temperature (200^oC) for 7 days and subsequent extraction and column chromatography led to obtain a pure product in a 1 % yield.

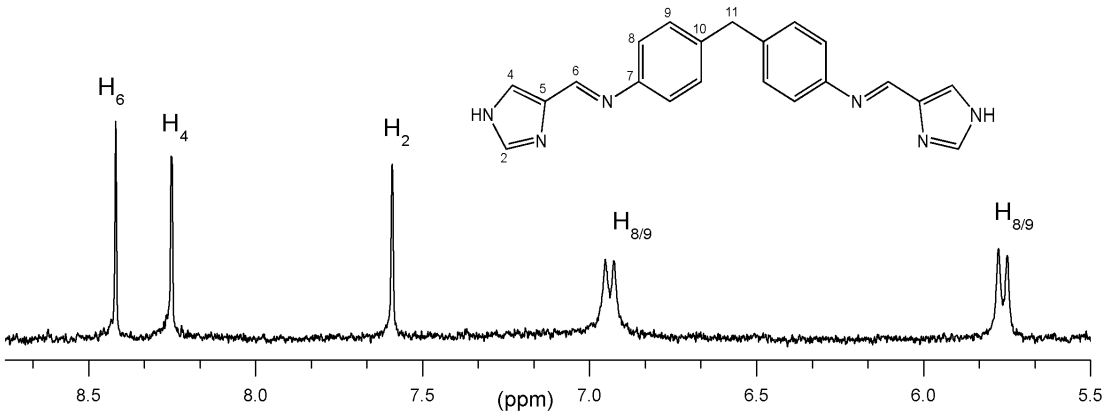

Fig. 2.18 Aromatic region of the ^{1}H NMR spectrum of $[Ru_2L^{4(5)\text{-}im}{}_3]Cl_4$ in MeOD

.

The ^{1}H NMR spectrum shows seven proton resonances, which confirm the high symmetry of the system (Fig. 2.18). The mass spectrum shows a peak at *m/z* 316.6 corresponding to the 4+ charged compound, $[Ru_2L^{4(5)\text{-}im}{}_3]^{4+}$, 421.7 that corresponds to $[Ru_2L^{4(5)\text{-}im}{}_3 - H]^{3+}$, and 632, which indicates $[Ru_2L^{4(5)\text{-}im}{}_3 - 2H]^{2+}$ formulation.

Multiple attempts to crystallize the compound with different counterions and from different solvent systems were undertaken, however no diffraction was observed from the crystals obtained.

The orange colour of $[Ru_2L^{4(5)\text{-}im}{}_3]^{4+}$ arises from the MLCT transitions, which are visible in the UV-Vis spectrum as a band centered at 423 nm. When excited at 375 nm an emission band with a maximum at 465 nm is observed (Fig. 2.19).

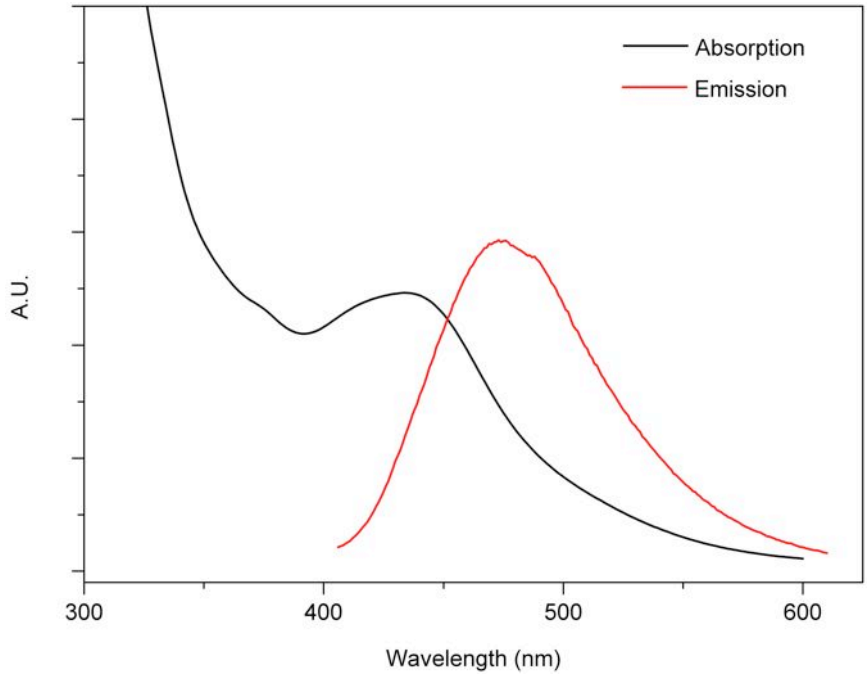

Fig. 2.19 Absorption (black) and emission (red) spectrum of $[Ru_2L^{4(5)\text{-}im}{}_3]Cl_4$ recorded in water (λ_{ex}= 375 nm). Spectra are not on the same scale.

2.3 DNA binding studies

Having established the synthetic procedures for several new ruthenium cylinders and knowing that supramolecular cylinder have the potential to modify the DNA secondary structures, the binding properties of all three new helicates using a range of biophysical techniques has been initiated.

Since the DNA-binding and further biological studies were to be undertaken in aqueous solutions the stability of the newly synthesized complexes had to be first determined. As seen in Fig. 2.20 the UV-Vis studies reveal that all three complexes are stable in aqueous solution. This is a valuable feature of ruthenium complexes and especially important for probing bio-molecular interactions and for biological studies.

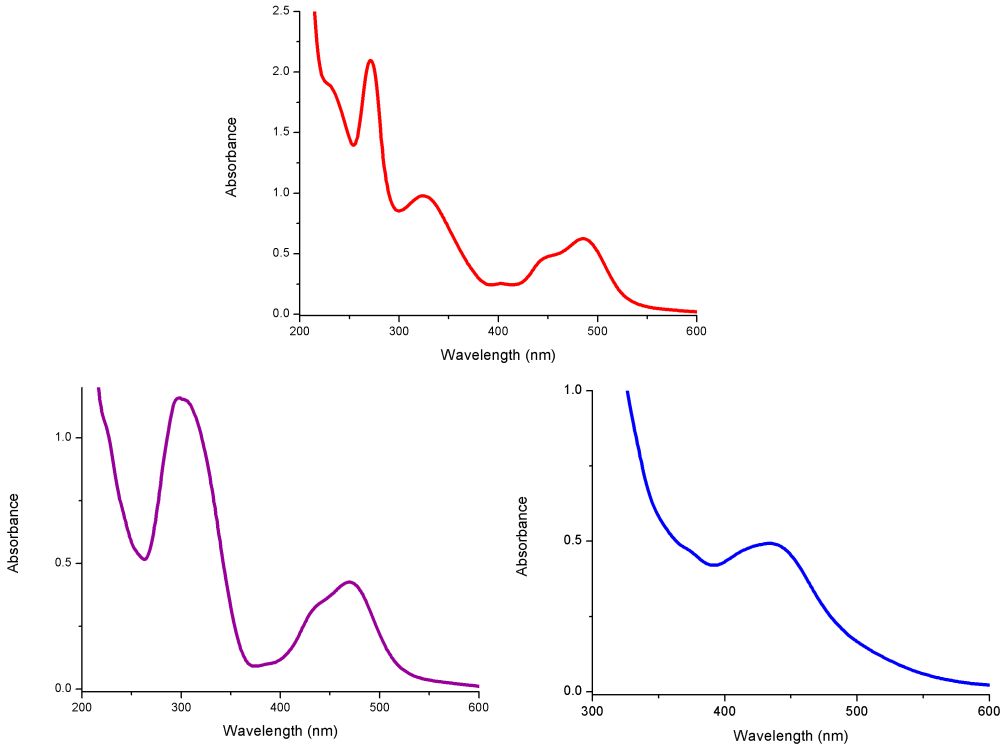

Fig. 2.20 UV-Vis absorption spectra of (red) $[Ru_2L^{o}{}_3]Cl_4$, (purple) $[Ru_2L^{2\text{-}im}{}_3]Cl_4$, (blue) $[Ru_2L^{4(5)im}{}_3]Cl_4$ recorded over a period of 24h in aqueous solution.

2.3.1 Circular dichroism

Circular dichroism (CD) is a UV-Vis absorption based spectroscopic technique that measures the differences in absorption of left and right hand circularly polarized light, which arise from the chirality of the molecule or its asymmetric character.[32]

$$CD = A_L - A_R$$

This spectroscopic technique is very useful and especially advantageous for providing the information about the structural features of biologically significant macromolecules in solution like proteins or nucleic acids, but also to monitor the macroscopic structural changes in the system while changing the environment

conditions or upon interaction with other chromophores and to assess their binding modes and affinities.

The DNA itself, as a chiral molecule, has an inherent CD signal and this signal is dependent on its conformation (*e.g.* A, B, Z). The typical B-DNA spectrum consists of two bands, positive centered at ~ 275 nm and negative centered at ~ 240 nm with zero based around 258 nm (Fig. 2.21). The spectrum results from the helical orientation of the aromatic bases and is 'a superimposed result of all the couplings of the transitions occurring in all the bases' and is also strongly affected by stacking interactions of the base pairs.[32] The bands observed around and below 190 nm originate from the chiral sugar moieties in the DNA backbone and there is no CD signal above 300 nm.

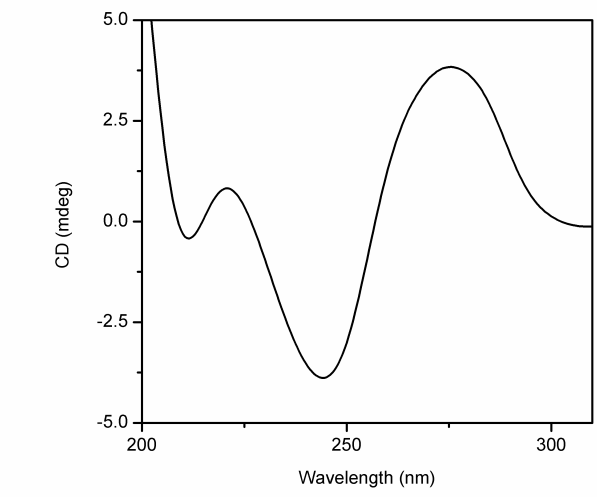

Fig. 2.21 Circular dichroism spectrum of ct-DNA

Non-chiral molecules have no inherent CD spectroscopy signal, however, if they bind to or interact with chiral molecules like DNA they will experience a chiral environment and induced CD signals may result (ICD). These will be

unique to the specific interaction and are most apparent on the spectrum in the region where the chromophore of the guest molecule(s) absorbs. This is a strong indication of an interaction between the two molecules.

Consequently, to probe the asymmetry of the system in the presence of the newly synthesized Ru cylinders, circular dichroism studies with B-DNA have been undertaken. CD titration experiments of Ru(II) cylinders with calf thymus DNA were conducted at constant DNA concentrations (300 μM), in a buffer containing 20 mM NaCl and 1 mM sodium cacodylate. The CD profiles of ct-DNA in the presence of increasing amounts of ruthenium complexes are shown in Fig. 2.22. The additions of cylinders to the DNA solutions result in strong induced MLCT CD signals in the 300 – 600 nm region indicating cylinder-DNA interactions. The increases in the intensities of these bands are linear in each of the three individual cases and this suggests that each complex interacts with DNA in a single binding mode. The DNA region in the spectra also shows changes upon addition of the complexes. For $[Ru_2L^o_3]Cl_4$ an increase of the positive band (275 nm) and decrease in the intensity of the negative band (245 nm) is observed and there is also a shift of these bands towards longer wavelengths. This effect could be the result of 'additive induced CD signals', due to the ligand-ligand transitions in the complex that overlap with the DNA bands, but it can also indicate the local unwinding of the DNA helix. In the case of imidazole-based complexes a decrease in the intensity of both the positive and negative bands is observed in each case. The retained shape of the DNA band upon interaction with all three complexes confirms that the B-DNA conformation is retained.

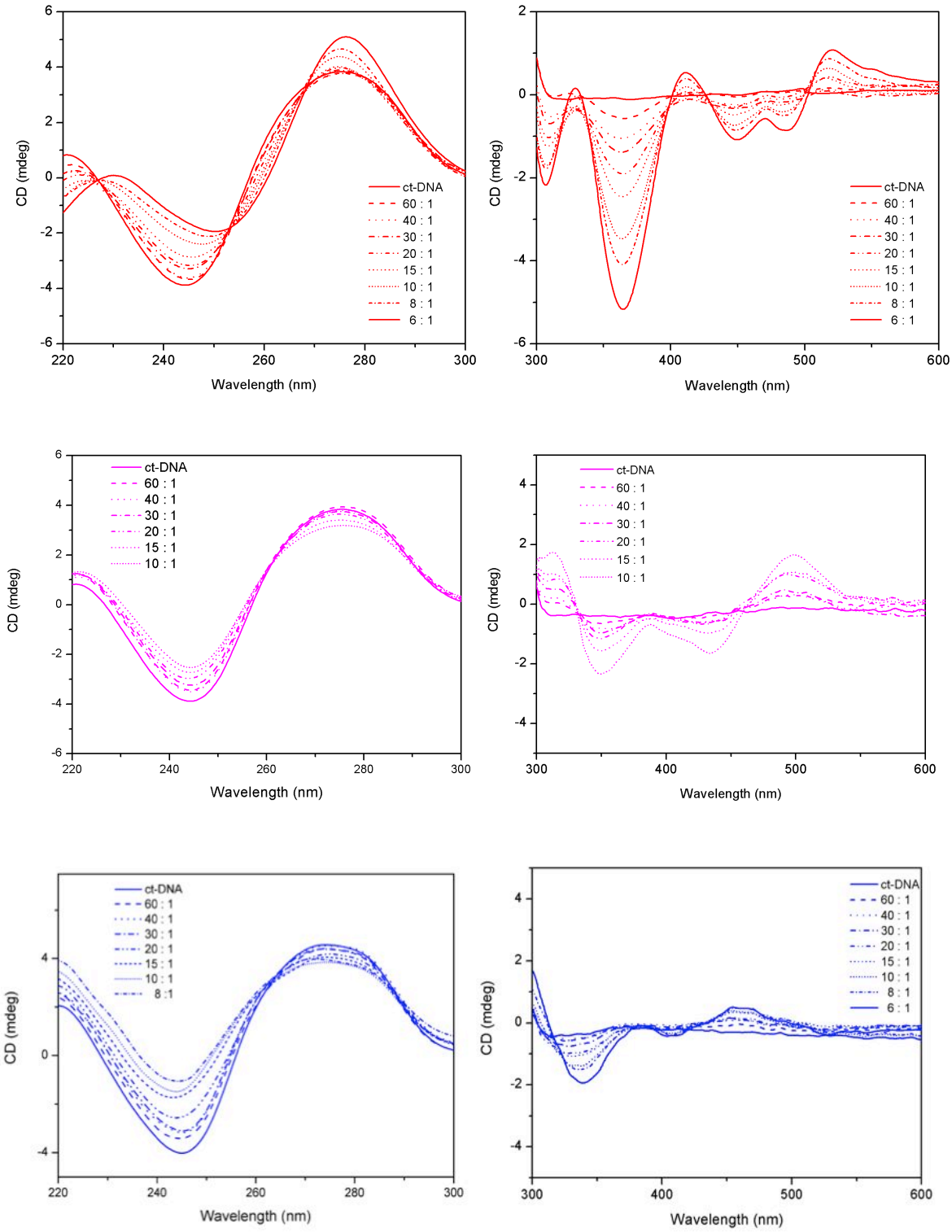

Fig. 2.22 CD spectra of DNA upon addition of (from top) $[Ru_2L^{o}{}_3]Cl_4$, $[Ru_2L^{2\text{-im}}{}_3]Cl_4$ and $[Ru_2L^{4(5)\text{-im}}{}_3]Cl_4$ (220 – 300 nm - 2 mm pathlength cuvette, 300 – 600 nm - 1 cm pathlength cuvette). Ratios are indicated as DNA base to complex.

2.3.2 Linear dichroism

Linear dichroism (LD) spectroscopy probes the electronic transitions of an oriented sample, which take place when linearly polarized electromagnetic radiation (parallel and perpendicular to an orientation axis) is applied.[32, 33]

$$LD = A_{II} - A_{L}$$

Linear dichroism can be a useful technique for probing the orientation, flexibility and conformation of the sample, but can also be utilized to study the molecular recognition processes.[34] In particular, LD can be very advantageous for exploring drug-biomolecule systems, as it provides key information about the binding geometries, therefore allowing for the determination of the alignment of a drug and the degree of orientation and flexibility of a biomolecular complex.

The principal requirement for LD spectroscopy is that the sample be oriented along the same vector, which can be achieved by a number of methods such as stretching the film, flowing the sample or applying an electric field. In this work a Couette flow cell (Fig. 2.23) was used to achieve orientation of a long DNA polymer by viscous drag generated in the sample chamber.

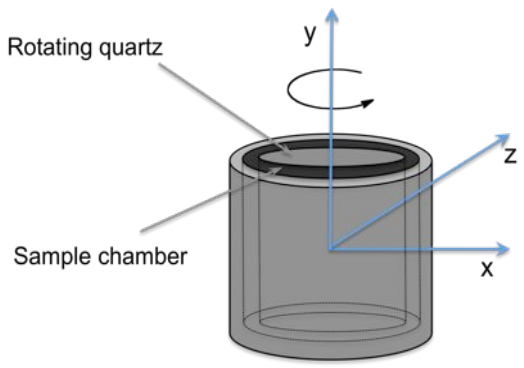

Fig. 2.23 Schematic representation of Couette cell used for linear dichroism measurements.

The LD spectrum of DNA is dominated by π–π* electronic transitions in the DNA bases, which are parallel to the nucleobases. This appears on the spectrum as a strong negative band with the minimum at 258 nm. The transitions within the DNA phosphodiester backbone result in the spectrum in the second negative band centered at 195 nm (Fig. 2.24).

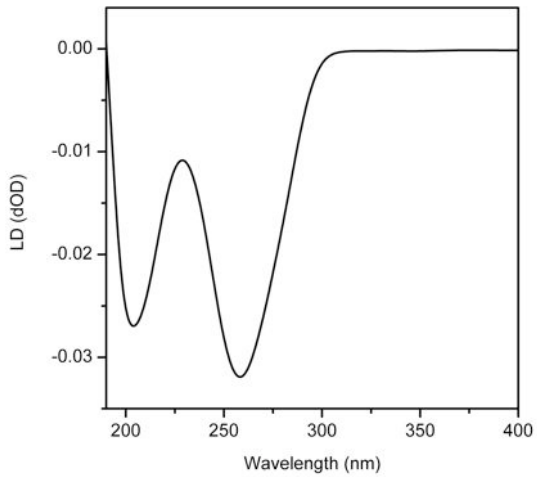

Fig. 2.24 Linear dichroism spectrum of calf thymus DNA

On interaction of the small molecules with DNA perturbations in the DNA LD signal(s) can be observed and, in addition, LD bands from the small molecule can appear in the spectrum. The latter will only happen if the small molecule becomes orientated due to its interaction with the DNA macromolecule. To probe these effects the linear dichroism titrations have been performed.

Flow linear dichroism experiments were performed under the same condition as used in the CD titrations described above (300 μM ct-DNA, 20 mM NaCl, 1mM sodium cacodylate buffer). The LD titration spectra are shown in Fig. 2.25. It is apparent that in all three cases upon addition of the complex the magnitude of the signal in the DNA region (259 nm) decreases. This is consistent with loss of

the DNA orientation, presumably a result of bending/kinking or coiling of the polymeric DNA by the helicates.

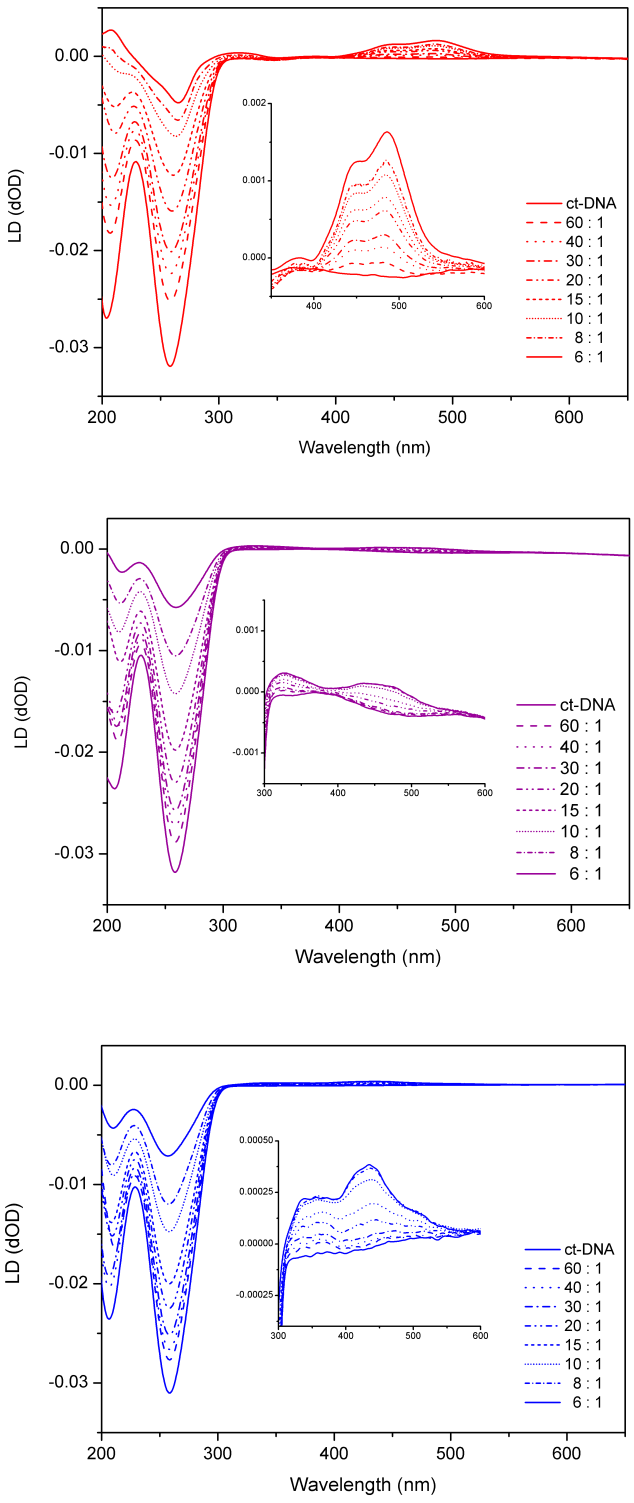

Fig. 2.25 LD spectra of ct-DNA (300 µM, 20 mM NaCl, 1 mM sodium cacodylate) in the presence of (from top) $[Ru_2L^{o}_3]Cl_4$, $[Ru_2L^{2\text{-im}}_3]Cl_4$, $[Ru_2L^{4(5)\text{-im}}_3]Cl_4$. Mixing ratios are indicated as DNA base to complex.

However, the degree of DNA coiling induced by interacting cylinders seems to be distinct for each complex (Fig. 2.26). The $[Ru_2L^{o}_3]Cl_4$ has the greatest effect on DNA orientation and this complex also appears to give rise to DNA coiling via different pathway to that of the two imidazole-based complexes.

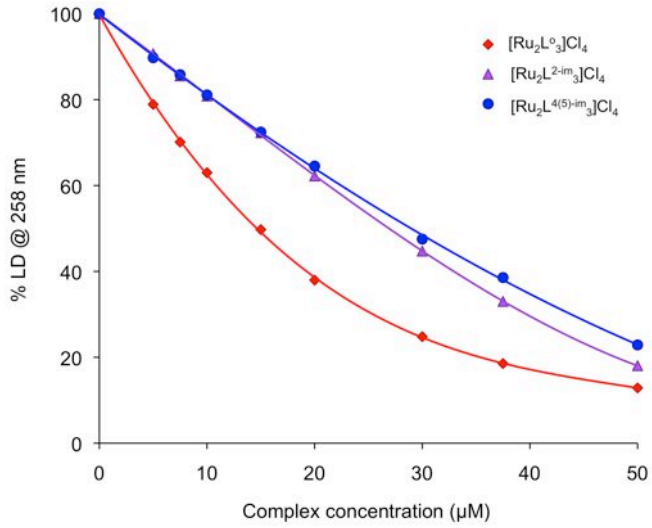

Fig. 2.26 % LD signal of DNA at 258 nm upon addition of (from top) $[Ru_2L^{o}_3]Cl_4$, $[Ru_2L^{2\text{-im}}_3]Cl_4$ and $[Ru_2L^{4(5)\text{-im}}_3]Cl_4$.

Addition of the cylinders to solutions of DNA results also in strong, induced positive LD signals in the cylinders MLCT regions, which increase systematically as more complex is added. This indicates that all compounds bind to polymeric DNA and the binding takes place in a specific orientation. The positive signs of these bands may suggest that cylinders are aligned more parallel than perpendicular to an orientation axis, which could be consistent with groove binding.

2.3.3 Agarose gel mobility shift assay

The agarose gel mobility shift assay is a technique used in molecular biology to separate and analyze biomolecules by their size and/or conformation.[35] To probe the effect of the studied ruthenium triple-stranded helicates on the superhelical DNA structure and assess their DNA helix unwinding potential a series of electrophoretic mobility shift assays have been performed. The DNA used in these studies was the negatively supercoiled pBR322 plasmid consisting of 4361 base pairs.

The plasmid DNA exists in two major forms: circular and supercoiled structure (Fig. 2.27).[36] However, upon interaction with other molecules, often as a result of the formation of a molecular complex, perturbations in the superhelical structure of the DNA may occur. These processes can be probed by the electrophoretic analysis of DNA.

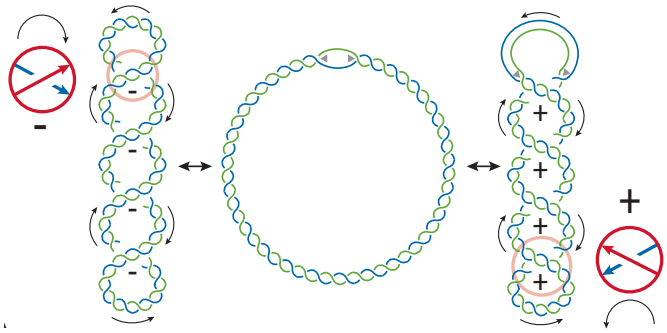

Fig. 2.27 Supercoiling: its handedness and sign. Adapted by permission from Macmillan Publishers Ltd: EMBO reports, 2004, 5, 256, copyright (2004).
http://www.nature.com/embor/index.html

Fig. 2.28 shows electrophoresis gels, in which pBR322 plasmid DNA has been mixed with increasing amounts of ruthenium complexes. It is apparent that as the concentration of Ru complexes increases the migration rate of the supercoiled DNA bands gradually decreases. It subsequently reaches the coalescence point, where all DNA supercoils are transformed to relaxed form, and after this

stage positive supercoiling is induced, resulting in an increase of the DNA migration rate.

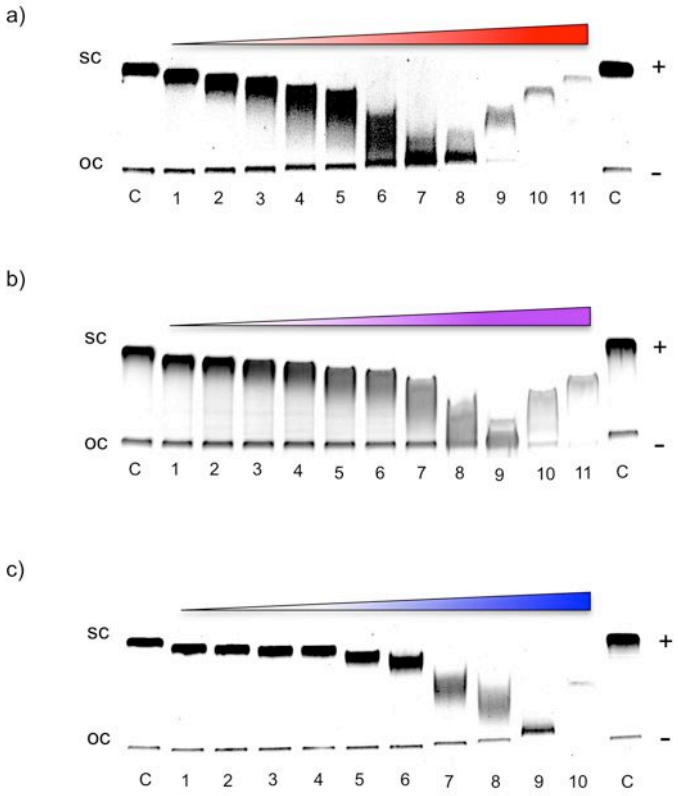

Fig. 2.28 Agarose gel electrophoresis of circular plasmid pBR322 after 1h of incubation with increased amount of complex a) $[Ru_2L^{o}_3]Cl_4$ lanes 1-11, r_b = 0.023, 0.025, 0.027, 0.031, 0.036, 0.038, 0.042, 0.045, 0.050, 0.060, 0.083, 0.125, 0.25; b) $[Ru_2L^{2\text{-im}}_3]Cl_4$ lanes 1-10, r_b= 0.05, 0.055, 0.06, 0.07, 0.08, 0.10, 0.125, 0.17, 0.25, 0.50; c) $[Ru_2L^{4(5)\text{-im}}_3]Cl_4$ lanes 1-10, r_b= 0.05, 0.055, 0.06, 0.07, 0.08, 0.10, 0.125, 0.17, 0.25, 0.50; C- control, sc – supercoiled DNA, oc – open circular DNA.

Using the coalescence points, on the assumption that at this stage all cylinders are bound to the DNA, the degree of DNA unwinding per bound drug, unwinding angle (ϕ), can be calculated:[37]

$$\phi = 18 \cdot \sigma / r_b(c)$$

where ϕ is the unwinding angle, σ is the superhelical density and $r_b(c)$ the number of cylinders bound per DNA base for which the supercoiled and

circular forms of plasmid co-migrate. Based on the DNA unwinding angle for cisplatin (13^o)[38] σ was found to be -0.059 and r_b values were determined from the DNA to complex mixing ratios. The calculated unwinding parameters for the studied cylinders are summarized in Table 2.1.

Compound	r_b(c)	unwinding angle (^{o})
$[Ru_2L_3](PF_6)_4$	0.08	13
$[Ru_2L_3]Cl_4$	0.042	25
$[Ru_2L^o{}_3]Cl_4$	0.06	17
$[Ru_2L^{2\text{-im}}{}_3]Cl_4$	0.13	8
$[Ru_2L^{4(5)\text{-im}}{}_3]Cl_4$	0.25	4

Table 2.1 DNA unwinding angles of Ru(II) triple helicates

The results herein demonstrate that all cylinders interact with DNA and relax negative supercoils to different extents, which confirms that all complexes interact with DNA dissimilarly. Of the three new Ru(II) helicates, $[Ru_2L^o{}_3]Cl_4$ appears to have the greatest unwinding properties (17 ± 3^o). This may indicate that $[Ru_2L^o{}_3]Cl_4$, while adopting a major groove binding, has a greater degree of insertion into the groove than $[Ru_2L^{2\text{-im}}{}_3]Cl_4$ and $[Ru_2L^{4(5)\text{-im}}{}_3]Cl_4$, possibly by 'fitting' one of the ligands between DNA bases. This effect might be restricted in the case of the imidazole-based helicates due to the additional -NH groups present at the metal-binding units, which could form hydrogen bonds with the phosphate backbone and thus limit the groove penetration. The position of -NH groups in the imidazole ring may also have an effect in the recognition process.

2.4 Cell viability assay

It has been shown that supramolecular cylinders possess promising anticancer activities against several human cancer cell lines.[39] In order to explore the anticancer properties of the new cylinders and access their possible structure-activity relationship, MTT cell proliferation assays have been performed. The MTT assay is a colorimetric assay used for quantification of the activity of reductase enzymes that convert MTT, 3-(4,5-dimethylthiazol-2-yl)-2,5-diphenyltetrazolium bromide, to formazan in viable cells (Fig. 2.29), therefore allowing for the evaluation of the mitochondrial activity in metabolically active cells.

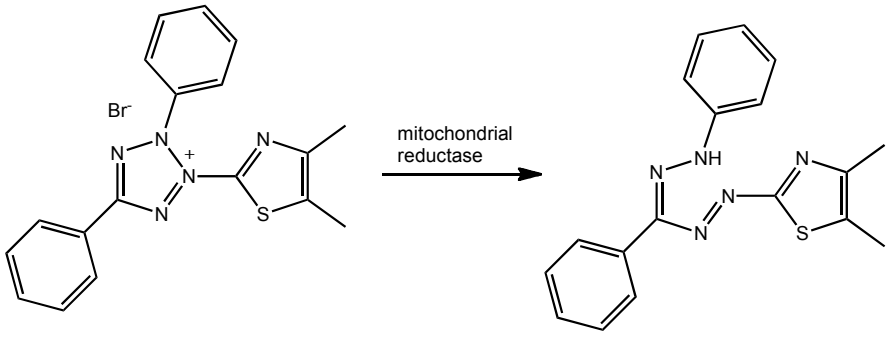

Fig. 2.29 Reduction of MTT to formazan crystals.

All three complexes were preliminarily tested in vitro for their cytotoxic activities against human breast cancer cell lines (T47D and MDA-MB-231) and the IC_{50} values were determined from the concentration-response curves. The results are shown in Fig. 2.30 (See also Table 2.2). The obtained IC_{50} values for $[Ru_2L_3]Cl_4$ and $[Ru_2L^o_3]Cl_4$ are very similar ~ 55 – 60 μM, which indicates that introducing the oxygen bridge in the centre of the ligand does not remarkably influence the cytotoxicity of the cylinder.

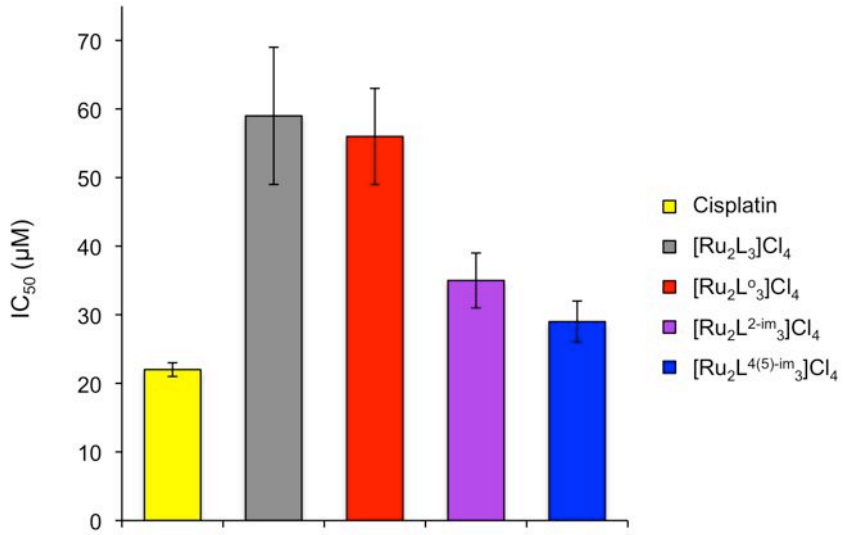

Fig. 2.30 IC_{50} values of ruthenium cylinders tested in breast cancer cell line (T47D).

However, changing the coordination sphere of ruthenium from pyridine to imidazole, while maintaining the shape of the cylinder seems to be causing a dramatic increase of the cytotoxicity of the cylinder. $[Ru_2L^{4(5)\text{-im}}{}_3]Cl_4$ is around two-fold more cytotoxic (IC_{50} = 29 ± 3 μM) than its pyridine analogue and initial testing of the second imidazole complex, $[Ru_2L^{2\text{-im}}{}_3]Cl_4$, shows that this compound also exhibits much greater cytotoxicities than pyridine-based complexes (IC_{50} = 35 ± 4 μM).

Compound	**IC_{50} (μM)**
cisplatin	22 ± 1
$[Ru_2L_3]Cl_4$	59 ± 10
$[Ru_2L^{o}{}_3]Cl_4$	56 ± 7
$[Ru_2L^{2\text{-im}}{}_3]Cl_4$	35 ± 4
$[Ru_2L^{4(5)\text{-im}}{}_3]Cl_4$	29 ± 3

Table 2.2 IC_{50} values of Ru cylinders tested in breast cancer cell line (T47D)

2.5. General discussion, conclusions and further work

New and improved methodologies for the synthesis and purification of the ruthenium triple-stranded helicates have been developed. Three new, stable and fluorescent ruthenium cylinders have been prepared and characterised and studies of their DNA binding properties and biological activities have been undertaken.

There are two important properties of the supramolecular helicates common to all three studied cylinders which are very important for the formation of their molecular complexes with DNA: the relatively large hydrophobic surface and cationic charge (+4). These two features are anticipated to have a substantial energetic contribution to the overall Gibbs free energy of the system and have a major impact on the thermodynamic characteristics of the system thus driving the formation of a molecular complex. The intermolecular supramolecular interactions between the helicates and the DNA *i.e.* hydrogen bonding, Van der Waals interactions and possibly π - π stacking are also expected to have a favorable energetic contribution to the binding free energy. Nevertheless, as anticipated from the linear dichroism studies and agarose gel mobility shift assays, the structural features of the three studied complexes and their ability to interact non-covalently with certain biomolecule moieties seems to have a great impact on the DNA secondary structure. While all complexes bind to and coil the polymeric DNA and cause unwinding of the supercoiled DNA, the magnitude of the structural changes caused by each complex is distinct. Both the DNA coiling and unwinding properties decrease as follows $[Ru_2L^{o}_3]Cl_4 > [Ru_2L^{2\text{-im}}_3]Cl_4 > [Ru_2L^{4(5)\text{-im}}_3]Cl_4$.

The cytotoxicity testing of the three ruthenium helicates proved that all complexes exhibit antiproliferative properties in human cancer cell lines with IC_{50} values below 60 μM. Interestingly, imidazole-based complexes seem to be around two-fold more cytotoxic than their pyridine analogues. The reason for this effect is not understood as yet and further, extensive cytotoxicity testing should be a feature of further investigations.

The cellular responses of supramolecular cylinders are believed to be due to their DNA binding properties, therefore full understanding of the molecular interaction between the complex and DNA at the structural, thermodynamic and kinetic level is crucial in order to obtain a full, detailed picture of the drug-DNA binding. In addition to the more detailed structural studies on the cylinder-DNA complex the investigation of the binding affinities and energetics of the molecular complex formation should be performed.

To access possible structure-activity relationships of the new compounds the effect of isomerism of the imidazole complexes should be explored. Preparation of modified cylinders such as these containing oxazole or *N*-substituted imidazole as the metal binding unit and studies of their biomolecule-binding properties and cytotoxic activities should be performed.

Further, more comprehensive cytotoxicity testing of the studied systems should be undertaken in order to explore the activities of these compounds in different cancer cell lines and to compare their effects. Following this, the studies of the uptake, cellular distribution, genotoxicity and finally mutagenicity of the new cytotoxic complexes should be performed.

2.6 References

[1] M. J. Hannon, *Chem. Soc. Rev.* **2007**, *36*, 280.

[2] M. Hannon, J., C. Painting, L., A. Jackson, J. Hamblin, W. Errington, *Chem. Commun.* **1997**, 1807.

[3] M. J. Hannon, V. Moreno, M. J. Prieto, E. Moldrheim, E. Sletten, I. Meistermann, C. J. Isaac, K. J. Sanders, A. Rodger, *Angew. Chem. Int. Ed.* **2001**, *40*, 879.

[4] I. Meistermann, V. Moreno, M. J. Prieto, E. Moldrheim, E. Sletten, S. Khalid, P. M. Rodger, J. C. Peberdy, C. J. Isaac, A. Rodger, M. J. Hannon, *Proc. Natl. Acad. Sci. USA* **2002**, *99*, 5069.

[5] C. Uerpmann, J. Malina, M. Pascu, G. J. Clarkson, V. Moreno, A. Rodger, A. Grandas, M. J. Hannon, *Chem. Eur. J.* **2005**, *11*, 1750.

[6] J. C. Peberdy, J. Malina, S. Khalid, M. J. Hannon, A. Rodger, *J. Inorg. Biochem.* **2007**, *101*, 1937.

[7] A. Oleksy, A. G. Blanco, R. Boer, I. Uson, J. Aymami, A. Rodger, M. J. Hannon, M. Coll, *Angew. Chem. Int. Ed.* **2006**, *45*, 1227.

[8] L. Cerasino, M. J. Hannon, E. Sletten, *Inorg. Chem.* **2007**, *46*, 6245.

[9] D. R. Boer, J. M. C. A. Kerckhoffs, Y. Parajo, M. Pascu, I. Usón, P. Lincoln, M. J. Hannon, M. Coll, *Angew. Chem. Int. Ed.* **2010**, *49*, 2336.

[10] J. Malina, M. J. Hannon, V. Brabec, *Chem. Eur. J.* **2007**, *13*, 3871.

[11] R. R. Sinden, *Nature* **2001**, *411*, 757.

[12] A. D. Richards, A. Rodger, M. J. Hannon, A. Bolhuis, *Int. J. Antimicrob. Agents* **2009**, *33*, 469.

[13] A. C. G. Hotze, N. J. Hodges, R. E. Hayden, C. Sanchez-Cano, C. Paines, N. Male, M. K. Tse, C. M. Bunce, J. K. Chipman, M. J. Hannon, *Chem. Biol.* **2008**, *15*, 1258.

[14] A. J. Pope, C. Bruce, B. Kysela, M. J. Hannon, *Dalton Trans.* **2010**, *39*, 2772.

[15] L. J. Childs, J. Malina, B. E. Rolfsnes, M. Pascu, M. J. Prieto, M. J. Broome, P. M. Rodger, E. Sletten, V. Moreno, A. Rodger, M. J. Hannon, *Chem. Eur. J.* **2006**, *12*, 4919.

[16] G. I. Pascu, A. C. Hotze, C. Sanchez-Cano, B. M. Kariuki, M. J. Hannon, *Angew. Chem. Int. Ed.* **2007**, *46*, 4374.

[17] G. I. Pascu, *PhD Thesis, University of Birmingham* **2008**.

[18] J. Malina, M. J. Hannon, V. Brabec, *Chem. Eur. J.* **2008**, *14*, 10408.

[19] M. H. W. Lam, S. T. C. Cheung, K.-M. Fung, W.-T. Wong, *Inorg. Chem.* **1997**, *36*, 4618.

[20] S. Torelli, S. Delahaye, A. Hauser, G. Bernardinelli, C. Piguet, *Chem. Eur. J.* **2004**, *10*, 3503.

[21] S. Torelli, D. Imbert, M. Cantuel, G. Bernardinelli, S. Delahaye, A. Hauser, J.-C. G. Bünzli, C. Piguet, *Chem. Eur. J.* **2005**, *11*, 3228.

[22] N. C. Fletcher, R. T. Brown, A. P. Doherty, *Inorg. Chem.* **2006**, *45*, 6132.

[23] C. R. K. Glasson, G. V. Meehan, J. K. Clegg, L. F. Lindoy, J. A. Smith, F. R. Keene, C. Motti, *Chem. Eur. J.* **2008**, *14*, 10535.

[24] S. Phongtongpasuk, *PhD Thesis, University of Birmingham* **2011**.

[25] C. Ducani, A. Leczkowska, N. J. Hodges, M. J. Hannon, *Angew. Chem. Int. Ed.* **2010**, *49*, 8942.

[26] C. Sanchez-Cano, *PhD Thesis, University of Birmingham* **2009**.

[27] Y. Parajo, J. Malina, I. Meistermann, G. J. Clarkson, M. Pascu, A. Rodger, M. J. Hannon, P. Lincoln, *Dalton Trans.* **2009**, 4868.

[28] M. Pascu, *PhD Thesis, University of Birmingham* **2007**.

[29] T. K. Ronson, H. Adams, T. Riis-Johannessen, J. C. Jeffery, M. D. Ward, *New J. Chem.* **2006**, *30*, 26.

[30] Z. Zhang, D. Dolphin, *Chem. Commun.* **2009**, 6931.

[31] A. Rodger, P. M. Rodger, *J. Am. Chem. Soc.* **1988**, *110*, 2361.

[32] A. Rodger, B. Norden, *Circular and Linear Dichroism*, Oxford University Press, Oxford, **1997**.

[33] M. R. Hicks, J. Kowalski, A. Rodger, *Chem. Soc. Rev.* **2010**, *39*, 3380.

[34] B. Norden, T. Kurucsev, *J. Mol. Recognit.* **1994**, *7*, 141.

[35] A. M. Guilliatt, *PCR Mutation Detection Protocols: Agarose and Polyacrylamide Gel Electrophoresis*, Humana Press, **2002**; S. Kaur Banwait, *PhD Thesis, University of Birmingham* **2010.**

[36] J. B. Schvartzman, A. Stasiak, *EMBO reports* **2004**, *5*, 256.

[37] W. R. Bauer, *Annu. Rev. Biophys. Bioeng.* **1978**, *7*, 287.

[38] S. F. Bellon, J. H. Coleman, S. J. Lippard, *Biochemistry* **1991**, *30*, 8026.

[39] T. Mossman, *J. Immunol. Methods* **1983**, *65*, 55.

3

Optical Isomers of

Ru(II) Triple-Stranded Helicate

Abstract

In this chapter the separation and characterisation of optical isomers of ruthenium triple-stranded helicates of a formula $[Ru_2L_3]Cl_4$, where L is bispyridylimine ligand $(C_6H_4N)C=N(C_6H_5)CH_2(C_6H_5)N=C(C_6H_4N)$, is presented. Both enantiomers have also been tested for their DNA binding properties using linear dichroism, fluorescence and agarose gel mobility shift assay. Both isomers interact with DNA, inducing coiling of duplex DNA and extensive unwinding of supercoiled DNA. The effect of the *M* enantiomer on DNA structure was found to be greater than that of its *P* analogue, consequently its binding constant was found to be higher.

3.1 Introduction

In recent years the importance of chirality has been widely explored in the field of supramolecular recognition. This is due to its considerable potential impact on the areas of bio- or nanotechnology, medicinal chemistry and drug development. Stereochemistry can play a critical role in determining the strength and selectivity of molecular recognition, therefore the asymmetric nature of the binding molecule can be a valuable tool in the recognition of biologically important molecules like DNA or RNA, but also in the recognition of synthetic nucleic acids such as PNAs.[1] In this field, chirality can be particularly effective for examining local alterations in nucleic acids structures but also for probing their conformational features.[2] For example, the Δ-enantiomer of $[Ru(DIP)_3]^{2+}$ (DIP-4,7-diphenyl-1,10-phenanthroline) (Fig. 3.1) was shown to preferentially recognize B-DNA while its Λ-stereoisomer favours binding to left-handed Z-DNA.[3]

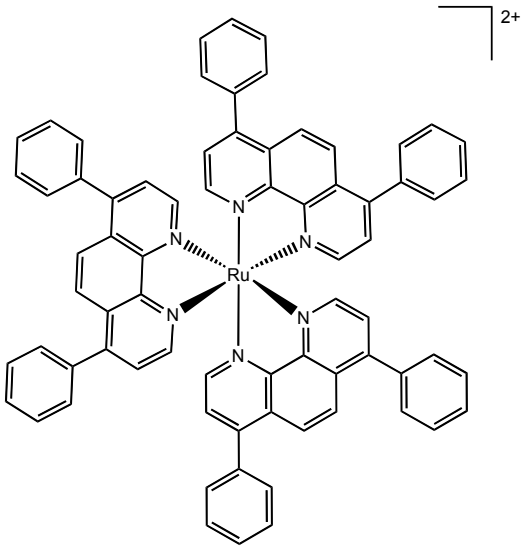

Fig. 3.1 Molecular structure of Δ-$[Ru(DIP)_3]^{2+}$

As highlighted by Barton,[4] the chiral discrimination in this kind of systems *i.e.* intercalators with DNA, is contingent upon the symmetry of the metal complex corresponding to that of the biomolecule.

Stereochemistry has also had a great impact on drug design and development.[5] The asymmetric properties of a potential therapeutic agent may play a crucial role in its action and biological activity and furthermore its cellular uptake, metabolism and/or delivery to the biological target may also be affected. However, the inherent features of chiral molecules include their potential for chiral inversion or racemisation, as seen in the case of thalidomide. This can have severe consequences for biological processes, hence studies of the nature of enantiopure drugs, their biomolecule recognition properties and cellular effects is mandatory.

The dinuclear triple-stranded complexes of the types described in Chapter 2 have a size and shape comparable to protein zinc-finger DNA recognition motifs and since these complexes adopt a helical structure, possess chiral properties (Fig. 3.2). Indeed the asymmetric character of supramolecular cylinders is distinct from this of intercalating agents, thus their molecular recognition properties and biological effects are unique yet not fully understood.

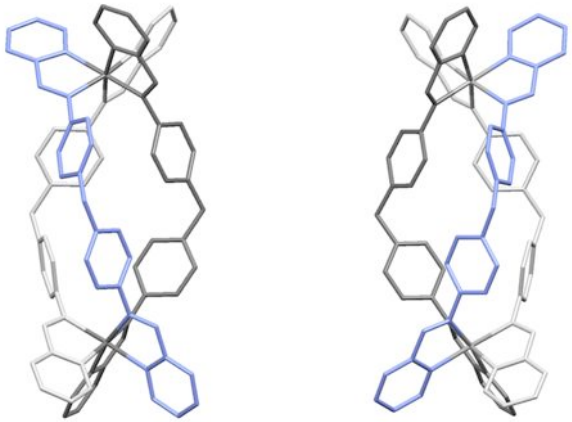

Fig.3.2 The optical isomers of the dinuclear triple-stranded helicates with bispyridylimine ligand; (left) left-handed *M* enantiomer, (right) right-handed *P* enantiomer.

Studies had been undertaken previously to explore the effect of the two enantiomers of an iron(II) helicate on the DNA structure.[6] It was found that both enantiomers bind strongly to the DNA, however the binding effects of the *M*-(ΛΛ)-enantiomer seemed to be the greater of the two. It was concluded that the two enantiomers bind strongly to natural polymeric DNA but might possess different binding modes. While the *M* enantiomer has been found to bind in the major groove of the duplex DNA, the location of the *P* enantiomer was less clear: it could also be binding in the major groove but has been proposed to be binding on top of the minor groove spanning the two phosphate backbones. More recently, Brabec and co-workers explored the chiral dinuclear Fe triple-helical systems for their interactions with DNA three-way junctions and found that the *M* enantiomer is more efficient in stabilization of these structures than the corresponding *P* enantiomer.[7]

The aim of the work presented in this chapter is to investigate and understand the binding effects of two enantiomers of ruthenium(II) triple-stranded helicate with the bispyridylimine ligand (Fig. 3.3) towards DNA structures. This is not

only to see how the complexes with different asymmetric properties interact with DNA, but also to understand the role of the metal center in the overall binding properties of the helicates.

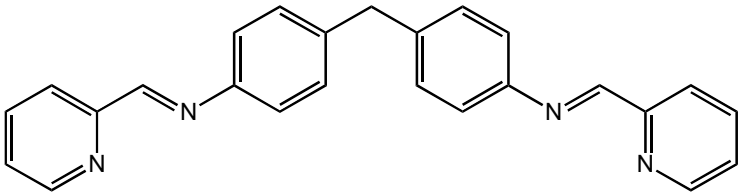

Fig. 3.3 Bispyridylimine ligand L

3.2 Results and discussion

3.2.1 Enantiomer separation

The compound, which is the subject of these studies, $[Ru_2L_3]Cl_4$ was synthesized and purified as a racemic mixture according to the procedure described in Chapter 2.

Separation of optically active species often involves the application of chiral ions for diastereoselective ion-pairing either in crystallization or extraction processes or in the chromatographic resolution on the stationary phase, where chiral ions serve as key components of the mobile phase.[8] These techniques give a very efficient resolution of chiral organic molecules, optical isomers of mononuclear polypyridyl metal complexes,[9] but can also be successfully used for the separation of more subtle structures like multinuclear metal-based helical arrangements.[10-12] Chiral stationary phases in column chromatography can also be employed for the resolution of these systems. Hannon *et al.* showed that simple paper chromatography and a 20 mM aqueous solution of

NaCl can afford the separation of two enantiomers of metallo-supramolecular helicates.[13] It was also found that this technique could be applied on the preparative scale using cellulose chromatography for the purification and resolution of enantiomeric helicates with different structural topologies.[14]

To initiate this work the separation of the two optical isomers of ruthenium triple stranded helicate, $[Ru_2L_3]^{4+}$, using the cellulose approach was explored. In all attempts the compound was used as an analytically pure sample in its chloride form.

The first explored approach for the resolution of Ru enantiomers was based on the Hannon technique, which employed cellulose (~20 micron) and 20 mM aqueous solution of NaCl as an eluent. Although in this method a partial resolution of enantiomers was obtained, the technique itself was found to be very inefficient for the separation of ruthenium triple-stranded helicates. As observed earlier for the iron cylinder, the two bands that formed after applying the eluent remained partially merged throughout the whole separation process and a part of a loaded compound remains on the column. This necessitated repeat column chromatography with a consequent loss of the compound and as a result of this only 5-10 % of the amount of initially loaded compound could be recovered as enantiopure isomers.

Further investigations led to the finding that using the same stationary phase (~20 micron cellulose) but increasing the concentration of eluent by 10 fold (0.2 M aq. NaCl) and introducing medium pressure on top of the column leads to the clear separation of the loaded compound into two distinct orange bands. It was also found that using this method no loss of the compound on the column

is observed and a total of 96 % of initially loaded complex can be eluted. These conditions also give clear separation for the iron cylinder.

The two obtained fractions were further examined using NMR, MS and UV-Vis spectroscopy and confirmed that the two enantiomers have been separated. The CD spectra of the two separated compounds, for the same absorbance, are identical in shape, equal in magnitude and opposite in sign throughout the whole range of the spectrum (Fig. 3.4), suggesting that complete separation of the optical isomers was achieved. The enantiopurity of the obtained fractions was further investigated and confirmed by NMR studies with Δ-TRISPHAT as a chiral shift reagent (see Chapter 4).

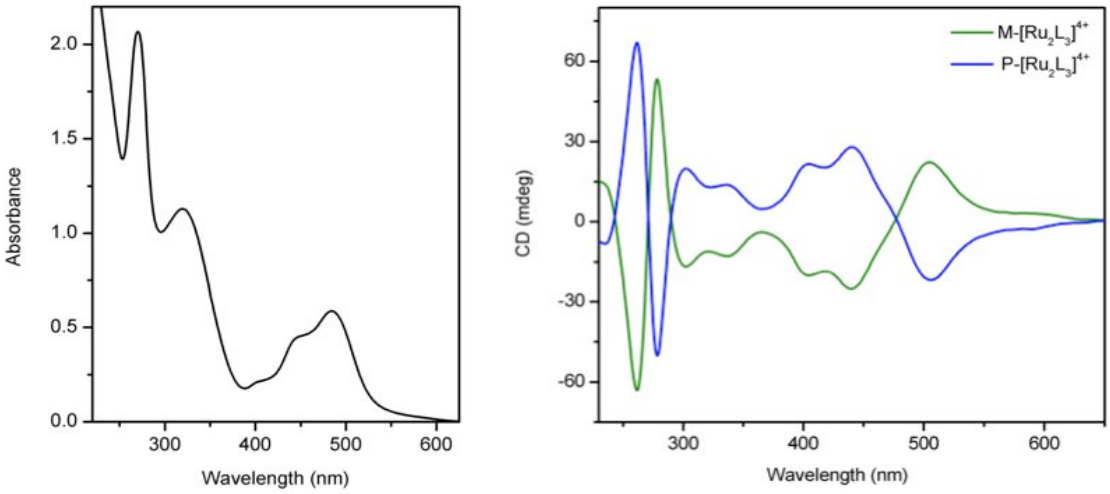

Fig. 3.4 UV-Vis absorption spectrum of $[Ru_2L_3]^{4+}$ (left) and CD spectra of M- and P-$[Ru_2L_3]^{4+}$ (right) in H_2O.

Total absolute configurations of the two enantiomers of $[Ru_2L_3]Cl_4$ were assigned from the CD spectra. On the basis of exciton theory and model compounds[15-17] the first eluted compound was found to be left-handed, ΛΛ-(*M*)-$[Ru_2L_3]^{4+}$ and the second right-handed ΔΔ-(*P*)-$[Ru_2L_3]^{4+}$. Further confirmation of this assignment comes from the X-ray structure detailed below.

The kinetic stabilities of both enantiomers in aqueous solution were measured by UV-Vis and CD spectroscopy. As expected, due to the high kinetic stability of Ru polypyridyl complexes, after four weeks at room temperature no changes in absorbance or optical activity were observed in either solution. This indicates that optically pure Ru triple-stranded helicates are configurationally stable and do not undergo racemisation in aqueous solution.

3.2.2 X-ray structure

X-ray quality crystals of the second eluting *P* enantiomer were successfully obtained by slow diffusion of diethyl ether into a methanolic solution of the chloride form of the compound at 4°C. The compound crystallized in the cubic crystal system with the enantiomorphic space group $I2_13$. The crystal structure shows that both metal centers adopt a Δ configuration and thus the overall molecule is right-handed (Fig. 3.5).

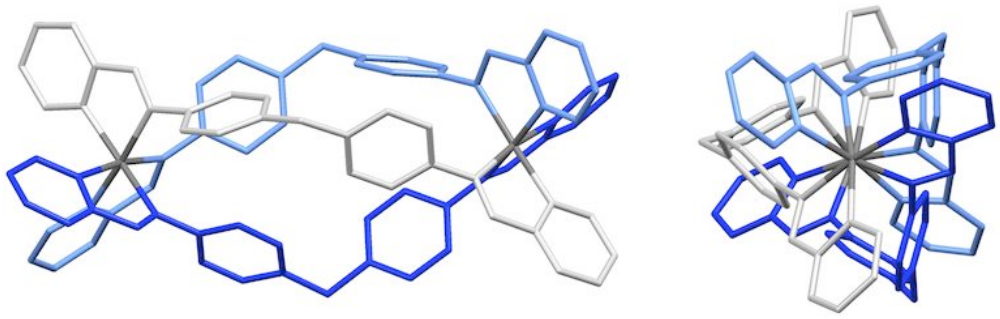

Fig. 3.5 Crystal structure of cation in *P*-$[Ru_2L_3]Cl_4$: side view (left), top view (right). The hydrogen atoms, counter ions and solvent molecules are omitted for clarity.

3.3 DNA binding studies

Having established an efficient methodology for the total resolution of optically active isomers of ruthenium triple-stranded helicate and determined their properties and solution behaviour an investigation of the DNA binding characteristics of both enantiomers has been initiated.

3.3.1 Flow linear dichroism spectroscopy

The LD studies of the effect of a racemic mixture of $[Ru_2L_3]Cl_4$ on ct-DNA showed that the metallo-helicate causes a dramatic loss of the DNA orientation, which was consistent with bending or coiling of the DNA.[18] To explore the binding/bending effects of the enantiopure isomers and compare them to the effect of the racemate the LD titration experiments with ct-DNA were performed. The experiments were carried out with a constant DNA concentration (300 μM) in the buffer containing 20 mM NaCl and 1 mM sodium cacodylate. The linear dichroism titration spectra are illustrated in Fig. 3.6.

The effect of both enantiomers, *M*-$[Ru_2L_3]^{4+}$ and *P*-$[Ru_2L_3]^{4+}$, on DNA structure is remarkable and it is apparent that with an increase of the cylinder concentration a systematic loss of LD signal at 258 nm occurs. Both isomers cause the loss of the magnitude of the DNA LD signal, consistent with either an increase in DNA flexibility or compound-induced kinking, bending or coiling of DNA, which could also be related to DNA aggregation or compaction. However, it is nonetheless evident that the *M* enantiomer has a more dramatic effect on DNA coiling/bending than its *P* analogue.

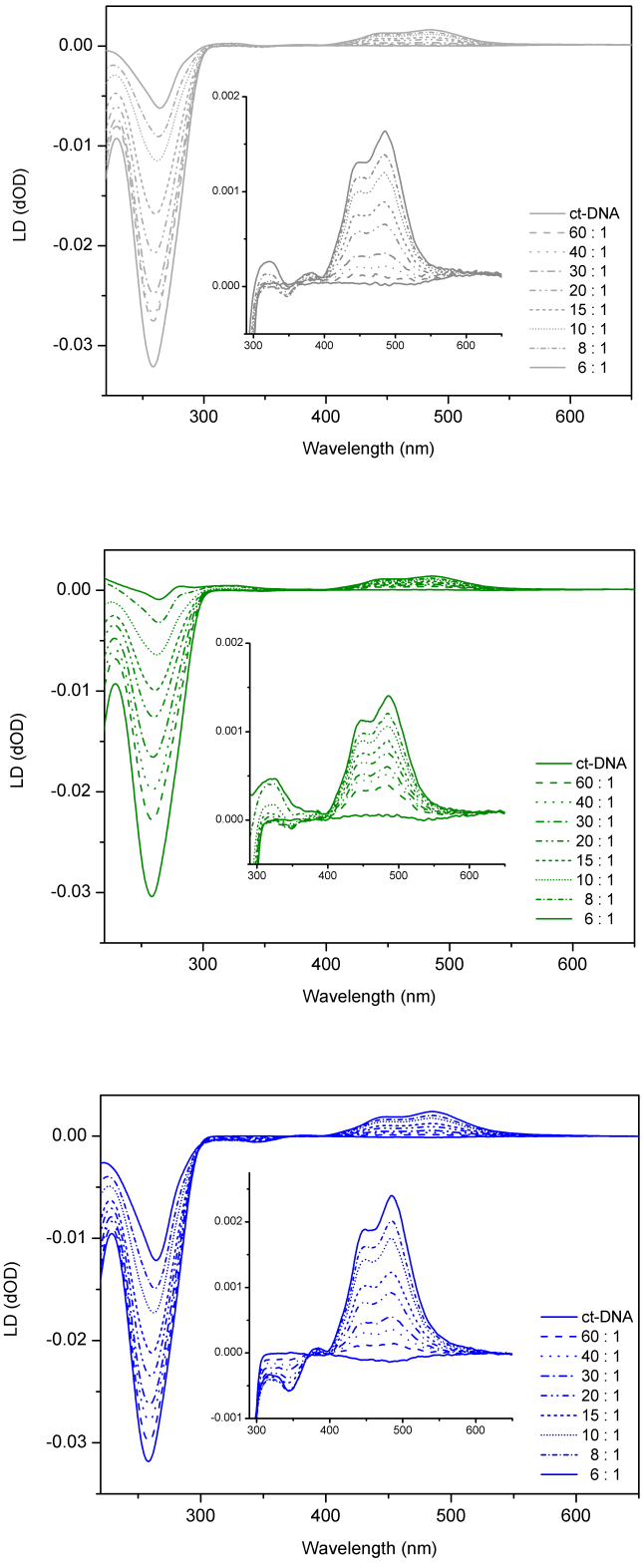

Fig. 3.6 LD spectra of ct-DNA (300 µM, 20 mM NaCl, 1 mM sodium cacodylate) upon addition of (from top) *rac*-, *M*- and *P*-$[Ru_2L_3]Cl_4$. Mixing ratios are indicated as DNA base to complex.

At a 60 : 1 ratio (DNA base : complex) a 25% loss of DNA LD signal is observed in the case of the *M* enantiomer and only a 6% decrease in the case of the *P* enantiomer. At a 6 : 1 ratio of DNA base to complex (10 times higher cylinder concentration) *M*-$[Ru_2L_3]^{4+}$ causes almost total loss of the DNA signal (98 %). This indicates stronger kinking of the DNA compared to the *P* enantiomer, which at the same ratio causes only 65% signal loss (Fig. 3.7). The racemic mixture induces a 15 and 82 % loss of LD signal at above ratios, which seems to be a combination of the effects of *M* and *P* helicates. This suggests that both enantiomers interact with the biomolecule independently.

Similar effects on DNA structures of left and right-handed helicates were observed for the *M*- and *P*-$[Fe_2L_3]^{4+}$ in the previous studies by Meistermann *et al*.. *M*-$[Fe_2L_3]^{4+}$ was found to cause more dramatic kinking than the *P* enantiomer.[6]

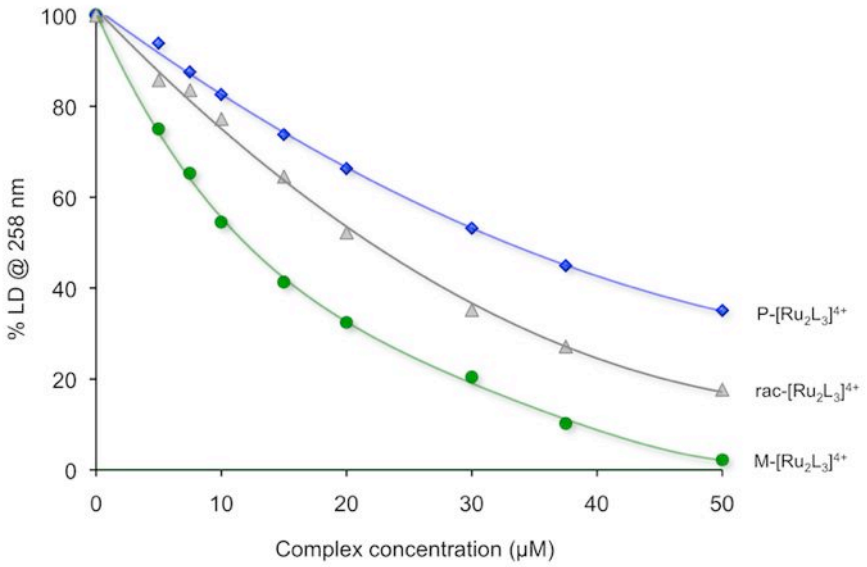

Fig. 3.7 % LD upon addition of increased amount of complexes.

Moreover, the supramolecular cylinders do not bind to DNA randomly yet in an oriented manner. As more complex is added to the DNA sample induced LD signals in the MLCT region appear in the spectra and increase gradually as the cylinder concentration increases. Although both enantiomers acquire orientation upon binding to the DNA the magnitude of the induced positive band at 485 nm is remarkably higher for *P* enantiomer. Indeed the positive signs of these bands indicate that the cylinders bind more parallel than perpendicular to the orientation axis, which would be consistent with groove binding. Interestingly, in the 300 – 400 nm region additional induced bands appear on the spectra upon addition of complexes and these have opposite signs for both enantiomers, positive for the *M* enantiomer and negative for the *P* enantiomer.

3.3.2 Fluorescence response

In the previous studies on the racemic mixture it was found that the ruthenium cylinder, when excited in the MLCT region (485 nm), gives rise to an emission band centered around 700 nm and upon binding to DNA this fluorescence is enhanced.[18] Therefore, having established through LD that the enantiomers have distinct effects on the structure of ct-DNA, causing different coiling effects, further spectroscopic studies were undertaken to determine the binding affinities of both enantiomers to ct-DNA. The fluorescence response of both enantiomers and a racemic mixture were studied as a function of increasing the DNA to cylinder ratio while maintaining the cylinder concentration constant (Fig. 3.8).

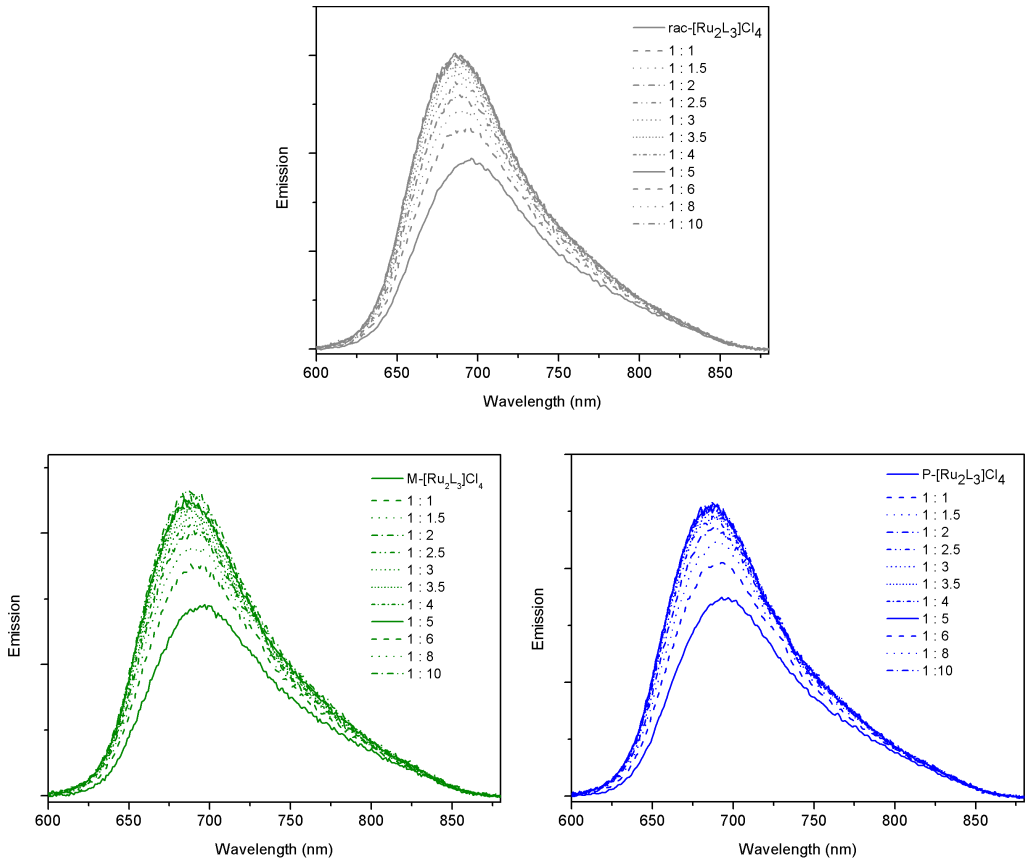

Fig. 3.8 Fluorescence response of *rac*-, *M*- and *P*-$[Ru_2L_3]Cl_4$ (λ_{ex}=485 nm), (25 μM, 20 mM NaCl, 1 mM sodium cacodylate) upon addition of ct-DNA. Mixing ratios are indicated as complex to DNA base.

It is apparent that the emission intensity of both enantiomers in aqueous solution increases concomitantly with an increase in the DNA to cylinder ratio (Fig. 3.9). This effect is due to DNA providing shielding for the excited state of Ru complex from quenching by water molecules.[19, 20] However, the fluorescence enhancement is greater in the case of *M*-$[Ru_2L_3]^{4+}$, which indicates that the *M* enantiomer is better protected by DNA than *P* isomer. This implies a higher binding equilibrium constant (K_b) for *M*-$[Ru_2L_3]^{4+}$.

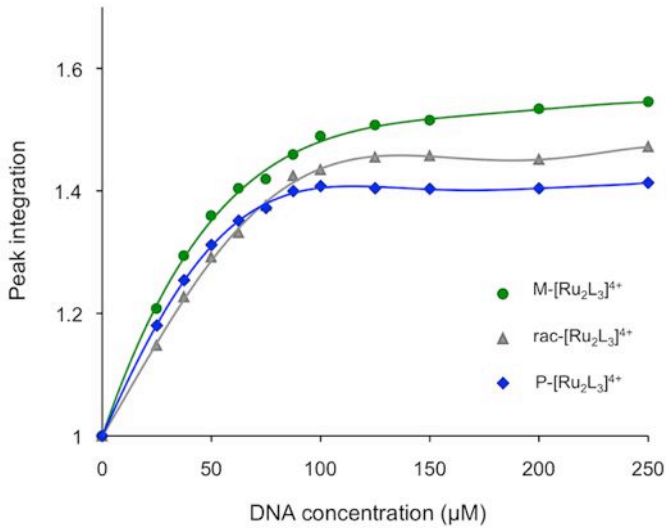

Fig. 3.9 Fluorescence response of *rac*-, *M*- and *P*-$[Ru_2L_3]^{4+}$ upon addition of increasing amount of ct-DNA.

Scatchard analysis of the emission titration data allowed for determination of the equilibrium binding parameters of the excited-state Ru(II) complexes with ct-DNA (Table 3.1).

Compound	K^{ex}_b (M^{-1})
rac-$[Ru_2L_3]Cl_4$	2.24 ± 0.9 x 10^5
M-$[Ru_2L_3]Cl_4$	3.10 ± 0.4 x 10^5
P-$[Ru_2L_3]C_4$	1.94 ± 0.5 x 10^5

Table 3.1 Equilibrium parameters for *rac*-, *M*-, and *P*-$[Ru_2L_3]Cl_4$ obtained from fluorescence titrations (each value represents the average of the values obtained from three independent experiments, errors represent standard deviations).

The analysis indicated that equilibrium binding constants of the ruthenium(II) triple-stranded helicate are greater than 10^5 M^{-1}. Interestingly, these results are consistent with the binding affinities of quaterpyridine-based tetracationic Ru(II) triple-stranded helicates obtained by Glasson.[11]

The equilibrium binding constants of the two enantiomers *M* and *P* were found to be 3.10 ± 0.4 x 10^5 M^{-1} and 1.94 ± 0.5 x 10^5 M^{-1} respectively. The *P* enantiomer seems to have a lower binding affinity compared to its *M* analogue and in thermodynamic terms this would suggest higher values of Gibbs free energies associated with formation the of *P*-$[Ru_2L_3]^{4+}$- DNA adduct compared to that of the M-$[Ru_2L_3]^{4+}$-DNA system. The approximate calculations gave rough evaluation of the free energies of the formation of the helicate-DNA molecular complexes. These were found to be -30.5 kJ mol^{-1}, -31.2 kJ mol^{-1} and -30.0 kJ mol^{-1} for racemic mixture, *M* and *P* enantiomer respectively. It is also apparent that the cylinder to DNA binding events proceed spontaneously (at room temperature) hence move the systems to lower, more thermodynamically stable energy states.

3.3.3. Agarose gel mobility shift assay

The unwinding effects of the negatively supercoiled plasmid DNA pBR322 upon interaction with the Ru cylinders was determined by agarose gel mobility shift assay as described in Chapter 2.

Figure 3.10 presents the electrophoresis gels of the plasmid-cylinder complexes, where the plasmid has been mixed with increasing amounts of *rac*-$[Ru_2L_3]Cl_4$, *M*-$[Ru_2L_3]Cl_4$ and *P*-$[Ru_2L_3]Cl_4$. Both enantiomers greatly unwind supercoiled DNA. *M*-enantiomer is more efficient in unwinding negatively supercoiled DNA than the *P*-enantiomer, though effects of both are similar to these observed for the corresponding Fe cylinders (32 ± 3^o and 22 ± 3^o for *M*- and *P*-$[Fe_2L_3]^{4+}$ respectively).[21]

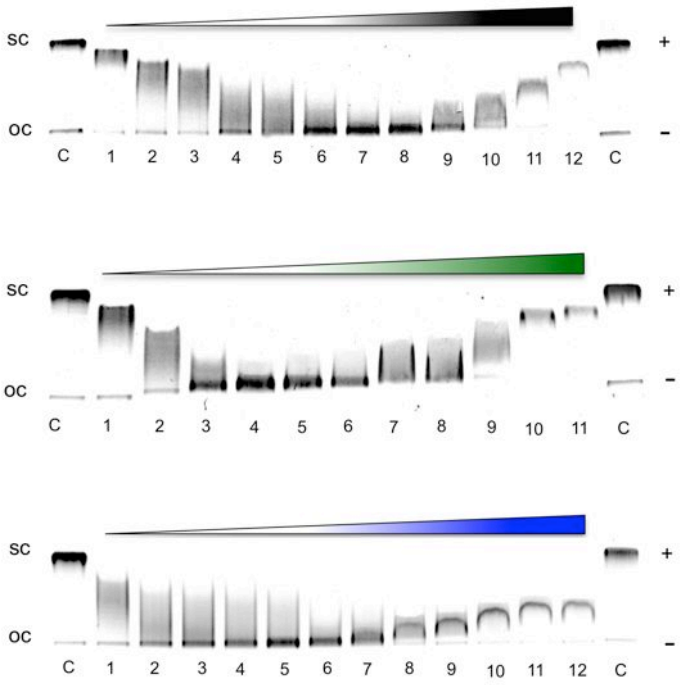

Fig.3.10 Agarose gel electrophoresis of circular plasmid pBR322 after 30 min of incubation with increased amount of complex: (black) *rac*-$[Ru_2L_3]Cl_4$ lanes 1-12, r_b = 0.023, 0.028, 0.031, 0.033, 0.036, 0.038, 0.042, 0.045, 0.050, 0.056, 0.071, 0.167; (green) *M*-$[Ru_2L_3]Cl_4$ lanes 1-11, r_b = 0.014, 0.02, 0.024, 0.028, 0.031, 0.033, 0.036, 0.038, 0.045, 0.071, 0.100; (blue) *P*-$[Ru_2L_3]Cl_4$ lanes 1-12, r_b = 0.028, 0.033, 0.036, 0.038, 0.042, 0.045, 0.05, 0.056, 0.063, 0.071, 0.100, 0.250; C- control, sc – supercoiled DNA, oc - open circular DNA.

The calculated unwinding angles are listed in Table 3.2

Compound	r_b (c)	unwinding angle (°)
rac – $[Ru_2L_3](PF_6)_4$	0.08	13 ± 2
rac – $[Ru_2L_3]Cl_4$	0.042	25 ± 3
M – $[Ru_2L_3]Cl_4$	0.031	34 ± 3
P – $[Ru_2L_3]Cl_4$	0.045	23 ± 4

Table 3.2 Coalescence points and unwinding angles for *rac*-, *M*- and *P*-$[Ru_2L_3]Cl_4$ (each value represents the average of the values obtained from three independent experiments, errors represent standard deviations).

The effect of *rac*-Ru cylinder on the superhelical DNA structure is presumably a combination of the effects of *M* and *P* helicate and, consistently with the linear

dichroism experiments, might indicate that both, left- and right-handed isomers interact independently with DNA. These results are also comparable to the results obtained for the *rac*-iron helicate (27 ± 3^{o}).[21] However, Malina *et al.* found that when plasmid DNA was treated with *rac*-$[Ru_2L_3](PF_6)_4$ (instead of the chloride salt of this complex, as studied here) the complex unwinds the supercoiled DNA by 13^{o} only,[22] which is only half of the effect observed for the chloride counterpart of the complex. This suggests the contribution of the counterion in the metal complex to the local unwinding of DNA.

3.4 General discussion, conclusions and further work

Recognition of DNA by supramolecular cylinders is expected to be predominantly driven by hydrophobic interactions and/or electrostatic attractions *i.e.* entropically favorable polyelectrolyte effects between the cylinder and polyanionic DNA. These two elements give a substantial contribution to the Gibbs free energy of the cylinder-DNA complexation. Although the tetracationic charge and large hydrophobic surface are common to both optical isomers, the different asymmetric character of the two enantiomers and thus different binding potential, gives rise to distinctive effects on DNA and thus should be reflected in the thermodynamics of the systems. The energetics of the drug – DNA binding event is a function of several factors, such as hydrophobic effects, polyelectrolyte effects, reorganization of water molecules, DNA structural changes, intermolecular interactions etc., all of which give rise to the distinctive energy gains and losses of the system and this is reflected in the binding affinities of the drug towards DNA and therefore in the stability of the system.

As discussed in previous paragraphs, the formation of $[Ru_2L_3]^{4+}$-DNA complexes gives rise to significant changes in the DNA secondary structure and these are remarkably different for both optical isomers of $[Ru_2L_3]^{4+}$. The linear dichroism studies showed that the *M* enantiomer has a greater effect on DNA structure than its corresponding *P* enantiomer, causing over 30 % more dramatic coiling of the DNA duplex compared to the effect of the *P* enantiomer at the same DNA base to complex ratio. This might be a consequence of more favourable shape features of the *M* enantiomer, which could fit deeper into the DNA groove and interact with the DNA bases either by inserting one its ligands between the stacked bases or alternatively by face to edge π-π interactions between the phenyl rings and DNA bases. The *P* enantiomer, assuming that it also adopts major groove binding, would be expected to be sterically hindered from these types of contacts and consequently the magnitude of the free energy component of non-covalent interaction of this class in this case would be different. The structural changes in the DNA molecule arising from cylinder binding are clearly visible also from the agarose gel mobility shift assay. Consequently, as we see in the linear dichroism studies the *M* enantiomer has a greater effect on the DNA superhelical structure than the *P* enantiomer. This could also be attributed to the ability of the cylinder to fit into the groove and insert its chelates in between the stacked bases.

The greater shape compatibility and thus the possible deeper groove penetration of the *M* enantiomer could also be extrapolated from fluorescence titration experiments. These indicated that the DNA provides better shielding from fluorescence quenching caused by water molecules to the *M* enantiomer.

In turn this could suggest that the *P* enantiomer is more freely bound to the DNA and this effect is reflected in the derived DNA affinities of the two enantiomers, which were found to be 3.10 ± 0.4 x 10^5 M^{-1} and 1.94 ± 0.5 x 10^5 M^{-1} for *M* and *P* enantiomer respectively. The attained binding free energies for *M* and *P* enantiomers show that the *M*-$[Ru_2L_3]^{4+}$-DNA adduct is more thermodynamically stable than P-$[Ru_2L_3]^{4+}$-DNA complex, however formation of both complexes proceeds spontaneously under experimental conditions.

In fact, both enantiomers induce a different level of structural changes in the biomolecule and therefore the magnitude of the free energy associated with these events should be different in both cases. However, distinctive fit of the cylinders to the major groove or alternatively recognition of two different DNA units by *M*- and *P*-$[Ru_2L_3]^{4+}$, would give rise to distinct reorganisation of water molecules in DNA and/or to different DNA hydration levels in both cases. This might also have its effect on the structural changes in the DNA and consequently affect the energetics and stabilities of the systems. Furthermore, the molecular recognition event is also associated with the energy penalties resulting from the losses in translational and rotational degrees of freedom of the two interacting molecules and this can also be different in the two studied cases.

The DNA recognition process by chiral triple-stranded helicates is a complex phenomenon and multiple factors need to be considered when discussing the binding features of the optical isomers and the outcomes of their complexation with DNA. For example, the structural changes that the enantiomers induce in the DNA structure might be associated not only with accommodation of the cylinder within the helix, which is attributed to molecular

symmetry properties of the interacting molecules but also with other factors like hydration levels, inter- and intramolecular interactions etc.. Indeed, all these events are related to the specific energy gains and losses and these are directly reflected in the thermodynamic profiles of the drug-DNA binding and the stabilities of the systems.

As anticipated, the metal ion in the helicate does not seem to play a significant role in the recognition of DNA structures. The binding characteristics of the *M* and *P* enantiomers of ruthenium helicates, their effects on DNA coiling and degree of unwinding of the superhelical structures are highly comparable to these obtained for the iron analogues. Each of the two, $[Fe_2L_3]^{4+}$ and $[Ru_2L_3]^{4+}$, have the same ionic charge and very similar structural features.

Understanding the molecular recognition in biological systems at the structural and thermodynamic level can be of prime importance for a rational drug design. Indeed chiral molecules can play a specific role in the understanding of the forces that drive the recognition processes. In this respect supramolecular cylinders, due to their unique symmetry properties, can be great models for better understanding of the major groove DNA recognition processes and, in the long term, for the design of sequence specific DNA binding drugs that target the DNA in a protein-like manner.

In this context, the exhaustive studies on the interaction of both *M* and *P* enantiomers with DNA should be undertaken as a future work. This could include the determination of the thermodynamic profiles of both systems in order to better understand the forces and the magnitude of the energy

components that are involved in the recognition process and the DNA-cylinder molecular complex formation.

Since both compounds have a potential as therapeutic agents against cancer, further detailed cytotoxicity testing on various different cancer cell lines should also be performed.

3.5 References

[1] R. Corradini, S. Sforza, T. Tedeschi, R. Marchelli, *Chirality* **2007**, *19*, 269.

[2] J. K. Barton, *Science* **1986**, *233*, 727.

[3] A. E. Friedman, C. V. Kumar, N. J. Turro, J. K. Barton, *Nucleic Acids Res.* **1991**, *19*, 2595.

[4] B. M. Zeglis, V. C. Pierre, J. K. Barton, *Chem. Commun.* **2007**, 4565.

[5] I. K. Reddy, R. Mehvar, *Chirality in drug Design and Development*, Marcel Dekker, Inc., New York, **2004**.

[6] I. Meistermann, V. Moreno, M. J. Prieto, E. Moldrheim, E. Sletten, S. Khalid, P. M. Rodger, J. C. Peberdy, C. J. Isaac, A. Rodger, M. J. Hannon, *Proc. Natl. Acad. Sci. USA* **2002**, *99*, 5069.

[7] J. Malina, M. J. Hannon, V. Brabec, *Chem. Eur. J.* **2007**, *13*, 3871.

[8] F. R. Keene, *Coord. Chem. Rev.* **1997**, *166*, 121.

[9] J. Lacour, S. Torche-Haldimann, J. J. Jodry, C. Ginglinger, F. Favarger, *Chem. Commun.* **1998**, 1733.

[10] G. Rapenne, B. T. Patterson, J. P. Sauvage, F. R. Keene, *Chem. Commun.* **1999**, 1853.

[11] C. R. K. Glasson, G. V. Meehan, J. K. Clegg, L. F. Lindoy, J. A. Smith, F. R. Keene, C. Motti, *Chem. Eur. J.* **2008**, *14*, 10535.

[12] J. J. Jodry, J. Lacour, *Chem. Eur. J.* **2000**, *6*, 4297.

[13] M. J. Hannon, I. Meistermann, C. J. Isaac, C. Blomme, J. R. Aldrich-Wright, A. Rodger, *Chem. Commun.* **2001**, 1078.

[14] J. M. C. A. Kerckhoffs, J. C. Peberdy, I. Meistermann, L. J. Childs, C. J. Isaac, C. R. Pearmund, V. Reudegger, S. Khalid, N. W. Alcock, M. J. Hannon, A. Rodger, *Dalton Trans.* **2007**, 734.

[15] M. Ziegler, A. von Zelewsky, *Coord. Chem. Rev.* **1998**, *177*, 257.

[16] S. G. Telfer, N. Tajima, R. Kuroda, *J. Am. Chem. Soc.* **2004**, *126*, 1408.

[17] S. G. Telfer, T. M. McLean, M. R. Waterland, *Dalton Trans.* **2011**, *40*, 3097.

[18] G. I. Pascu, A. C. Hotze, C. Sanchez-Cano, B. M. Kariuki, M. J. Hannon, *Angew. Chem. Int. Ed.* **2007**, *46*, 4374.

[19] N. J. Turro, V. Ramamurthy, J. C. Scaino, *Principles of Molecular Photochemistry - An Introduction*, Scaino University Science Books, Sausalito, **2009**.

[20] J. R. Lakowicz, *Principles of Fluorescence Spectroscopy*, 3rd ed., Springer, New York, **2006**.

[21] J. Malina, M. J. Hannon, V. Brabec, *Nucleic Acids Res.* **2008**, *36*, 3630.

[22] J. Malina, M. J. Hannon, V. Brabec, *Chem. Eur. J.* **2008**, *14*, 10408.

4

The Enantiodifferentiation of Chiral Ruthenium(II) Triple-Stranded Helicates by Δ-TRISPHAT

Abstract

The interaction of Δ-TRISPHAT with a racemic mixture and two enantiopure Ru(II) triple-stranded helicates, *M*(ΛΛ)- and *P*(ΔΔ)-enantiomer, have been investigated by ^{1}H NMR. The proton spectra of the Ru compounds in the presence of the chiral shift reagent indicate that Δ-TRISPHAT induces the NMR enantiodifferentiation of the two diastereomers by interacting with both isomers independently and appears to show chiral discrimination towards the interaction site. It is proposed that the Δ-TRISPHAT interacts with the ΛΛ–enantiomer along the C_2 axis, having an effect mainly on the phenyl rings and methylene group in the central part of the helicate whereas with the ΔΔ – isomer it interacts along the C_3 axis of the complex, thus affecting exclusively the pyridine protons.

4.1 Introduction

Chiral molecular recognition has been of great interest in asymmetric chemistry, because of its considerable potential in bio- and nanotechnology, but also in pharmaceutical science and drug discovery. Indeed selective chiral discrimination and diastereoselective ion pairing phenomenon can be a valuable tool for supramolecular stereocontrol, diastereoselective synthesis and catalysis but also for development of resolving agents and NMR chiral solvating agents.[1] Particularly successful in these fields have been chiral hexacoordinated phosphates,[1-7] a representative example being the Δ-tris(tetrachloro-1,2-benzenediolato)phosphate(V) ion, commonly known as TRISPHAT (Fig. 4.1). TRISPHAT is an anionic coordination complex, where three bidentate tetrachlorocatecholate ligands are coordinated to a phosphorus atom. The compound exists in two isomeric forms: left-handed, Λ enantiomer and right-handed, Δ enantiomer and, importantly, both stereoisomers were found to be configurationally stable in solution.

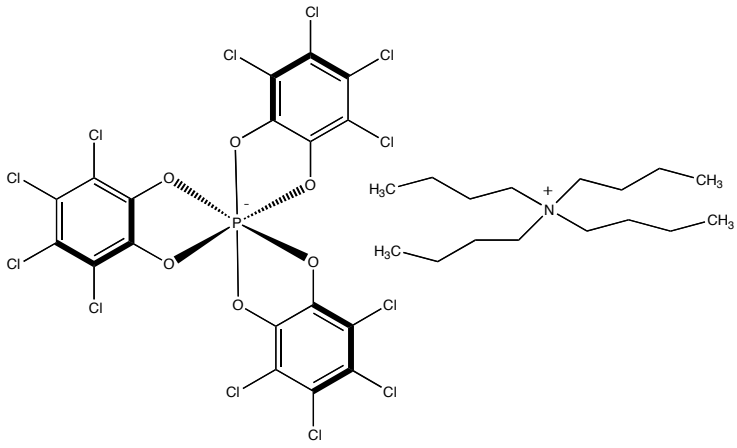

Fig. 4.1 Structure of [Tetrabutylammonium] [Δ-tris(tetrachloro-1,2-benzenediolato)phosphate(V)].

TRISPHAT has been found to be especially useful as a chiral recognition agent for cationic molecules. Unlike other chiral shift reagents such as lanthanide-

based [Eu(fod)$_3$] or neutral (*R*)-*α*-methoxy-*α*-trifluoromethylphenylacetic acid, also known as Mosher's acid (Fig. 4.2), TRISPHAT being an anionic species means it can act as a counterion for cationic molecules and thereby distinguish the two diastereomers by chiral ion pairing.[4]

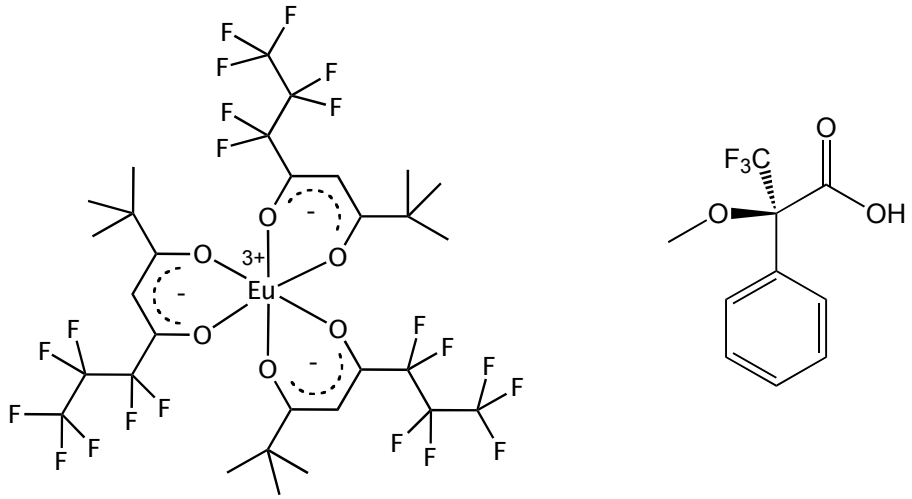

Fig. 4.2 Molecular structures of chiral shift reagents: (left) Eufod, (right) Mosher's acid

Consequently, it can be successfully used as a chiral resolving agent for mono- or dinuclear metal complexes.[5, 8] Lacour and co-workers used TRISPHAT as a diastereomeric resolving agent for dinuclear triple-stranded helicate systems by asymmetric extraction.[9] A similar approach was also applied by Raymond, where, by using a chiral cation (*S*)-*N*-Methylnicotinium (Fig. 4.3), it was possible to separate *M* and *P* enantiomers of anionic gallium dinuclear triple-stranded helicate.[10]

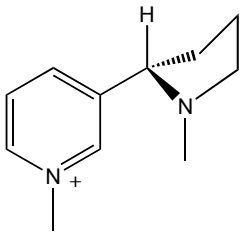

Fig. 4.3 Chiral cationic resolving agent, (*S*)-*N*-Methylnicotinium

It was shown that TRISPHAT can also act as a NMR chiral shift reagent[11] and therefore it can be successfully used to determine the enantiopurity of the optical isomers, being more efficient in enantiodifferentiation than commonly used lanthanide shift reagent.[12]

Previous studies on the interaction of TRISPHAT with an iron(II) triple-helicate carried out in Hannon group by C. R. Pearmund showed that in the presence of chiral TRISPHAT anion the splitting of some proton signals in the NMR spectrum of the Fe(II) cylinder occurs. This implies that the anion induces enantiodifferentiation of the two isomers present in the solution.[13]

To examine the binding properties of the TRISPHAT and *M* and *P* enantiomers and possibly explore their interaction site(s) and to assess the enantiopurity of the complexes, NMR studies of the interaction between the racemic mixture, *M* and *P* isomer of the ruthenium triple-stranded helicate and Δ-TRISPHAT have been undertaken.

Since the improved methodologies for the synthesis and purification and also enantiomer resolution of the Ru cylinder with ligand L (Fig. 4.4) have been successfully developed (See Chapter 2 and 3) and the enantiomers were found

to be configurationally stable, this cylinder was chosen as a model compound for our systems.

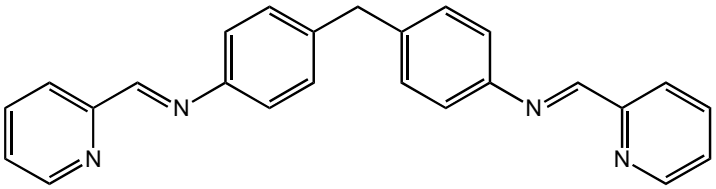

Fig. 4.4 Bispyridylimine ligand L

4.2 Results and discussion

As described in previous chapters the supramolecular Ru(II) triple-stranded helicate is assembled from three symmetrical bis(bidentate) ligands (L), which are wrapped around two metal centers, aligned along the C_3 axis of the complex. The compound exhibits a very high degree of symmetry and thus ^{1}H NMR spectrum shows 8 signals at room temperature. The ^{1}H NMR spectrum of the hexafluorophosphate salt of racemic mixture, $[Ru_2L_3](PF_6)_4$, in CD_3CN is shown in Fig. 4.5.

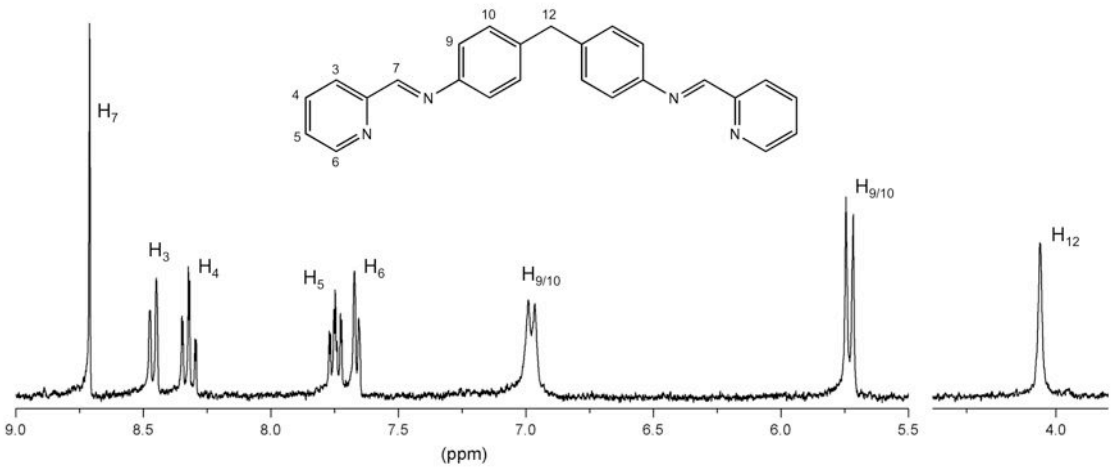

Fig. 4.5 ^{1}H NMR spectrum of $[Ru_2L_3](PF_6)_4$ in CD_3CN

The resonance that corresponds to the imine proton is the most shifted and appears at 8.71 ppm. Next we observe four signals coming from the pyridine ring protons, which appear at 8.45 (H_3), 8.29 (H_4), 7.72 (H_5) and 7.65 ppm (H_6). The two resonances corresponding to the phenyl protons in the centre of the molecule are visible in the spectrum as two doublets at the highest field of the aromatic region and appear at 6.96 and 5.71 ppm. There is one aliphatic signal in the spectrum, a singlet at 4.04 ppm, and it belongs to the methylene protons at the centre of symmetry of the ligand.

To investigate the interactions of our helicate with the chiral TRISPHAT the conditions reported in earlier work from our group were used.[13] Four equivalents of [n-Bu_4N][Δ-TRISPHAT] were added to a solution of $[Ru_2L_3](PF_6)_4$ in CD_3CN and the ^1H NMR spectrum recorded. At this ratio no precipitation occurred but dramatic changes in the spectrum were observed.

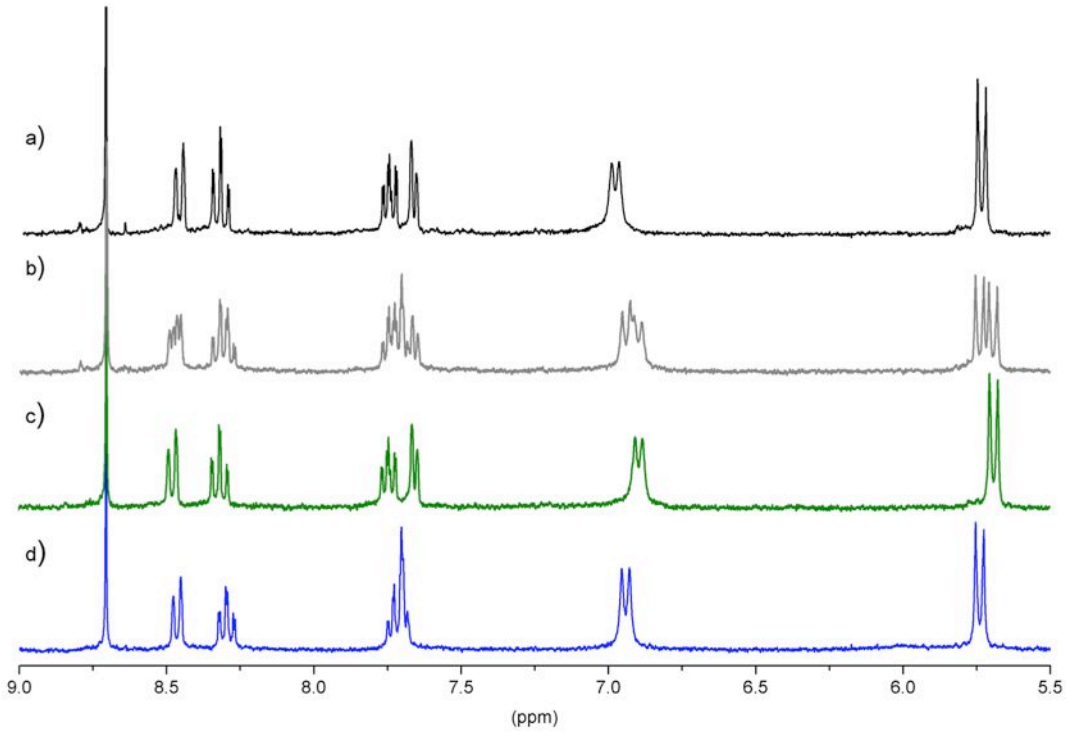

Fig. 4.6 Aromatic region of ^1H NMR spectra of a) *rac*-$[Ru_2L_3](PF_6)_4$, b-d) $[Ru_2L_3](PF_6)_4$ with Δ-TRISPHAT 1:4, b) rac, c) *M*, d) *P*.

The resonance corresponding to the imine proton is the only one that remains undisturbed when TRISPHAT is added, while the other 7 resonances are strongly influenced by the chiral reagent (shifted and/or split) (Fig. 4.6b). The most visible and remarkable change that appears in the spectrum is the splitting of the signal coming from the aliphatic proton into two resonances. The two signals now appear at 3.94 and 4.02 ppm. The induced splitting of the resonances is also clearly visible in the phenyl region of the spectrum. The resonances, which previously appeared as doublets, now became doublets of doublets. It now becomes apparent that in the 3.90-7.10 ppm region the appearance of second set of signals has been induced, where, as described by Pearmund,[13] one set of resonances remains in the position of the native signals, before adding the shift reagent, and the second set of signals appears to be shifted towards higher field.

In the pyridine region the changes in the spectrum are also significant. It is clear that the H_6 and H_5 resonances, which previously appeared on the spectrum as doublet and triplet, split and now become a combined multiplet with a center at 7.71 ppm. Furthermore, the signal corresponding to H_3 has transformed from a doublet to a doublet of doublets and the triplet coming from H_4 has now become a multiplet.

The observed changes in the spectrum of the racemic mixture of triple helicate upon addition of Δ-TRISPHAT indicate that the system now experiences an asymmetric environment, which is caused by enantiodifferentiation of the two optical isomers present in solution by the chiral agent.

TRISPHAT has been shown to interact dissimilarly with the two optical isomers of triple-helicates.[9] Therefore, to explore the interaction of TRISPHAT with the two enantiomers of the studied system, and possibly determining their interaction site(s) preferences, the experiment, which was performed for the racemic mixture, under the same conditions was undertaken for the enantiopure, configurationally stable isomers (for enantiomer separation see Chapter 3).

The ^{1}H NMR of both *M* and *P* enantiomers are identical and are consistent with the NMR spectrum of the racemic mixture. However, when Δ-TRISPHAT was added (four equivalents as for racemic mixture) the two systems became non-equivalent.

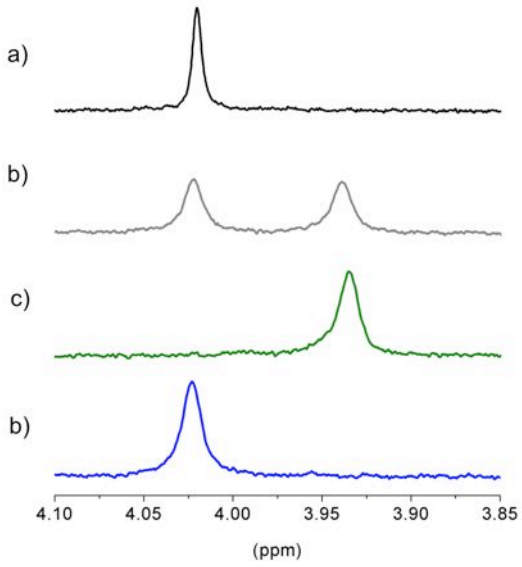

Fig. 4.7 Aliphatic region of ^{1}H NMR spectra of a) *rac*-$[Ru_2L_3](PF_6)_4$, b-d) $[Ru_2L_3](PF_6)_4$ with Δ-TRISPHAT 1:4, b) *rac*, c) *M*, d) *P*.

In the ^{1}H NMR spectrum of the *M* enantiomer, a 0.08 ppm upfield shift of the resonance corresponding to the aliphatic proton is observed compared to the

original spectrum (Fig. 4.7). The phenyl resonances are also shifted towards higher field, but there are no significant changes in the spectrum in the pyridine region apart from a small downfield shift of the H_3 and H_4 resonances.

The spectrum of the *P* enantiomer in the presence of Δ-TRISPHAT also differs from the one before adding the chiral agent. However, in this case the most influenced resonances seem to be the ones situated at the periphery of the cylinder. H_6 and H_5 are now becoming more equivalent and appear on the spectrum as one multiplet, while the other pyridine protons do not seem to be significantly affected by the Δ-TRISPHAT. Unlike in the case of the *M* enantiomer, the signals corresponding to the central part of the helicate, methylene and phenyl protons remain essentially unchanged, thus the environment in this part of the right-handed helicate must be not affected (undisturbed) by the presence of the chiral shift reagent. This gives a key indication about the interaction site(s) between the optically active helicates and chiral hexacoordinated phosphate.

It is clear that Δ-TRISPHAT induces the NMR enantiodifferentiation of the *M* and *P* enantiomer by interacting with the two isomers independently and showing chiral discrimination towards the interaction site. The two chiral molecules, or their 'active moieties', interact with each other via geometrical complementarities. Therefore, it can be proposed that the Δ-TRISPHAT recognises primarily the central part of the left-handed helicate (*M*), possibly by interacting with the phenyl rings along the C_2 axis of the cylinder.

The opposite effect is present in the case of the *P* helicate, where the electronic environment of central part of the complex seems to be undisturbed by presence of Δ-TRISPHAT while the terminal protons seem to be affected the

most. In this case the two molecules might 'communicate' with each other along the C_3 axis of the long molecule, probably with phosphate atom pointing at the metal center, which may also be assisted by π-π stacking or edge to face interactions between the pyridine rings of the helicate and phenyl rings of Δ-TRISPHAT. This kind of interaction can be an effect of the structural preferences but ultimately a consequence of the homochiral ion pairing. A similar mode of recognition was also proposed by Correia *et al.* for the chiral mononuclear polypyridyl Ru(II) complexes.[14]

4.3 General discussion, conclusions and further work

Chiral molecular recognition is predominantly based on the molecular symmetry features of the two interacting species. This in turn is closely associated with the stereoselective intermolecular interactions and consequently with energy gains and losses while driving the system to the most thermodynamically stable state.

The NMR studies presented in this chapter have shown that Δ-TRISPHAT recognizes both optical isomers of the ruthenium triple-stranded helicate. Indeed, it appears that the TRISPHAT interacts independently with both enantiomers, however the recognition processes seem to be controlled by the stereochemical compatibility of the two interacting molecules leading to chiral discrimination between the interaction sites.

There are two elements that are anticipated to drive the molecular recognition between the TRISPHAT and optical isomers of the $[Ru_2L_3]^{4+}$: hydrophobic effects and electrostatic attractions. These interactions are expected to be the

dominant factors affecting the binding energetics of both *M* and *P* enantiomers to an approximately equal extent. Nevertheless the thermodynamics of the two discussed cases can be strongly differentiated by other elements of molecular recognition, which, in structural terms, could arise from the symmetry properties of the two interacting species.

The ^{1}H NMR spectra of the two enantiomers in the presence of Δ-TRISPHAT display distinctive shielding and deshielding effects suggesting that the different functional units of the *M* and *P* enantiomers are involved in the interactions with the hexacoordinated phosphate anion. The interaction of Δ-TRISPHAT with the *M* enantiomer results in more shielding of the phenyl and aliphatic protons of the cylinder and thus in lower values of *δ*. This could be consistent with π-π stacking of the two phenyl rings of the TRISPHAT molecule with the central phenyl rings of the left-handed helicate. Furthermore, this would give an additional energy gain to the system arising from the π-π interactions of the aromatic rings. However, in the case of the right handed, *P* enantiomer the same kind of interactions would be expected to be sterically hindered and hence less favorable. Indeed the NMR spectrum of the *P* enantiomer with Δ-TRISPHAT shows the central protons to be unaffected by the presence of TRISPHAT while the protons at the edges of the helicate *i.e.* pyridine protons, seem to be influenced. The high symmetry of the system suggests that the chiral hexacoordinated phosphate anion approaches the *P* helicate from the ruthenium site(s) along the C_3 axes. This homochiral ion pairing, with the phosphorus atoms pointing at the ruthenium centers, would be expected to give rise to greater association of TRISPHAT moieties with the helicate units

allowing intermolecular interactions, which in turn would result in additional energy gain to the system.

The different recognition sites of the *M* and *P* enantiomer could also lead to different level of loss in translational and rotational degrees of freedom and such factors would need to be taken into consideration while exploring the energetics of the *M* and *P* systems with TRISPHAT. Moreover, all the above factors would lead to certain energy benefits and penalties and this could be reflected in the distinctive binding affinities of Δ-TRISPHAT towards chiral helicates and consequently binding energetics.

Although the NMR studies presented in this chapter do not give detailed information about the recognition event between the TRISPHAT and chiral helicates, and only a hypothesis about the binding sites can be drawn, the enantiodifferentiation of the *M*- and *P*-$[Ru_2L_3]^{4+}$ by chiral hexacoordinated phosphate ions enables the enantiopurity of the dinuclear triple-stranded cylinders to be determined with greater precision than could previously be obtained. Indeed these NMR studies confirmed the efficiency of the methodology used for the separation of the optical isomers of the ruthenium triple-stranded helicates and can be successfully used to examine the purity of the enantiomeric complexes.

Understanding the molecular insights of chiral recognition can have a great impact on development of new approaches for enantioselective synthesis or catalysis, host-guest chemistry, molecular aggregation, separation processes or drug design. In this context, the TRISPHAT – supramolecular chiral triple-stranded helicate systems can serve as great model systems to study the

forces that drive this kind of molecular recognition hence to better understand the homo- and heterochiral ion pairing phenomenon. Therefore, comprehensive studies of the interactions of enantiomeric hexacoordinated phosphate ions with chiral triple-stranded helicates at the structural, kinetic and thermodynamic level should be a feature of further studies.

4.4 References

[1] J. Lacour, R. Frantz, *Org. Biomol. Chem.* **2005**, *3*, 15.

[2] J. Lacour, *C. R. Chim.* **2010**, *13*, 985.

[3] O. Maury, J. Lacour, H. Le Bozec, *Eur. J. Inorg. Chem.* **2001**, 201.

[4] J. Lacour, J. J. Jodry, C. Ginglinger, S. Torche-Haldimann, *Angew. Chem. Int. Ed.* **1998**, *37*, 2379.

[5] J. Lacour, C. Goujon-Ginglinger, S. Torche-Haldimann, J. J. Jodry, *Angew. Chem. Int. Ed.* **2000**, *39*, 3695.

[6] H. Amouri, R. Thouvenot, M. Gruselle, B. Malezieux, J. Vaissermann, *Organometallics* **2001**, *20*, 1904.

[7] A. Damas, J. Moussa, M. N. Rager, H. Amouri, *Chirality* **2010**, *22*, 889.

[8] J. Lacour, S. Torche-Haldimann, J. J. Jodry, C. Ginglinger, F. Favarger, *Chem. Commun.* **1998**, 1733.

[9] J. J. Jodry, J. Lacour, *Chem. Eur. J.* **2000**, *6*, 4297.

[10] R. M. Yeh, M. Ziegler, D. W. Johnson, A. J. Terpin, K. N. Raymond, *Inorg. Chem.* **2001**, *40*, 2216.

[11] J. Lacour, C. Ginglinger, F. Favarger, S. TorcheHaldimann, *Chem. Commun.* **1997**, 2285.

[12] G. Bruylants, C. Bresson, A. Boisdenghien, F. Pierard, A. Kirsch-De Mesmaeker, J. Lacour, K. Bartik, *New J. Chem.* **2003**, *27*, 748.

[13] C. Pearmund, *PhD Thesis, University of Warwick* **2002**

[14] I. Correia, H. Amouri, C. Cordier, *Organometallics* **2007**, *26*, 1150.

5

Synthesis, Characterisation and DNA Binding Studies of Ru(II) Complexes With Ammine and Azopyridyl Building Units

Abstract

The DNA binding effects of di- and mononuclear Ru(II) complexes of the formula $[Ru_2L(NH_3)_8]Cl_4$ and $[RuL^{azpy}(NH_3)_4]Cl_2$, where L is the bisazopyridine ligand $(C_5H_4N)N=N(C_6H_4)CH_2(C_6H_4)N=N(C_5H_4N)$ and L^{azpy} is the azopyridine ligand $(C_5H_4N)N=N(C_6H_5)$, have been investigated by UV-Vis spectroscopy, circular and linear dichroism and agarose gel electrophoretic mobility shift assays. Both complexes bind non-covalently to ct-DNA inducing bending/coiling in the biomolecule. The binding of the dinuclear complex was found to be much stronger and appears to be more specific than the binding of the mononuclear complex. Both complexes were found to have no antiproliferative effects in human cancer cell lines.

5.1 Introduction

Studies to probe the structural effects of a drug on biological systems and investigate the dependence of the structure of the 'active' moiety on its binding ability/properties have been a fast growing area of research in the past few decades. The effects of small molecules on DNA structures are of particular interest because of their potential to control or interfere with the processing of genetic information.

Polyamine species such as spermidine or spermine (Fig. 5.1) are often involved in regulation of cell proliferation and cell differentiation.[1]

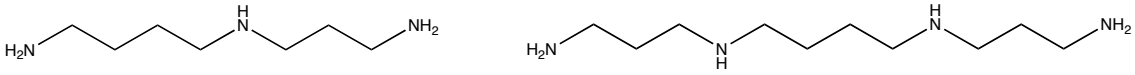

Fig. 5.1 Molecular structures of (left) spermidine, (right) spermine

They neutralize the chromosomal DNA and protect it from damage by oxygen species.[2] As cationic molecules they bind to the DNA, acting either in the major or minor groove, and also induce structural changes in the biomolecule.[3] Some amine-based metal complexes can act as polyamine mimics, for example $[Co(NH_3)_6]^{3+}$, which induces the structural transition of B- to Z- form of DNA.[4] Interestingly, this complex is more effective in stabilizing the Z-DNA structure than Na^+ or Mg^{2+} ions.[5] Other analogues of this compound, such as the Ru analogue, are also able to induce DNA structural transitions, however, it was found that the Ru dication is less effective in stabilising the Z-DNA structure than

the parent Co(III) compound. The crystal structures of both complexes with oligonucleotides show that both ions particularly interact through hydrogen bonding with guanine residues (Fig. 5.2).[6] Such hydrogen-bonding is a feature of ammine based ligands.

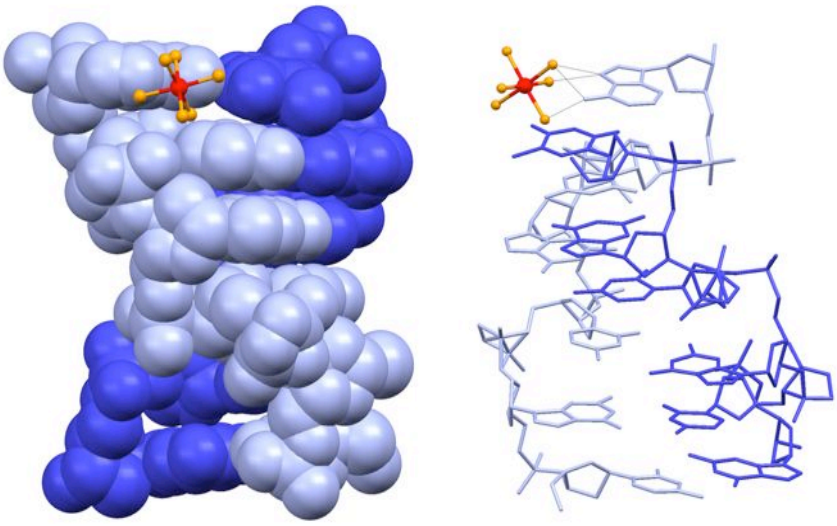

Fig. 5.2 The interaction of ion $[Ru(NH_3)_6]^{2+}$ with Z-DNA; (left) spacefill representation, (right) hydrogen bonding between Ru cation and guanine residues (PDB ref. 2HTO).[6]

In $[Ru(NH_3)_4(diimine)]^{2+}$, where the bidentate diimine is a large, aromatic heterocyclic ligand suited to intercalation, the NH_3 ligands also tend to be involved in hydrogen bonding with the intrastrand nucleobases assisting the intercalation of diimine between the bases.[7] These intercalating complexes also induce some DNA structural changes and were shown to cleave DNA.[8] When irradiated, NH_3 ligands can act as photolabile species. Turro *et al.* showed that photolysis of *cis*-$[Ru(bpy)_2(NH_3)_2]^{2+}$ (bpy - 2,2′-bipyridine) in water led to the photoinduced loss of NH_3 ligands and formation of a cationic aqua-species, which could then coordinate to the bases of ss- and/or ds-DNA.[9] This opens up the potential use of this class of compounds as therapeutic prodrugs

in the field of photodynamic therapy (PDT). A number of ammine compounds have been already explored in biological systems. For example, an ammine-rich mixed-valence oxygen-bridged trinuclear ruthenium compound, commonly known as ruthenium red (Fig. 5.3) was found to bind to calcium-binding proteins and particularly inhibit Ca^{2+} uptake by mitochondria.[10]

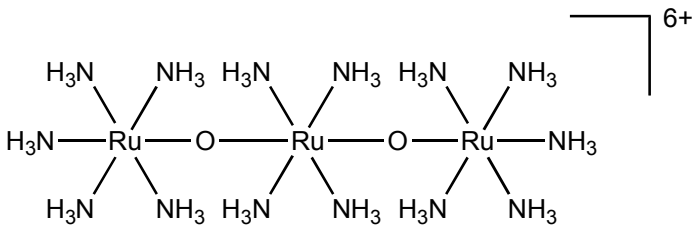

Fig. 5.3 Molecular structure of ruthenium red

Farrell and co-workers developed a series of polynuclear platinum ammine-based complexes, which were found to bind along the DNA phosphate backbone[11] and also exhibit micromolar cytotoxicity against cancer cells.[12] Other ammine-based transition metal complexes such as mononuclear $[Ru(NH_3)_4Cl_2]Cl$ or $[Ru(NH_3)_3Cl_3]$ also show promising cytotoxic activity against tumours.[13, 14] This kind of complexes bind to histidine imidazoles in proteins such as albumin and transferrin, which have been suggested to mediate their uptake into cells.[15]

An alternative promising class of potential anticancer drugs are azopyridyl metal complexes (See Chapter 1). Reedijk and co-workers reported isomers of $[RuL^{azpy}{}_2Cl_2]$ and showed that the σ- isomer of this compound shows remarkably higher cytotoxic activity against a range of tumour cell lines compared to its β- and γ-analogues.[16] More recently Hotze prepared a set of isomeric dinuclear

bis-azopyridine cylindrical complexes, $[Ru_2L_2Cl_4]$, which exhibit up to 10 fold higher cytotoxic activities against tumour cells than cisplatin.[17]

Since cylinders have dramatic effects on DNA structure (coiling) and metal ammine complexes, also affect DNA structure (altering its conformation), and since both offer different types of non-covalent DNA recognition we decided to explore whether introducing both aspects within the same molecule might create species with unusual DNA binding. Creating such species involves replacing one or more strands of the cylinder with ammine groups (using single-stranded or double-stranded cylinders). To initiate this work we chose to investigate the dinuclear single stranded species since this avoids the isomers observed with the double-stranded helicates.[17] Alongside this, a mononuclear analogue was prepared to compare its properties. Herein we combine the bis-azopyridine approach with the ammine complex approach and present the DNA binding of the two Ru(II) mixed ammine- and azopyridine complexes. A symmetrical dinuclear ruthenium(II) complex with bisazopyridine bridging ligand (L^a) and ammine co-ligands and a mononuclear analogue of this compound with azopyridine ligand (L^{azpy}), (Fig. 5.4) are reported along with their action on the DNA structure and in cells.

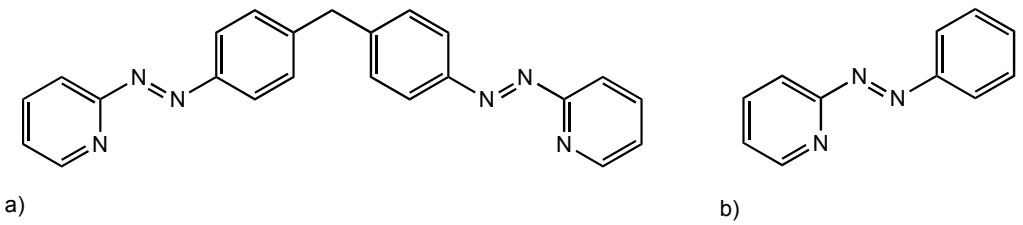

Fig. 5.4 a) bisazopyridine ligand, b) azopyridine ligand

These compounds are designed to have no or very little potential to bind coordinatively to the DNA or to intercalate between base pairs, but this leaves open the possibility of binding along the grooves and/or interacting with the phosphate backbone.

5.2 Results and discussion

5.2.1 Synthesis

5.2.1.1 Synthesis and characterisation of $[Ru_2L^a(NH_3)_8]Cl_4$

Ligand L^a (Fig. 5.5) was prepared from 2-nitrosopyridine and 4,4'-methylenedianiline according to the previously described method.[18, 19]

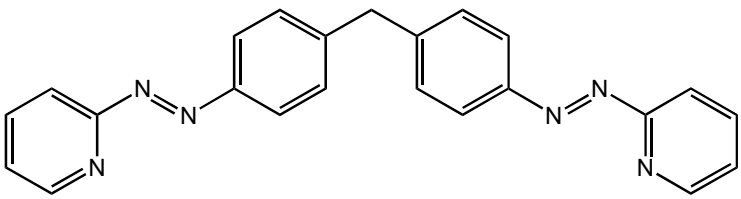

Fig. 5.5 Chemical structure of bisazopyridine ligand L^a

Ligand L^a was coordinated to the Ru(II) by stirring a solution of the ligand with $[Ru(NH_3)_5(H_2O)](PF_6)_2$ in acetone under an argon atmosphere. The complex was purified by flash chromatography on a neutral alumina column to afford a pure compound in 62 % yield. The ^1H NMR spectrum of the dinuclear complex shows one aliphatic signal corresponding to the bridging $-CH_2$ group in the centre of the ligand and six aromatic proton signals, indicating the presence of single, symmetrical species in the solution (Fig. 5.6).

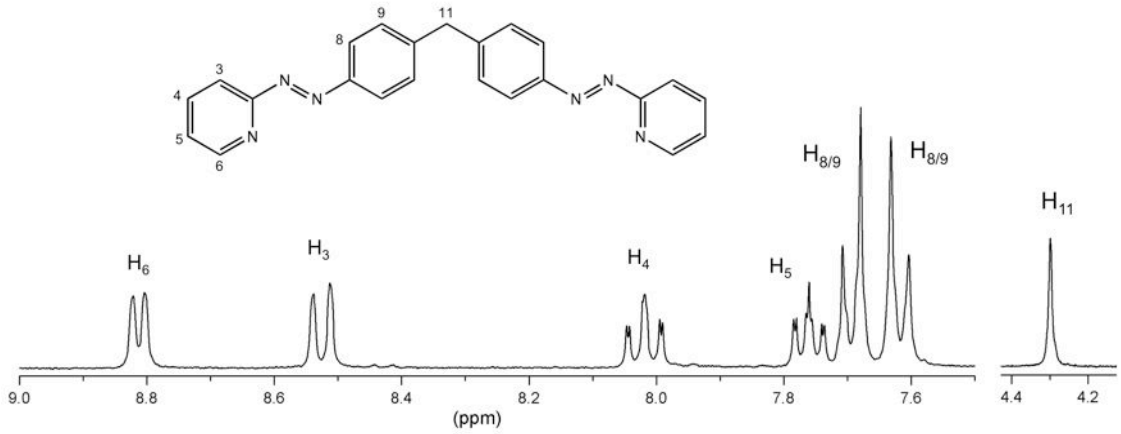

Fig. 5.6 ^{1}H NMR spectrum of $[Ru_2L^a(NH_3)_8]Cl_4$ in MeOD

The mass spectrum is dominated by peaks corresponding to $[Ru_2L^a(NH_3)_8]Cl^{3+}$ (*m/z* 250.1) $[Ru_2L^a(NH_3)_7]Cl^{3+}$, (*m/z* 245.2) $[Ru_2L^a(NH_3)_6]Cl^{3+}$, (*m/z* 239.1) $[Ru_2L^a(NH_3)_5]Cl^{3+}$, (*m/z* 233.3) and $[Ru_2L^a(NH_3)_8]^{2+}$ (*m/z* 358.4). Elemental analysis data was consistent with a formulation of $[Ru_2L^a(NH_3)_8]Cl_4$. Red needle – shaped crystals suitable for X-ray analysis were obtained by slow diffusion of Et_2O into a methanolic solution of the chloride salt of the compound. As expected, the crystal structure shows the cation to be a symmetrical dinuclear species where two octahedral Ru centers are linked by one bisazopyridine ligand, which separates the two Ru centers by 9.5 Å. There is no helical twist of the linking ligand about the Ru atoms and this results in orientation of all ammonia ligands to one side of the complex with the linking ligand acting as a bridge between the two metal centers (Fig. 5.7). Each Ru atom has also four coordinated ammonia ligands with Ru-N (NH_3) distances of 2.11-2.16 Å. The central phenyl rings are twisted with respect to each other with an inter planar angle of 85^o. The phenyl rings are also twisted with respect to the neighbouring pyridine rings (torsion angles 52 and 44^o).

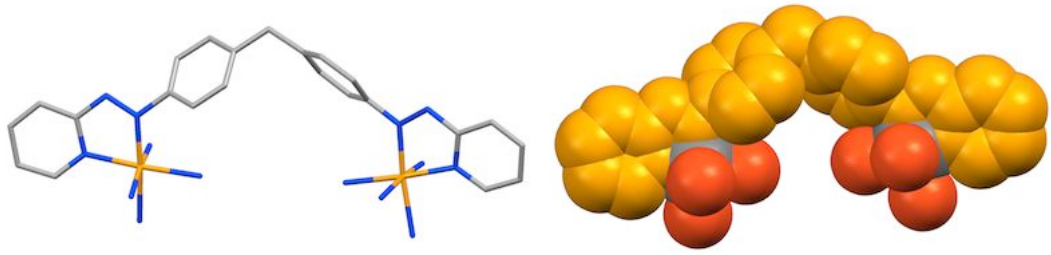

Fig. 5.7 Crystal structure of the cation in $[Ru_2L^a(NH_3)_8]Cl_4$. Hydrogen atoms and counterion are omitted for clarity

Fig. 5.8 shows the crystal packing diagram for $[Ru_2L^a(NH_3)_8]^{4+}$. The tetra-cations are arranged in parallel chains, which are held together by hydrogen bonding. Each metal complex cation is engaged in hydrogen bonding between its ammine groups and Cl^- counterions, which in turn are involved in hydrogen bonding with the two other neighbouring cations enabling the large highly organised scaffold to be formed.

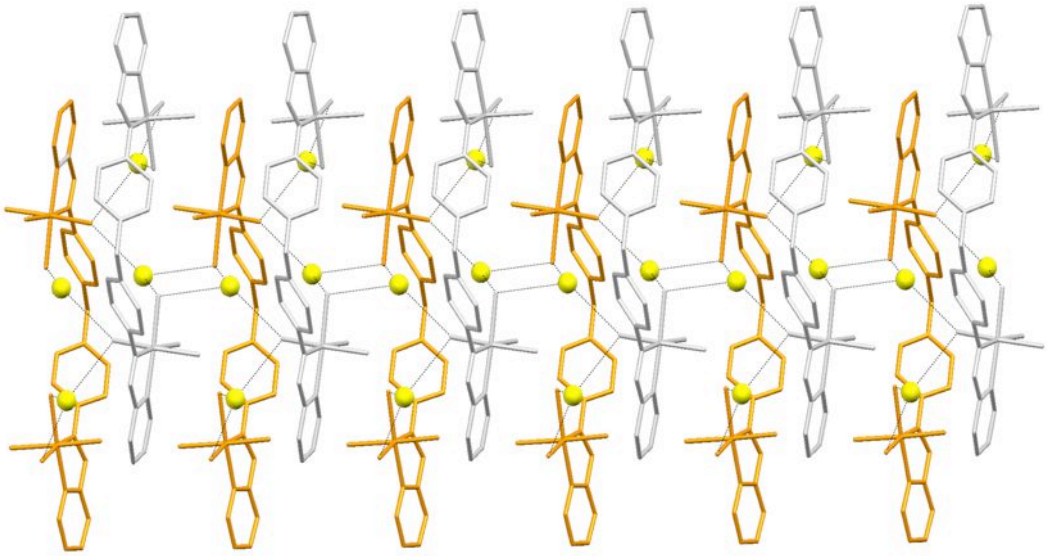

Fig. 5.8 Packing diagram for $[Ru_2L^a(NH_3)_4]^{4+}$ showing hydrogen bonding interaction between the ammine groups and chloride counterions (yellow). Hydrogen atoms and solvent molecules have been removed for clarity.

The $[Ru_2L^a(NH_3)_8]^{4+}$ was also crystallized as a hexafluorophosphate salt. The large red crystals were obtained by slow diffusion of acetonitrile from an acetonitrile/H_2O solution of the compound. The complex crystallized in a monoclinic crystal system with the space group P2(1)/n. The crystal structure shows two crystallographically unique $[Ru_2L^a(NH_3)_8]^{4+}$ cations in the asymmetric unit cell (Fig. 5.9).

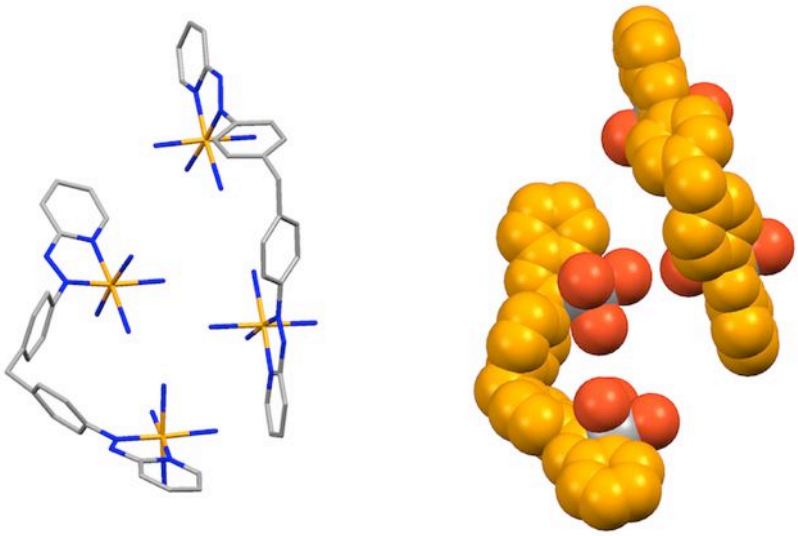

Fig. 5.9 Crystal structure and specefill representation of cations in $[Ru_2L^a(NH_3)_8](PF_6)_4$. Hydrogen atoms, counterions, and solvent molecules have been omitted for clarity.

Differences between the two unique cations in the structure arise primarily from dissimilarity in the Ru···Ru distances in the two molecules (9.2 Å and 7.8 Å), which are smaller than in the previous structure. As seen in the structure of $[Ru_2L^a(NH_3)_8]Cl_4$, no helical twist of the linking ligand is observed in either molecule.

5.2.1.2 Synthesis and characterisation of $[RuL^a(NH_3)_4]Cl_2$

One of the side products of the reaction towards the dinuclear single–stranded compound, described above, was the mononuclear complex of formula $[RuL^a(NH_3)_4]Cl_2$. The equilibrium of the reaction towards this compound was changed by increasing the molar ratios of the reagents (1: 1). Reaction of L with $[Ru(NH_3)_5(H_2O)](PF_6)_2$ was carried out in acetone under argon atmosphere. Purification of the product by column chromatography afforded the pure compound in 55 % yield. Under all conditions explored both, mononuclear and dinuclear species formation was observed.

The $[RuL^a(NH_3)_4]^{4+}$ is not symmetrical due to the coordination of the Ru atom only on one site of the bis-bidentate ligand and that results in the appearance of two sets of peaks in the ^1H NMR spectrum (Fig. 5.10). Assignment of the peaks was performed on the basis of 2D NMR experiments (see Supplementary information).

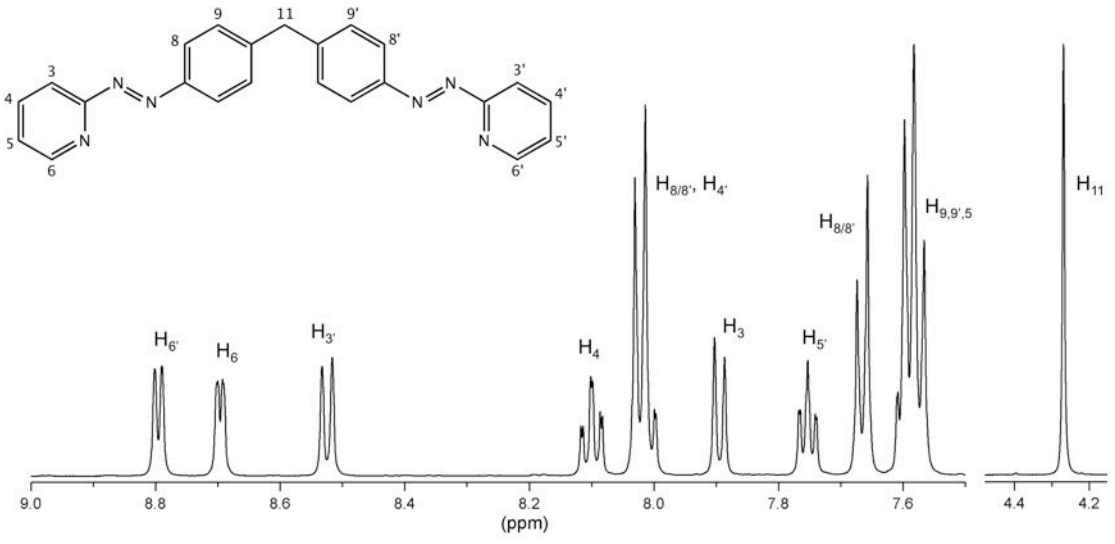

Fig. 5.10 ^1H NMR spectrum of $[RuL^a(NH_3)_4]Cl_2$ in MeOD

X-ray quality crystals were obtained by slow diffusion of benzene into an acetonitrile solution of its hexafluorophosphate salt of the compound. The crystal structure shows four ammonia ligands and one azopyridine ligand coordinated to one Ru atom (Fig. 5.11) with Ru-N (NH_3) distances 2.14 - 2.17 Å.

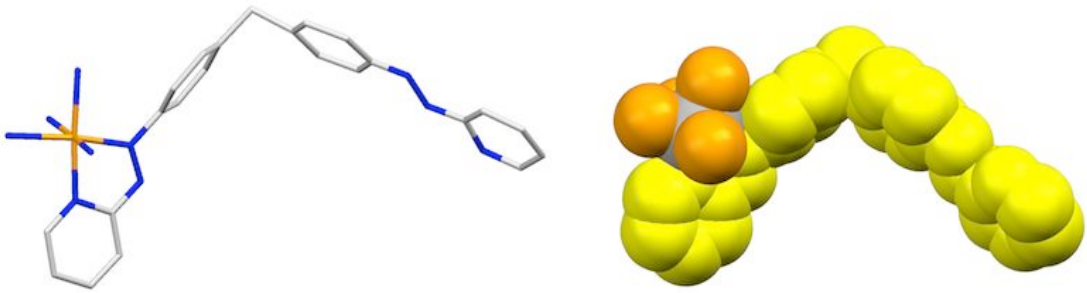

Fig. 5.11 Crystal structure and spacefill representation of cation in $[RuL^a(NH_3)_4](PF_6)_2$. Hydrogen atoms, counterions and solvent molecules have been omitted for clarity.

The ligand is bent about the central CH_2 group by 75.24^o and it adopts the *trans* configurations of the phenyl and pyridine rings about the central N-N bonds on both sites. In the 'free', uncoordinated, part of the ligand the phenyl and pyridine rings are in the same plane, while the coordination of the Ru atom causes the twist of the pyridine and phenyl ring planes by 58^o. Unlike in the dinuclear complex, here the ruthenium atom with four coordinated ammonia ligands is pointing away from the rest of the ligand.

Analysis of the crystal packing (Fig. 5.12) reveals that the metal complex cations are aligned in chains through π-π stacking between the phenyl rings of alternating complexes. The inter-planar distance between the adjacent phenyl rings is ~ 3.6 Å. Each chain aligns with two other chains in head-to-head or tail-to-tail fashion.

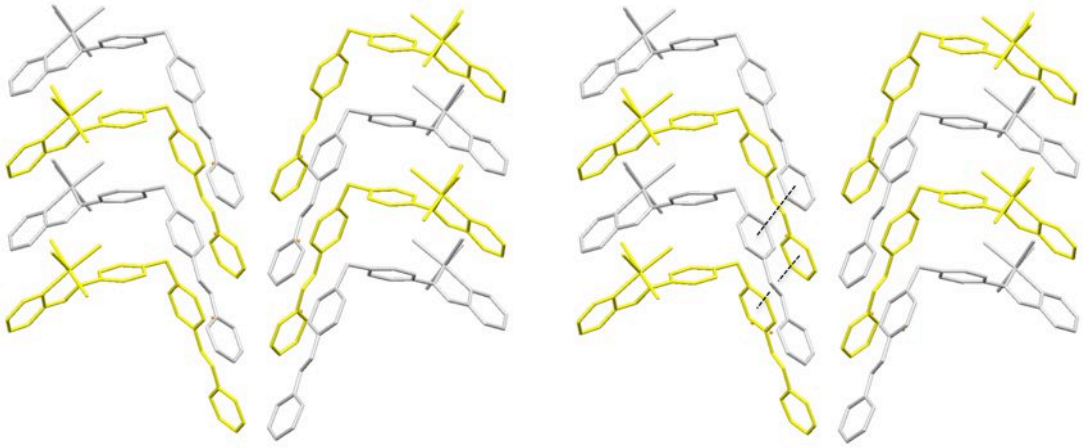

Fig. 5.12 Crystal packing diagram for $[RuL^{a}(NH_3)_4]^{2+}$ showing the π-π stacking interactions between phenyl rings. Hydrogen atoms, counterions and solvent molecules have been removed for clarity.

The $[RuL^{a}(NH_3)_4]Cl_2$ was found to be unstable in solution. Upon standing in methanolic or aqueous solution a change in the colour of the solution from orange to deep red/purple was observed. Given that the mass spectral data indicated the presence of species of a formulation $[RuL^{a}(NH_3)_4]^{2+}$ and $[Ru_2L^{a}{}_2(NH_3)_4]^{4+}$ and NMR data demonstrated the presence of numerous entities that could be assigned to several different isomers of dinuclear product(s), it would appear that the complex $[RuL^{a}(NH_3)_4]Cl_2$ undergoes dimerisation under these conditions and for this reason, further biological studies with this compound have not been undertaken.

5.2.1.3 Synthesis and characterisation of $[RuL^{azpy}(NH_3)_4]Cl_2$

The literature procedure for the synthesis of ligand L^{azpy} (Fig. 5.13) involves a condensation reaction between 2-aminopyridine and nitrosobenzene and further purification by recrystallization from petroleum ether.[20, 21]

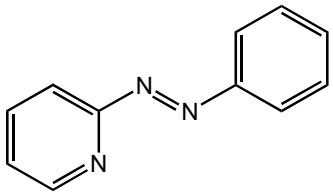

Fig. 5.13 Chemical structure of azopyridine ligand L^{azpy}

In these studies the ligand was prepared by analogous procedures by instead reacting 2-nitrosopyridine and aniline in dichloromethane with one drop of glacial acetic acid. It was found that the compound could be successfully purified by silica gel column chromatography with chloroform as an eluent giving a yield of 74 %. The characterisation data was in agreement with that reported in the literature.

Coordination of the ligand L^{azpy} to the ruthenium centre was performed by stirring $[Ru(NH_3)_5(H_2O)](PF_6)_2$ and ligand L^{azpy} in acetone under an argon atmosphere. The precipitation of the product afforded a desired compound, $[RuL^{azpy}(NH_3)_4]Cl_2$, in 29 % yield. The ^1H NMR spectrum of the compound reveals only one set of aromatic peaks suggesting that a single compound is formed (Fig. 5.14).

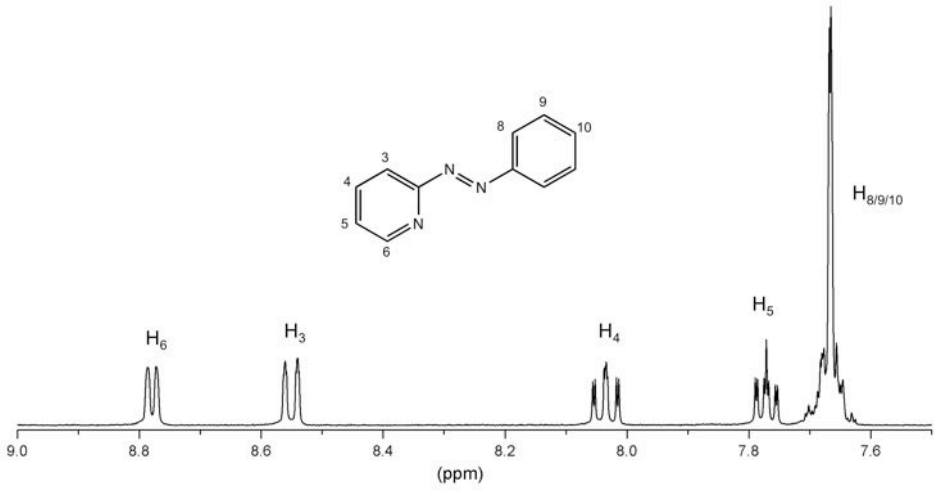

Fig. 5.14 ^1H NMR spectrum of $[RuL^{azpy}(NH_3)_4]Cl_2$ in MeOD

The electrospray mass spectrometry analysis shows peaks corresponding to the cations $[RuL^{azpy}]Cl^{+}$ (*m/z* 320.1), $[RuL^{azpy}(NH_3)_2]Cl^{+}$ (*m/z* 354.1), $[RuL^{azpy}(NH_3)_3]Cl^{+}$ (*m/z* 371.1), $[RuL^{azpy}(NH_3)_4]Cl^{+}$ (*m/z* 388.2) and partial microanalytical data were consistent with the formulation $[RuL^{azpy}(NH_3)_4]Cl_2$.

X-ray quality crystals of this compound were obtained by slow diffusion of benzene into an acetonitrile solution of the hexafluorophosphate salt of the complex. The compound crystallized in the monoclinic crystal system with the space group P2(1)/c. The structure contains two PF_6^- ions per ruthenium complex and a molecule of solvent benzene. The crystal structure of the cation shows one azopyridine ligand to be coordinated to the ruthenium atom, which has also coordinated four ammonia ligands (Fig. 5.15) with Ru-N distances of 1.91 – 2.13 Å. In the azopyridine unit the phenyl and pyridine rings adopt a trans conformation about the central N=N bond. The torsion angle between N=N and phenyl ring is 50^{o}.

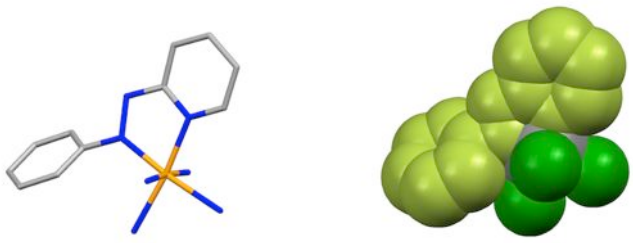

Fig. 5.15 Crystal structure and spacefill representation of $[RuL^{azpy}(NH_3)_4]Cl_2$. Hydrogen atoms and counterions are omitted for clarity.

The analysis of crystal packing shows that the metal complex cations are aligned in chains (Fig. 5.16). The initial analysis shows that each cation interacts via hydrogen bonding with the neighbouring PF_6^- ion, which further

hydrogen bonds with another neighbouring $[RuL^{azpy}(NH_3)_4]^{4+}$. However, due to the high disorder of one of the PF_6^- ions in the structure further discussion cannot be undertaken.

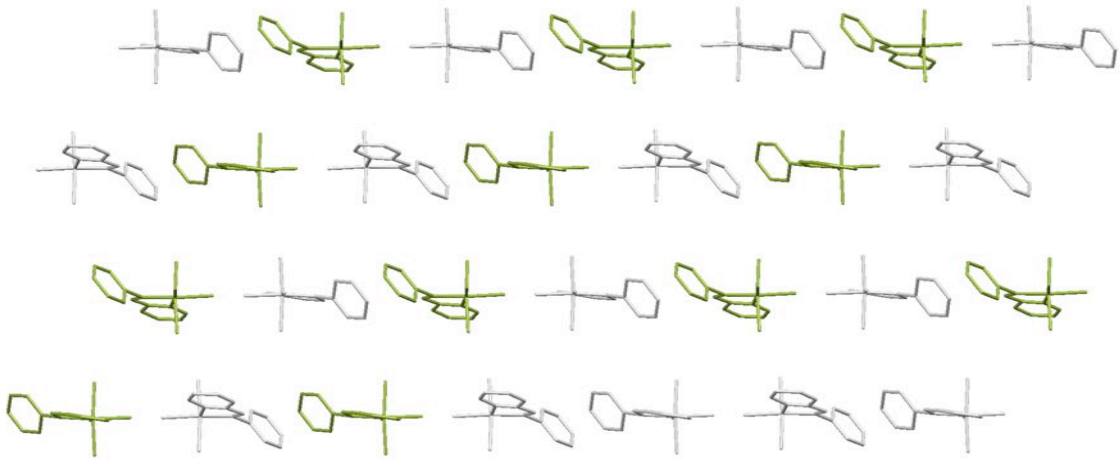

Fig. 5.16 Crystal packing of $[RuL^{azpy}(NH_3)_4]^{2+}$. Hydrogen atoms, counterions and solvent molecules have been omitted for clarity.

5.2.2 Interaction with DNA

Compound $[Ru_2L^a(NH_3)_8]Cl_4$ and $[RuL^{azpy}(NH_3)_4]Cl_2$ were selected for further studies. These complexes show the potential to bind to DNA through a range of non-covalent interactions: electrostatic interactions between cationic complex and polyanionic DNA, hydrophobic interactions within DNA grooves, hydrogen bonding of ammine ligands with phosphate backbone or within intrastrands guanine nucleobases and/or partial intercalation of the azopyridine ligand between the stacked bases. To probe the complexes interactions with DNA the absorption based spectroscopic techniques such as circular and linear

dichroism as well as agarose gel electrophoretic mobility shift assay and DNA thermal denaturation analysis were employed.

5.2.2.1 Absorption spectral studies

The UV-Vis absorption spectra of the two complexes selected for the DNA binding studies, $[Ru_2L^a(NH_3)_8]^{4+}$ and $[RuL^{azpy}(NH_3)_4]^{2+}$, reveal intense π-π* transition bands centered at ~225 nm and ~330 nm and, corresponding to the red/orange colour of the chromophore, broad metal to ligand charge transfer bands (MLCT) with the maximum at ~ 477 nm.

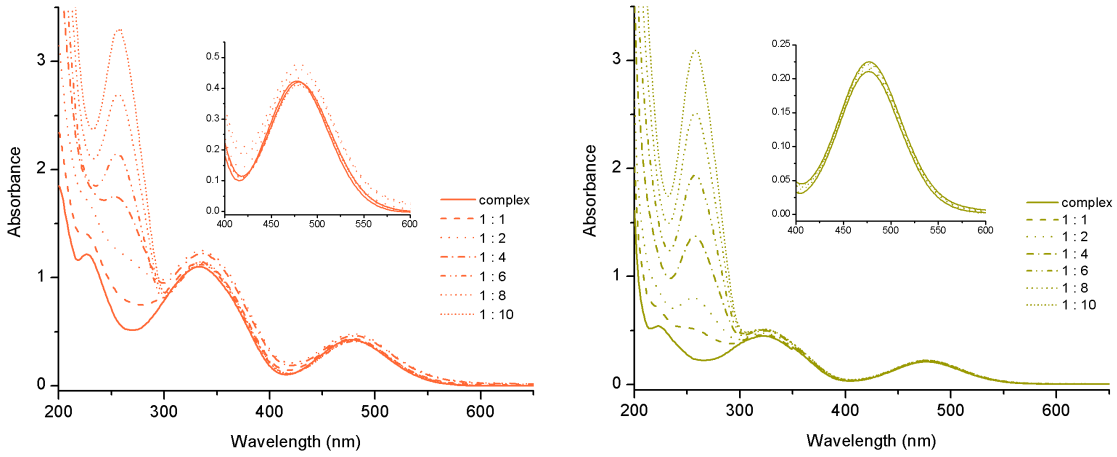

Fig. 5.17 UV-Vis titration spectra of complex (50 μM, 20 mM NaCl, 1 mM sodium cacodylate) upon addition of DNA; (left) $[Ru_2L^a(NH_3)_8]Cl_4$, (right) $[RuL^{azpy}(NH_3)_4]Cl_2$. Mixing ratios are indicated as complex to DNA base.

Upon addition of ct-DNA no significant changes in the MLCT regions of the compounds are observed indicating that the compounds are not altered upon binding to DNA (Fig. 5.17). Moreover, a small hyperchromic effect in the MLCT band of $[RuL^{azpy}(NH_3)_4]Cl_2$ was observed upon addition of DNA, while

$[Ru_2L^a(NH_3)_8]Cl_4$ displayed first hyper-[4] and then hypochromicity[5] implying two DNA binding modes for this complex.

5.2.2.2 Circular dichroism

To further explore the possible effect of the compounds on the DNA structure CD titrations of the compounds into a solution of the ct-DNA (300 μM, 20 mM NaCl, 1 mM sodium cacodylate) were performed.

Upon addition of $[Ru_2L^a(NH_3)_8]Cl_4$ into DNA solution a strong induced CD signal in the in-ligand region of the compound is observed, clearly indicating binding of the compound to the DNA. The retained shape of the DNA CD bands below 300 nm confirms that a B-DNA conformation is maintained throughout the titration (Fig. 5.18).

The addition to DNA of the mononuclear analogue $[RuL^{azpy}(NH_3)_4]Cl_2$ causes less dramatic effects. Only very small changes in the DNA region are observed upon addition of the complex to the solution of DNA and no induced CD signal in the MLCT region of the complex is observed throughout the titration.

[4] hyperchromicity – increase of absorbance of a substance

[5] hypochromicity – decrease of absorbance of a substance

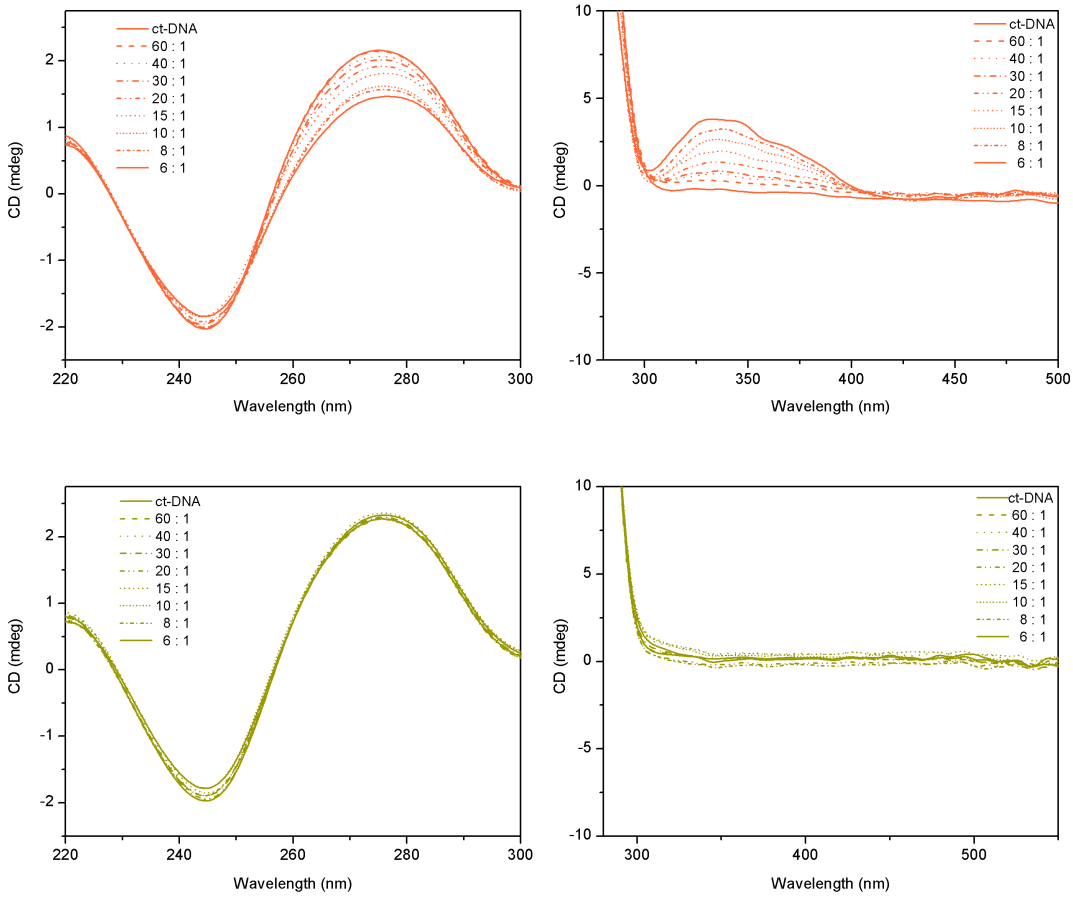

Fig. 5.18 CD spectra of DNA (300 μM, 20 mM NaCl, 1 mM sodium cacodyate) upon addition of: (top) $[Ru_2L^a(NH_3)_8]Cl_4$, (bottom) $[RuL^{azpy}(NH_3)_4]Cl_2$; (mixing ratios are indicated as DNA base to complex, 220-300 nm – 1 mm pathlength cuvette, 280-500 – 1 cm cuvette).

5.2.2.3 Flow linear dichroism (LD)

The linear dichroism titrations were conducted using the same conditions as used for CD experiments (300 μM ct-DNA, 20 mM NaCl, 1 mM sodium cacodylate). The LD spectra of ct-DNA alone and in the presence of different concentrations of Ru complexes are shown in Fig. 5.19.

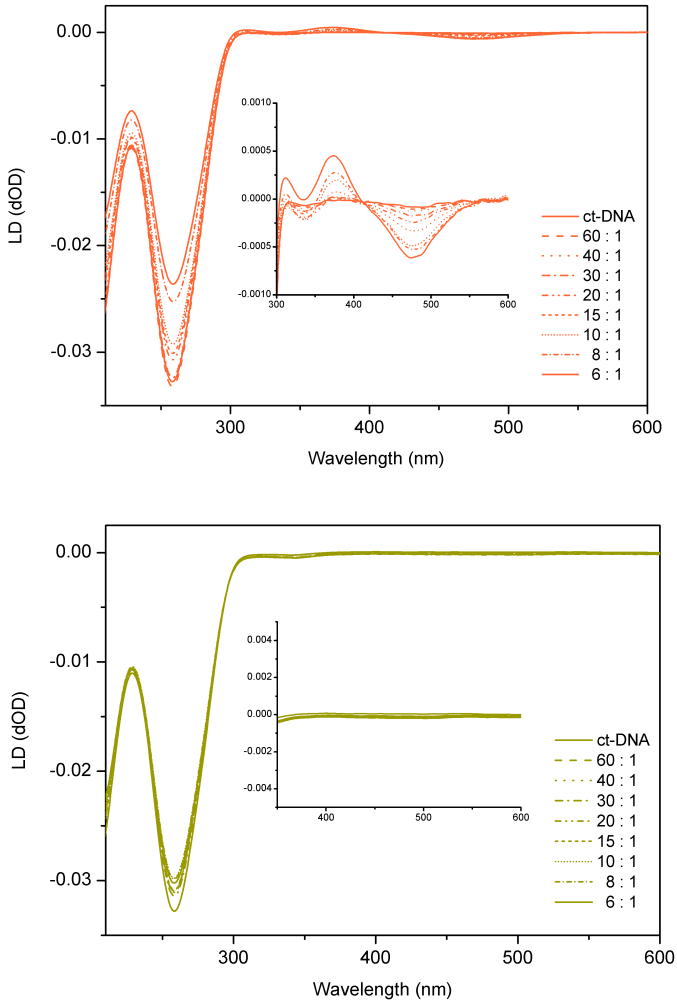

Fig. 5.19 LD spectra of DNA (300 μM, 20 mM NaCl, 1 mM sodium cacodylate) upon addition of complex (top) $[Ru_2L^a(NH_3)_8]Cl_4$, bottom $[RuL^{azpy}(NH_3)_4]Cl_2$. Mixing ratios are indicated as DNA base to complex.

Additions of the dinuclear complex to DNA solution gives rise to an induced LD signal in the 350 – 550 nm region. This indicates that the compound binds the DNA in a specific orientation(s). This effect is not observed for the mononuclear complex. However, in both cases a loss of the magnitude of the signal in the DNA region (260 nm) upon addition of the compound(s) is observed that indicates a loss in orientation of the DNA. This is consistent with coiling/bending of the biomolecule or an increase in its flexibility, but this effect is much weaker

for the mononuclear complex. Nevertheless, the loss of the signal (in the absence of DNA precipitation) is confirmation that the mononuclear compound does bind to the DNA. The weaker effect could reflect a lower coiling/bending efficacy or the expected lower binding constant or both.

5.2.2.4 DNA thermal denaturation

DNA thermal denaturation experiments involve analysis of the DNA absorption under heating and cooling conditions. When the temperature increases the hydrogen bonding between the strands is interrupted, base-stacking is lost and consequently DNA strands become separated. This results in the hyperchromic effect, where the UV absorption of the DNA increases and this can be monitored by UV-Vis spectroscopy. The melting temperature, the T_m, is the midpoint at which half of the DNA is denatured into single strands and half remains in a double helical state (Fig. 5.20).

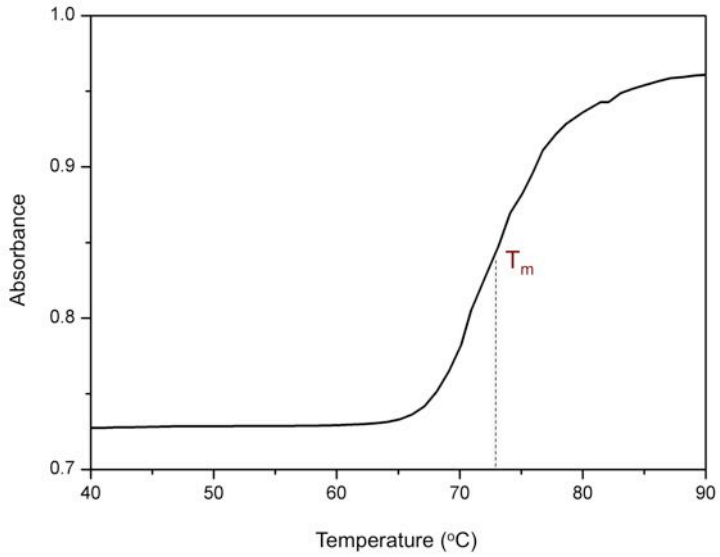

Fig. 5.20 Thermal denaturation profile of ct-DNA (20 mM NaCl, 1 mM sodium cacodylate).

When the small molecule binds to the DNA the strand separation is often reduced and the DNA duplex stabilised. This in turn gives rise to higher DNA melting temperatures.

The effect of temperature on the stability of the ct-DNA-compound complex was investigated. The profiles of thermal denaturation of DNA in the presence and absence of the compounds show that the interacting drugs stabilize the duplex DNA. The stabilization effect(s) seems to be much stronger for the dinuclear complex compared to the mononuclear analogue. On addition of $[Ru_2L^a(NH_3)_8]Cl_4$ to a ct-DNA solution (100 μM, 20 mM NaCl, 1 mM sodium cacodylate) the DNA melting temperature (T_m) was found to increase from 2^oC at the ratio 40 : 1 (DNA base: complex) to 7^oC at the ratio 5 : 1. However, a much weaker stabilization effect was observed for the mononuclear $[RuL^{azpy}(NH_3)_4]Cl_2$, where the T_m changes were smaller than 1^oC even at the highest used ratio 5 : 1 (DNA base : complex) (Table 5.1).

Complex concentration (μM)	**ΔT_m (^oC)**	
	$[Ru_2L^a(NH_3)_8]Cl_4$	**$[RuL^{azpy}(NH_3)_4]Cl_2$**
2.5	2	<1
5	4	<1
10	6	<1
20	7	<1

Table 5.1 ΔT_m of ct-DNA in the presence of Ru(II) complexes

5.2.2.5 Agarose gel electrophoretic mobility shift assay

To explore whether the compounds can interfere with the DNA supercoiling, agarose gel electrophoresis experiments with negatively supercoiled DNA were performed. Fig. 5.21 displays electrophoresis gels in which a mixture of relaxed and negatively supercoiled pBR322 plasmid DNA was treated with increasing amounts of ruthenium complexes (left to right). However, in both cases no unwinding of supercoiled DNA was observed in the tested range of concentrations.

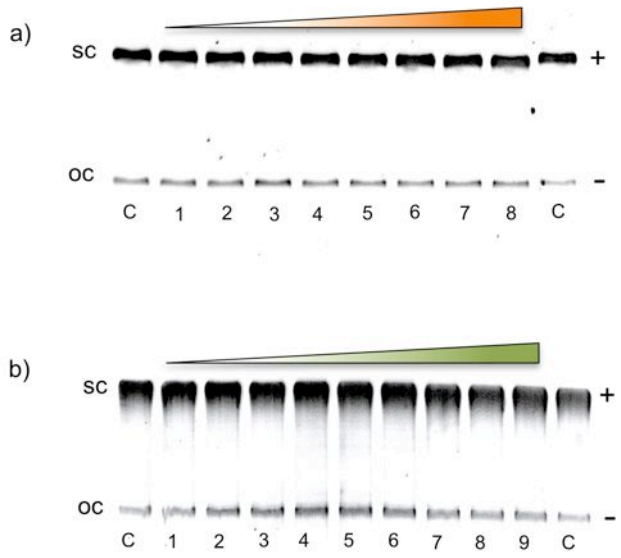

Fig. 5.21 Agarose gel electrophoresis of circular plasmid pBR322 after 30 min of incubation with increased amount of complex a) $[Ru_2L^a(NH_3)_8]Cl_4$, lanes 1-8, r_b = 0.033, 0.05, 0.063, 0.083, 0.1, 0.125, 0.167, 0.25; b) $[RuL^{azpy}(NH_3)_4]Cl_2$, lanes 1-9, r_b = 0.025, 0.033, 0.05, 0.063, 0.083, 0.1, 0.125, 0.167, 0.25; C-control, sc – supercoiled DNA, oc – open circular DNA.

5.2.3 Cell tests

Both complexes were also investigated for their antiproliferative properties in human cancer cell lines. Compounds were tested *in vitro* in breast cancer cells (MDA-MB-231, T47-D) using cell viability assay (MTT). However,

the initial studies of the cytotoxicity of both compounds indicated that the compounds were not active against tested cell lines (IC_{50} > 100).

5.3 General discussion, conclusions and further work

The above DNA binding studies of Ru-NH_3 complexes show that both compounds interact with DNA. However, $[Ru_2L^a(NH_3)_8]^{4+}$ shows a greater binding effect than its mononuclear analogue. This can be a consequence of a number of factors. The larger hydrophobic surface and the higher charge of the dinuclear complex has presumably considerable impact on the strength of the attractive forces between the complex and DNA and thus might be determining the binding affinity of the drug towards biomolecule. Nevertheless, the greater amount of ammonia ligands can also contribute to the overall binding affinity of the complex by direct hydrogen bonding with bases and/or the phosphate backbone. The size and shape of the binding molecule probably also can play a significant role in the recognition process.

In conclusion, three new ruthenium complexes based on ammine and azopyridine moieties have been prepared and characterised. The binding studies of the $[Ru_2L^a(NH_3)_8]^{4+}$ and $[RuL^{azpy}(NH_3)_4]^{2+}$ showed that the dinuclear, higher charged compound has a greater effect on the DNA structure than its mononuclear analogue. Both complexes interact with DNA causing coiling/bending of the biomolecule and stabilize the duplex DNA at high temperatures while the structures of the complexes themselves seem to be unaltered upon interaction. However, the effects on DNA structure are less than those of the literature ammine complexes and cylinders indicating that, at

least within these compounds studied herein, a combination of their two individual effects is not achieved. Consistent with this, neither compound was active in breast cancer cell lines.

Therefore, the work indicates that retaining the multistrand cylinder shape is crucial for the cylinder-like activity and that also the presence of an intercalator is important in the activity of metal-mixed ammine diimine complexes.

Further work on these systems should include testing the above compounds for their photoactive properties. Following this approach, the dinuclear double stranded compounds with azopyridine linking ligands and ammine co-ligands should be prepared and tested for their biomolecule binding properties and activities in cancer cells.

5.4 References

[1] K. Igarashi, K. Kashiwagi, *Int. J. Biochem. Cell Biol.*, *42*, 39.

[2] E. LÿVaas, S. Helmut, in *Adv. Pharmacol., Vol. 38*, Academic Press, **1996**, pp. 119.

[3] T. J. Thomas, U. B. Gunnia, T. Thomas, *J. Biol. Chem.* **1991**, *266*, 6137.

[4] A. Rodger, K. J. Sanders, M. J. Hannon, I. Meistermann, A. Parkinson, D. S. Vidler, I. S. Haworth, *Chirality* **2000**, *12*, 221.

[5] R. V. Gessner, G. J. Quigley, A. H. J. Wang, G. A. Van der Marel, J. H. Van Boom, A. Rich, *Biochemistry* **1985**, *24*, 237.

[6] D. Bharanidharan, S. Thiyagarajan, N. Gautham, *Acta Crystallogr. F* **2007**, *F63*, 1008.

[7] P. U. Maheswari, M. Palaniandavar, *Inorg. Chim. Acta* **2004**, *357*, 901.

[8] P. U. Maheswari, M. Palaniandavar, *J. Inorg. Biochem.* **2004**, *98*, 219.

[9] T. N. Singh, C. Turro, *Inorg. Chem.* **2004**, *43*, 7260.

[10] M. A. Matlib, Z. Zhou, S. Knight, S. Ahmed, K. M. Choi, J. Krause-Bauer, R. Phillips, R. Altschuld, Y. Katsube, N. Sperelakis, D. M. Bers, *J. Biol. Chem.* **1998**, *273*, 10223.

[11] S. Komeda, T. Moulaei, K. K. Woods, M. Chikuma, N. P. Farrell, L. D. Williams, *J. Am. Chem. Soc.* **2006**, *128*, 16092.

[12] A. L. Harris, X. H. Yang, A. Hegmans, L. Povirk, J. J. Ryan, L. Kelland, N. P. Farrell, *Inorg. Chem.* **2005**, *44*, 9598.

[13] M. J. Clarke, F. Zhu, D. R. Frasca, *Chem. Rev.* **1999**, *99*, 2511.

[14] M. J. Clarke, *Coord. Chem. Rev.* **2002**, *232*, 69.

[15] P. Som, Z. H. Oster, K. Matsui, G. Gugliemi, B. Persson, M. L. Pellettieri, S. C. Srivastava, P. P. Richards, H. L. Atkins, A. B. Brill, *Eur. J. Nucl. Med.* **1983**, *8*, 491.

[16] A. H. Velders, H. Kooijman, A. L. Spek, J. G. Haasnoot, D. de Vos, J. Reedijk, *Inorg. Chem.* **2000**, *39*, 2966.

[17] A. C. G. Hotze, B. M. Kariuki, M. J. Hannon, *Angew. Chem. Int. Ed.* **2006**, *45*, 4839.

[18] L. J. Childs, *PhD Thesis, University of Warwick* **2003**.

[19] M. Pascu, *PhD Thesis, University of Birmingham* **2007**.

[20] R. A. Krause, K. Krause, *Inorg. Chem.* **1980**, *19*, 2600.

[21] S. J. Dougan, M. Melchart, A. Habtemariam, S. Parsons, P. J. Sadler, *Inorg. Chem.* **2006**, *45*, 10882.

6

Experimental

6.1 General

All starting materials were purchased from Sigma Aldrich, Fluorochem or Acros Organics and used without further purification. NMR spectra were recorded on a Bruker AVIII300, AVIII400 or AV500 NMR spectrometer. UV-Vis spectra were recorded on a Cary 5000 Varian spectrophotometer using quartz cuvettes and far UV grade solvents. Fluorescence spectra were obtained using Shimadzu RF-5301 PC spectrofluorimeter. Electrospray Ionisation (ES) and High Resolution MS (HRMS) analyses were performed on a Micromass LCT Time of Flight mass spectrometer in positive ionisation mode. Microanalyses were carried out on a Leeman Labs CE44 CHN analyser. Infrared spectra were recorded using a Perkin Elmer Spectrum 100 FTIR spectrometer as neat films.

6.2 Syntheses

6.2.1 Synthesis of *cis*-$[Ru(DMSO)_4Cl_2]$

The compound was prepared by slight modification of a procedure described by Evans *et al.* [1]

$RuCl_3 \cdot xH_2O$ (1.1 g) was added to DMSO (10 mL) and the mixture was heated to reflux and then maintained at reflux for 5 min. The dark brown solution was allowed to stand and cooled to room temperature, when acetone (10 mL) was added and the mixture was left overnight in an open beaker in the fume cupboard at room temperature. The yellow hexagonal crystals that formed were filtered off, washed with ice-cold acetone, diethyl ether and dried in *vacuo*. Yield (1.2 g, 59 % for x=3)

EA (%): Found: C: 20.1, H: 4.9; Calc. for $Ru(C_2H_6SO)_4Cl_2$: C: 19.8, H: 5.0

IR, ν (cm^{-1}): 3008 (w), 1603 (m), 1525 (m), 1441 (m), 1340 (m), 1305 (m), 1209 (w), 1112 (s), 1084 (s), 1018 (s), 991 (s), 961 (s), 931 (s), 843 (m), 791 (m), 717 (m), 675 (s).

6.2.2 Synthesis of L

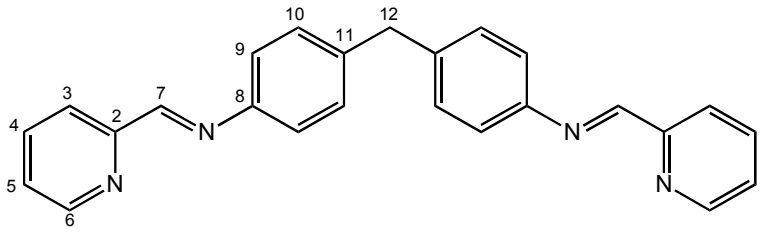

$C_{25}H_{20}N_4$

FW: 376.5

The compound was prepared as described by Painting.[2, 3]

Pyridine-2-carboxaldehyde (0.214 g, 2.0 mmol) and 4,4'-methylenedianiline (0.198 g, 1.0 mmol) were stirred in ethanol (50 mL) at room temperature for 4h. The resulting white-cream precipitate was collected by vacuum filtration, washed with ethanol (20 mL) and dried *in vacuo.* Yield (0.31 g, 82 %)

^{1}H NMR (400MHz, $CDCl_3$) δ = 8.71 (ddd, J = 4.8, 1.6, 0.9 Hz, 1H, H_6), 8.63 (s, 1H, H_7), 8.20 (d, J = 7.9 Hz, 1H, H_3), 7.79 (td, J = 7.7, 1.5 Hz, 1H, H_4), 7.35 (ddd, J = 7.5, 4.8, 1.2 Hz, 1H, H_5), 7.27 (s, 4H, $H_{9/10}$), 4.04 (s, 1H, H_{12})

^{13}C NMR (400 MHz, $CDCl_3$) δ = 160.05 (C_7), 154.69 (C_2), 149.7 (C_6), 149.05 (C_8), 139.76 (C_{11}), 136.63 (C_4), 129.7 ($C_{9/10}$), 125.04 (C_5), 121.86 (C_3), 121.41 ($C_{9/10}$), 41.08 (C_{12})

MS (ES+, $CHCl_3$) *m/z* = 399.1 $[M + Na]^+$

EA (%): Found: C: 80.0, H: 5.3, N: 14.9; Calc. for $C_{25}H_{20}N_4$: C: 79.8, H: 5.4, N: 14.9.

IR, ν (cm^{-1}): 3062 (w), 1625 (m), 1581 (m), 1566 (m), 1503 (m), 1466 (m), 1433 (s), 1348 (w), 1198 (w), 1147 (m), 1089 (w), 990 (m), 881 (m), 827 (s), 817 (s), 741 (s), 783 (s), 651 (m), 616 (s), 578 (s).

6.2.3 Synthesis of $[Ru_2L_3]Cl_4$

The compound was prepared and purified by modification of the literature procedure described by G. *Pascu et al.* [4]

Method 1

cis-$[Ru(DMSO)_4Cl_2]$ (0.242 g, 0.50 mmol) and ligand L (0.282 g, 0.75 mmol) in ethylene glycol (35 mL) in a 50 mL Schlenk flask were placed in a preheated 200^oC oil bath and the reaction mixture was stirred at reflux under argon atmosphere for 6 days when a dark orange solution was formed. The solution was cooled down to room temperature and a saturated aqueous solution of NH_4PF_6 (10 mL) was added. The dark brown precipitate that formed was filtered off, washed with water (200 mL) and vacuum dried. The precipitate was dissolved in CH_3CN (20 mL) and diethyl ether (150 mL) was added. The precipitate was filtered off, washed with water and diethyl ether and dried in vacuum. The crude was purified by column chromatography using silica gel and 5-15 mM NH_4PF_6 in CH_3CN/H_2O (3:1). The compound was eluted as a second intensive orange band following the small pink/orange band, which was discarded. The corresponding chloride salt of the complex was obtained by anion metathesis with n-tetrabutylammonium chloride. Yield (41 mg, 11 %)

An alternative method of purification involved the positive ion exchange chromatography on the Sephadex C-50 (Sigma Aldrich).

Sephadex was swell overnight in H_2O and then packed onto a column to form a surface of 25 mm/250 mm. Crude compound was dissolved in H_2O and ten loaded onto a column. Once the solution was loaded, the column was washed with H_2O until no more colour was observed and then washed/eluted with aqueous solutions of NaCl (0.05, 0.1, 0.4, 0.4, 0.8 M). The pure compound was eluted with 0.4 M aq. NaCl and further desalted using C-18 Sep-Pak cartridges (Waters). Yield (59 mg, 16 %)

^{1}H NMR (400 MHz, MeOD) δ = 9.00 (s, 1H, H_7), 8.60 (d, J = 7.4, 1H, H_3), 8.41 (td, J = 7.7, 1.5, 1H, H_4), 7.90 - 7.78 (m, 2H, $H_{5\&6}$), 7.08 (d, J = 7.3, 2H, H_{Ph}), 5.79 (d, J = 8.5, 2H, H_{Ph}), 4.09 (s, 1H, H_{12})

^{13}C NMR (400 MHz, MeOD) δ = 171.9 (C_7), 158.1 ($C_{2/8}$), 153.9 (C_6), 150.4 ($C_{2/8}$), 143.0 (C_{11}), 140.2 (C_4), 132.3 (C_3), 131.4 (C_{Ph}), 131.2 (C_5), 122.5 (C_{Ph}), 40.6 (C_{12})

MS (ES+, MeOH) *m/z* = 333.1 $[Ru_2L_3]^{4+}$, 444.0 $[Ru_2L_3]^{3+}$, 683.7 $[Ru_2L_3]Cl^{2+}$, 701.2 $[Ru_2L_3]Cl_2^{2+}$

EA (%): Found: C: 46.4, H: 3.2, N: 8.7, Calc. for $Ru_2C_{75}H_{60}N_{12}P_4F_{24}(H_2O)$: C: 46.7, H: 3.2, N: 8.7

EA (%): Found: C: 61.4, H: 4.1, N: 11.3, Calc. for $Ru_2C_{75}H_{60}N_{12}Cl_4$: C: 61.1, H: 4.1, N: 11.4

IR, ν (cm^{-1}): 2960 (m), 1608 (w), 1550 (w), 1501 (m), 1469 (m), 1437 (m), 1254 (w), 1206 (m), 1109 (w), 1017 (w), 865 (w), 817 (w), 781 (s), 748 (s), 654 (s)

Crystal structure data for $C_{75}H_{60}N_{12}Ru_2$, 4Cl, 6(H_2O), M = 1581.39, Cubic, a = 25.7546(5) Å, b = 25.7546(5) Å, c = 25.7546(5) Å, β = 90°, U = 17083.0(6) Å^3, T = 120 (2) K, space group $I2_13$, Z = 8, 22771 reflections measured, 5010 unique

(R_{int} = 0.0453) which were used in all calculations. Final *R*-indices (I>2σ(I)): *R1* = 0.0752, *wR2* = 0.2241.

Method 2

cis-[Ru(DMSO)$_4$Cl$_2$] (0.242 g, 0.50 mmol) and ligand L (0.282 g, 0.75 mmol) in ethylene glycol (35 mL) were placed in a microwaveable sealed vessel and reacted using microwave energy during 3-4 1h long cycles at 180^{o}C (60% of 400W in pressure vessel). The solution was cooled down to room temperature and a saturated aqueous solution of NH_4PF_6 (20 mL) was added. The dark brown precipitate that formed was filtered off, washed with water (200 mL) and vacuum dried. The precipitate was dissolved in a minimum amount of CH_3CN (10 mL) and the crude was re-precipitated with diethyl ether (100 mL). The precipitate was filtered off, washed with diethyl ether and dried *in vacuo*. The crude was purified by column chromatography on a silica gel stationary phase and 5-15 mmol solution of NH_4PF_6 in CH_3CN/H_2O (3:1) as an eluent. The compound was eluted as a second intensive orange band. The corresponding chloride salt of the complex was obtained by anion metathesis with n-Bu_4NCl. Yield (45 mg, 12 %)

6.2.3.1 Separation of optical isomers of $[Ru_2L_3]Cl_4$

Cellulose (~ 20 μm, Sigma Aldrich) was mixed with 0.2 M aq. solution of NaCl to form a slurry. The packing was performed by pouring the slurry onto a column (19 x 250 mm) and applying pressure from a peristaltic pump. A total column length of ~ 200 mm was prepared and the excess solvent was eluted.

The analytically pure racemic mixture of $[Ru_2L_3]Cl_4$ (15 mg) was dissolved in 0.2 M aq. NaCl (3 mL) and loaded on top of a column. Elution with 0.2 M aq. NaCl with applied pressure on top of the column afforded formation of two distinct orange bands. The two separate fractions were collected. Each fraction was desalted by loading onto C18 Sep-Pak cartridges (Waters), washed with H_2O (~ 200 mL each) and further eluted with MeOH (10 mL). The solutions were concentrated and addition of diethyl ether afforded brown precipitates, which were filtered off, washed with diethyl ether and dried *in vacuo*. The two samples were analyzed by UV-Vis and CD spectroscopy (See chapter 3) and further enantiopurity was confirmed by NMR studies with Δ-TRISPHAT (See chapter 4).

6.2.4 Synthesis of L^o

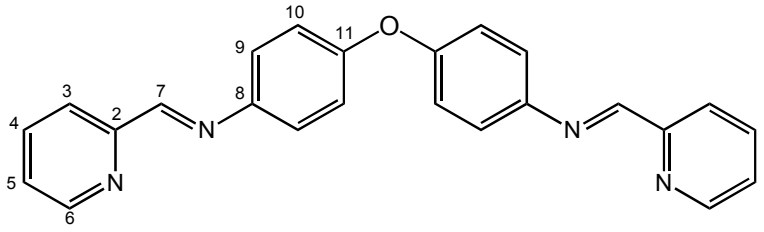

$C_{24}H_{18}N_4O$

FW: 378.4

Ligand L^o was prepared according to the previously published method.[5]

Pyridine-2-carboxaldehyde (0.430 g, 4 mmol) and 4,4'-diaminodiphenyl ether (0.400g, 2 mmol) were stirred at reflux in EtOH (50 mL) for 4h. The solution was cooled down and the volume was reduced to half when pale yellow solid precipitated. The solid was filtered off, washed with cold ethanol (50 mL) and dried in vacuum. Yield (0.62 g, 82 %)

^{1}H NMR (400 MHz, $CDCl_3$) δ = 8.72 (ddd, J = 4.9, 1.6, 0.9 Hz, 1H, H_6), 8.65 (s, 1H, H_7), 8.21 (dt, J = 7.8, 0.9 Hz, 1H, H_3), 7.81 (td, J = 7.7, 1.5 Hz, 1H, H_4), 7.40 - 7.32 (m, 3H, $H_{5, 9/10}$), 7.10 (d, J = 8.9 Hz, 2H, $H_{9/10}$)

^{13}C NMR (400 MHz, $CDCl_3$) δ = 159.6 (C_7), 156.3 (C_{11}), 154.7 (C_2), 149.7 (C_6), 146.2 (C_8), 136.6 (C_4), 125.0 (C_5), 122.8 ($C_{9/10}$), 121.8 (C_3), 119.5 ($C_{9/10}$)

MS (ES+, $CHCl_3$) m/z = 401.2 $[M + Na]^+$

EA (%): Found: C: 76.4, H: 4.7, N: 14.6; Calc. for $C_{24}H_{18}N_4O$: C: 76.2, H: 4.8, N: 14.8

IR, ν (cm^{-1}): 3048 (w), 1623 (m), 1581 (m), 1566 (m), 1493 (s), 1433 (m), 1344 (m), 1274 (m), 1238 (s), 1195 (s), 1110 (m), 1089 (w), 1046 (m), 993 (m), 959 (m), 858 (s), 830 (s), 775 (s), 742 (s), 715 (m), 616 (m), 582 (m).

6.2.5 Synthesis of $[Ru_2L^o_3]Cl_4$

cis-$[Ru(DMSO)_4Cl_2]$ (0.20 g, 0.41 mmol) and L^o (0.23 g, 0.62 mmol) were placed in a flask containing ethylene glycol (15 mL) and the flask was placed into a hot oil bath (200 ^oC). The reaction mixture was stirred and heated under reflux for 7 days leading to a brown/orange solution. After cooling the solution was loaded directly onto a silica gel column. The compound was eluted with CH_3CN/H_2O with NH_4PF_6 to give an initial crude separation. The eluted orange band was concentrated, desalted from NH_4PF_6, washed with H_2O and diethyl ether and dried in *vacuo*. The crude mixture was then placed onto a fresh silica gel column. The compound was eluted with gradient 5 to 15 mM NH_4PF_6 in CH_3CN/H_2O (1:3) as a second orange band following the initial red band, which was discarded (from colour and NMR suspected some double-stranded

complexes). The chloride salt of the compound was obtained by anion metathesis using t-Bu_4NCl. Yield (26 mg, 8 %)

Crystals suitable for X-ray analysis were obtained by slow diffusion of diethyl ether into CH_3CN solution of the compound at 4°C.

^1H NMR (300 MHz, MeOD) δ = 9.04 (s, 1H, H_{im}), 8.59 (d, J = 7.2 Hz, 1H, H_3), 8.39 (td, J = 7.8, 1.3 Hz, 1H, H_4), 7.83 (dd, J = 9.8, 3.6 Hz, 1H, H_5), 7.73 (d, J = 4.9 Hz, 1H, H_6), 6.93 (br, 2H, H_{Ph}), 5.97 (d, J = 8.9 Hz, 2H, H_{Ph})

^1H NMR (300 MHz, CD_3CN) δ = 8.76 (s, 1H, H_{im}), 8.48 (d, J = 7.4, 1H, H_3), 8.32 (t, J = 7.3, 1H, H_4), 7.75 (t, J = 6.8, 1H, H_5), 7.62 (d, J = 5.0, 1H, H_6), 6.85 (br, 2H, H_{Ph}), 5.92 (d, J = 8.7, 2H, H_{Ph})

MS ES+ *m/z* (CH_3CN): 334.3 $[Ru_2L^o_3]^{4+}$, 494.4 $[Ru_2L^o_3](PF_6)^{3+}$, 813.6 $[Ru_2L^o_3](PF_6)_2^{2+}$

MS (ES+, CH_3OH) *m/z* = 334.6 $[Ru_2L^o_3]^{4+}$, 457.5 $[Ru_2L^o_3]Cl^{3+}$

UV-Vis (H_2O) λ max/nm, (ε /dm^3 mol^{-1} cm^{-1}): 270 (75 000), 322 (33 300), 445 (15 600), 485 (21 500)

IR, ν (cm^{-1}): 3330 (m, br), 1589 (m), 1489 (s), 1438 (m), 1232 (s), 1198 (s), 1163 4 (m), 866 (m), 835 (m), 767 (m), 575 (s), 565 (s)

Crystal structure data for $C_{72}H_{54}N_{12}O_3Ru_2$, 4($PF_6$), 0.5($C_4H_{10}O$), 1.5($CH_3NO_2$), 0.5($C_2H_3N$), H_2O, M = 2084.46, Orthorhombic, a = 20.948(3) Å, b = 23.018(3) Å, c = 36.845 (4) Å, β = 90 (?)°, U = 17766(4) $Å^3$, T = 120 (2) K, space group *Pbca*, Z = 8, 56287 reflections measured, 14615 unique (R_{int} = 0.1040) which were used in all calculations. Final R-indices (I>2σ(I)): *R1* = 0.1880, *wR2* = 0.3931.

6.2.6 Synthesis of $L^{2\text{-im}}$

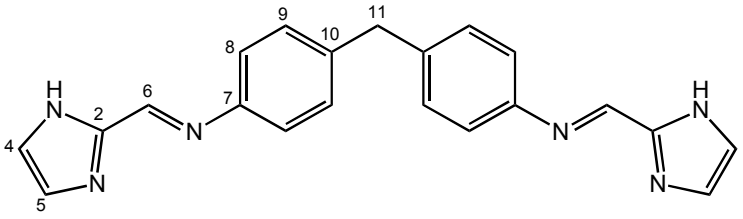

$C_{21}H_{18}N_6$

FW: 354.4

The ligand was synthesized following the literature procedure.[6]

Imidazole-2-carboxaldehyde (0.384 g, 4 mmol) and 4,4'-methylenedianiline (0.396 g, 2 mmol) were stirred in methanol (30 mL) and two drops of glacial acetic acid were added. The mixture was further stirred under reflux for 2 h. An off-white solid that precipitated was collected by filtration, washed with methanol and dried *in vacuo.* Yield (0.68 g, 96 %)

^{1}H NMR (400 MHz, d_6-DMSO) δ = 13.05 (s, 1H, H_{NH}), 8.41 (s, 1H, H_6), 7.45 - 7.05 (m, 6H, $H_{4,5,8,9}$), 3.99 (s, 1H, H_{10})

^{13}C NMR (400 MHz, d_6-DMSO) δ = 149.88 (C_6), 148.68 (C_7), 144.95 (C_{10}), 139.42 (C_7), 130.67 (C_4), 129.57 ($C_{8/9}$), 121.11 ($C_{8/9}$), 120.13 (C_5), 40.07 (C_{11}).

MS (ES+, DMSO) *m/z* = 377.2 $[M + Na]^+$

EA (%): Found: C: 71.1, H: 4.9, N: 23.6; Calc. for $C_{21}H_{18}N_6$: C: 71.2, H: 5.1, N: 23.7

IR, ν (cm^{-1}): 3048 (w), 1624 (m), 1581 (w), 1493 (m), 1433 (m), 1238 (m), 1196 (m), 1110 (m), 1047 (w), 993 (m), 858 (m), 830 (s), 774 (s), 756 (s), 743 (s), 716 (m), 617 (m).

6.2.7 Synthesis of $[Ru_2L^{2\text{-im}}{}_3]Cl_4$

cis-$[Ru(DMSO)_4Cl_2]$ (0.273 g, 0.564 mmol) and $L^{2\text{-im}}$ (0.300 g, 0.846 mmol) in ethylene glycol (35 mL) were stirred at reflux under argon atmosphere for 6 days. After cooling to room temperature a saturated aqueous solution of NH_4PF_6 was added (10 mL) and the solution was left overnight in the fridge. The brown solid was filtered off, washed with water (300 mL) and diethyl ether and dried *in vacuo*. The crude was then dissolved in CH_3CN (10 mL) and re-precipitated with Et_2O. The precipitate was filtered off washed with Et_2O and dried *in vacuo*. The crude compound was then placed in 500 ml beaker and EtOH was added (400 mL). This was stirred at room temperature for 1 hour. The solution was filtered off and the orange filtrate was concentrated under reduced pressure. The concentrated solution was then loaded onto a fresh silica gel column. The pure compound was eluted as a second orange band with 5 mM NH_4PF_6 in CH_3CN. Yield (1.7 mg, 1 %)

Brown/orange crystals of the hexafluorophosphate salt suitable for X-Ray analysis were obtained by slow diffusion of diethyl ether into a CH_3CN solution of compound.

^{1}H NMR (400 MHz, CD_3CN) δ = 11.98 (s, 1H, H_{NH}), 8.37 (s, 1H, H_{im}), 7.69 (dd, *J* = 2.8, 1.4 Hz, 1H, H_4), 6.93 (d, *J* = 8.0 Hz, 2H, H_{Ph}), 6.73 (t, *J* = *1.2, 0.9* Hz, 1H, H_5), 5.79 (d, *J* = 8.5 Hz, 2H, H_{Ph}), 4.01 (s, 1H, H_{CH2})

MS ES+(CH_3CN) *m/z* = 316.5 $[Ru_2L^{2\text{-im}}{}_3]^{4+}$, 632.5 $[Ru_2L^{2\text{-im}}{}_3]^{2+}$

UV-Vis (H_2O) *λ* max/nm, (ε/dm^3 mol^{-1} cm^{-1}): 297 (48 300), 470 (24 100)

IR, ν (cm^{-1}): 3025 (m, br), 1627 (w), 1536 (m), 1502 (m), 1433 (s), 1335 (m), 1259 (w), 1194 (m), 1008 (s), 1016 (m), 895 (m), 860 (m), 762 (s), 709 (m)

Crystal structure data for $C_{63}H_{54}N_{18}Ru_2$, $4(PF_6)$, $4(C_2H_6OS)$, $4(H_2O)$, M = 2229.84, Monoclinic, a = 34.894(2) Å, b = 13.3476(4) Å, c = 23.2616(12) Å, β = 125.597(2)°, U = 8809.6(7) Å^3, T = 120 (2) K, space group $C\ 2/c$, Z = 4, 35588 reflections measured, 9016 unique (R_{int} = 0.0918) which were used in all calculations. Final R-indices (I>2σ(I)): $R1$ = 0.0735, $wR2$ = 0.1681.

6.2.8 Synthesis of $L^{4(5)\text{-im}}$

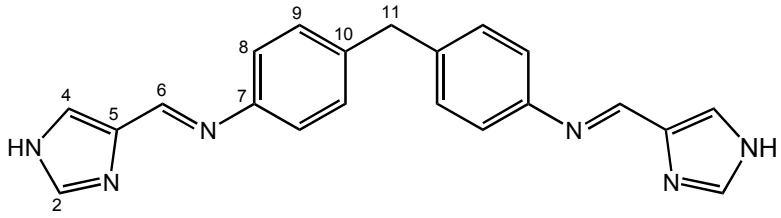

$C_{21}H_{18}N_6$

FW: 354.4

The compound was prepared following the literature procedure.[7]

4(5)-imidazolecarboxaldehyde (0.288 g, 3.0 mmol), 4,4'-methylenedianiline (0.300 g, 1.5 mmol) and 1 drop of glacial acetic acid were stirred at reflux in methanol (30 mL) for 2h. An off-white solid that precipitated was collected by vacuum filtration, washed with methanol (30 mL) and dried *in vacuo*. Yield (0.52 g, 97 %)

^{1}H NMR (400 MHz, d_6-DMSO) δ = 12.8 (s, 1H, H_{NH}), 8.43 (s, 1H, H_6), 7.82 (s, 1H, $H_{2/4}$), 7.62 (s, 1H; $H_{2/4}$), 7.22 (d, J = 7.8 Hz, 2H, $H_{8/9}$), 7.16 (d, J = 7.8 Hz, 2H, $H_{8/9}$), 3.98 (s, 1H, H_{11})

^{13}C NMR: compound not soluble enough

MS (ES+, DMSO) m/z = 377.2 $[M + Na]^+$

EA (%): Found: C: 70.9, H: 5.2, N: 23.7; Calc. for $C_{21}H_{18}N_6$: C: 71.2, H: 5.1, N: 23.7

IR, ν (cm^{-1}): 1350 (w), 1625 (m), 1581 (m), 1494 (s), 1433 (m), 1345 (w), 1239 (s), 1225 (m), 1197 (s), 1110 (m), 1091 (m), 1047 (w), 994 (m), 974 (m), 859 (m), 830 (s), 775 (s), 716 (m), 618 (s).

6.2.9 Synthesis of $[Ru_2L^{4(5)\text{-im}}{}_3]Cl_4$

cis-$[Ru(DMSO)_4Cl_2]$ (0.273 g, 0.564 mmol) and $L^{4(5)\text{-im}}$ (0.300 g, 0.846mmol) were placed in the flask containing ethylene glycol (20 mL) and the flask was placed into a hot oil bath (200 ^oC). The reacting mixture was stirred under reflux for 6 days when the brown/orange solution formed. After cooling the saturated aqueous solution of NH_4PF_6 (10 mL) was added and the precipitate that formed was filtered off, washed with water (200 mL) and dried in *vacuo*. The crude was then dissolved in CH_3CN (10 mL) and reprecipitated with diethyl ether. The dark brown solid was filtered off, washed with diethyl ether and dried in *vacuo*. The compound was extracted with ethanol and further purified on the fresh silica gel column with CH_3CN/15mM aq NH_4PF_6 (3:1). The pure compound was eluted as a second orange band. The counterion was then exchanged to chloride using t-Bu_4NCl. Yield (1.9 mg, 1 %)

^1H NMR (300 MHz, MeOD) δ = 8.42 (s, 1H, H_6), 8.25 (s, 1H, $H_{4/2}$), 7.59 (s, 1H, $H_{4/2}$), 6.94 (d, *J* = 7.6, 1H, $H_{8/9}$), 5.76 (d, *J* = 8.0, 1H, $H_{8/9}$), 3.98 (s, 1H, H_{11})

MS ES+ (MeOH) *m/z* = 316.4 $[Ru_2L^{4(5)\text{-im}}{}_3]^{4+}$, 421.9 $[Ru_2L^{4(5)\text{-im}}{}_3 - H]^{3+}$, 632.2 $[Ru_2L^{4(5)\text{-im}}{}_3 - 2H]^{2+}$

UV-Vis (H_2O) λ max/nm, (ε/dm^3 mol^{-1} cm^{-1}): 423 (21 000)

IR, ν (cm^{-1}): 3128 (m, br), 1961 (w), 1673 (s), 1596 (m), 1501 (m), 1279 (m), 1201 (s), 1130 (s), 799 (s), 720 (s).

6.2.10 Synthesis of L^{ox}

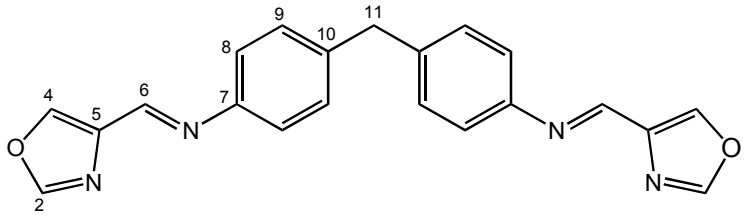

$C_{21}H_{16}N_4O_2$

FW: 356.4

4-oxazolecarboxaldehyde (0.097 g, 1 mmol) and 4,4'-methlenedianiline (0.099 g, 0.5 mmol) were stirred in ethanol (50 mL) at room temperature for 4 hours. The volume was reduced to half and the solution was left in the fridge for 2h. The resultant yellow precipitate that formed was filtered off, washed with ethanol and dried *in vacuo*. Yield (0.114 g, 64 %)

^{1}H NMR (400 MHz, $CDCl_3$) δ = 8.47 (s, 1H, H_6), 8.21 (d, J = 0.6, 1H, $H_{2/4}$), 7.99 (d, J = 0.4, 1H, $H_{2/4}$), 7.27 - 7.18 (m, 4H, $H_{8\&9}$), 4.03 (s, 1H, H_{11})

^{13}C NMR (400 MHz, $CDCl_3$) δ = 151.62 ($C_{2/4}$), 150.30 (C_6), 149.35 (C_{10}), 140.23 ($C_{2/4}$), 139.52 (C_7), 139.22 (C_5), 129.7 ($C_{8/9}$), 121.14 ($C_{8/9}$), 41.01 (C_{11})

MS (ES+): *m/z* = 379.1 $[M + Na]^+$

HRMS (ES+) *m/z*: Found: 379.1158, Calc. for $C_{21}H_{16}N_4O_2Na$: 379.1165

EA (%): Found: C: 70.8, H: 4.5, N: 15.7; Calc. for $C_{20}H_{16}N_4O_2$: C: 70.8, H: 4.5, N: 15.7

IR, ν (cm^{-1}): 3460 (w), 3085 (w), 1727 (w), 1670 (w), 1636 (m), 1574 (w), 1530 (m), 1499 9m), 1430 (w), 1381 (w), 1293 (m), 1238 (m), 1166 (m), 1091 (m), 1050 (m), 1073 (w), 905 (m), 864 (m), 795 (m), 755 (s), 743 (m), 699 9 (m), 613 (s)

mp (^{o}C): 155 – 160.

6.2.11 Synthesis of L^1

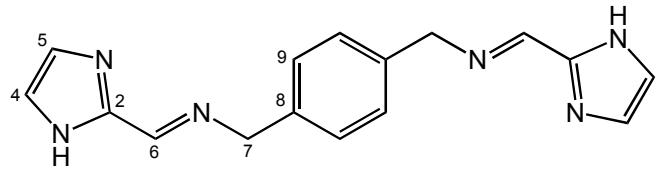

$C_{16}H_{16}N_6$

FW: 292.3

Imidazole-2-carboxaldehyde (0.192 g, 2.0 mmol) and p-xylenediamine (0.136 g, 1.0 mmol) were stirred in methanol (30 ml) for 30 min, 1 drop of glacial acetic acid was added and the reacting mixture was stirred at reflux for further 2 hours. An off white solid that precipitated was collected by vacuum filtration, washed with methanol (20 mL) and dried in *vacuo*. Yield (0.26 g, 89 %)

^{1}H NMR (400 MHz, d_6-DMSO) δ = 12.73 (s, 1H, H_{NH}), 8.31 (s, 1H, H_6), 7.32 (s, 2H, H_9), 7.21 (s, 1H, $H_{4/5}$), 7.08 (s, 1H, $H_{4/5}$), 4.77 (d, J = 1.2, 2H, H_7)

^{13}C NMR: compound not soluble enough

MS (ES+): m/z = 293.2 $[M + H]^+$

EA (%): Found: C: 65.9, H: 5.3, N: 28.8; Calc. for $C_{16}H_{16}N_6$: C: 65.7, H: 5.5, N: 28.8

IR, ν (cm^{-1}): 3009 (w, br), 2883 (w, br), 2770 (w, br), 1645 (s), 1557 (w), 1457 (m), 1444 (s), 1418 (m), 1388 (m), 1348 (m), 1304 (m), 1109 (m), 1044 (m), 1002 (m), 988 (m), 909 (s), 823 (m), 804 (s), 770 (s), 752 (s)

mp (^{o}C): 222 – 234 (decomposition).

6.2.12 Synthesis of L^2

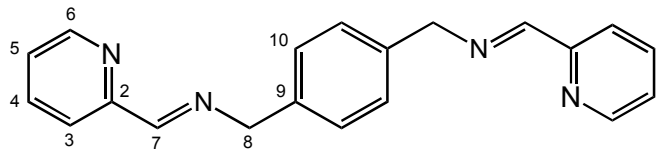

$C_{20}H_{18}N_4$

FW: 314.4

Pyridine-2-carboxaldehyde (0.214 g, 2.0 mmol) and p-xylenediamine (0.136 g, 1.0 mmol) were stirred in ethanol (30 mL) at 60^{o}C for 2h. The solution was cooled down to room temperature and then left in the fridge for 3h. The crystalline material that formed was then re-crystallized from ethanol. The white crystalline compound was filtered off washed with cold ethanol (5 mL) and dried *in vacuo*. Yield (0.21 g, 67 %)

^{1}H NMR (400 MHz, $CDCl_3$) δ = 8.66 (dd, *J* = 4.8, 0.7 Hz, 1H, H_6), 8.50 (s, 1H, H_7), 8.07 (d, *J* = 7.9 Hz, 1H, H_3), 7.75 (t, *J* = 7.7 Hz, 1H, H_4), 7.39 - 7.30 (m, 3H, $H_{5,Ph}$), 4.89 (d, *J* = 0.9 Hz, 2H, H_8)

^{13}C NMR (400 MHz, $CDCl_3$) *δ* = 162.78 (C_6), 154.54 (C_2), 149.38 (C_4), 137.61 (C_9), 136.56 (C_7), 128.46 (C_{10}), 124.82 (C_5), 121.35 (C_3), 64.65 (C_8)

MS (ES+) *m/z* = 337.2 $[M + Na]^+$

HRMS (ES+) *m/z* = Found: 337.1433, Calc. for $C_{20}H_{18}N_4Na$: 337.1424

EA (%): Found: C: 76.5, H: 5.6, N: 17.7; Calc. for $C_{20}H_{18}N_4$: C: 76.4, H: 5.8, N: 17.8

IR, ν (cm^{-1}): 3049 (w), 2903 (w), 1698 (m), 1639 (m), 1587 (m), 1565 (m), 1512 (m), 1470 (m), 1434 (m), 1358 (m), 1322 (m), 1194 (w), 1150 (w), 1090 (w), 1045 (m), 1015 (m), 990 (m), 981 (m), 916 (w), 896 (w), 848 (s), 775 (s), 754 (m), 738 (m), 662 (m), 616 (s), 571 (s)

mp (^{o}C): 122-123.

6.2.13 Synthesis of L[a]

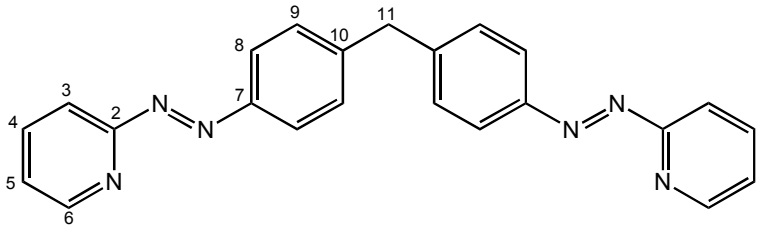

$C_{23}H_{18}N_6$

FW: 378.4

Ligand L was prepared according to literature procedures.[6, 8]

2-Nitrosopyridine (0.24 g, 2.2 mmol) was dissolved in 30 ml of dichloromethane. 4,4'-methylenedianiline (0.20 g, 1.0 mmol) and one drop of glacial acetic acid were added and the orange solution was stirred at room temperature for 2 days. The solvent was evaporated to dryness and the crude product was purified by column chromatography on a silica gel column with $CHCl_3$/MeOH (98/2). Yield (0.26 g, 68 %)

^{1}H NMR (400 MHz, $CDCl_3$) δ = 8.63 (ddd, J = 4.8, 1.8, 0.8, 1H, H_6), 7.92 (d, J = 8.4, 2H, $H_{8/9}$), 7.77 (ddd, J = 7.8, 1.9, 0.6, 1H, H_4), 7.71 (dt, J = 8.1, 1.0, 1H, H_3), 7.32 - 7.25 (m, 3H, $H_{8/9\&5}$), 4.04 (s, 1H, H_{11})

^{13}C NMR (400 MHz, $CDCl_3$) δ = 162.92 ($C_{2/7/10}$), 151.1 ($C_{2/7/10}$), 149.52 (C_6), 144.85 ($C_{2/7/10}$), 136.31 (C_4), 129.79 ($C_{8/9}$), 125.14 (C_5), 123.96 ($C_{8/9}$), 115.52 (C_3), 41.77 (C_{11})

MS (ES+) m/z = 401.2 $[M + Na]^+$

EA (%): Found: C: 73.1, H: 4.3, N: 22.2; C: Calculated for $C_{23}H_{18}N_6$: C: 73.0, H: 4.8, N: 22.2

IR, ν (cm^{-1}): 3063 (w), 1578 (m), 1499 (m), 1461 (m), 1412 (s), 1309 (w), 1218 (w), 1184 (w), 1134 (m), 1110 (m), 1113 (w), 989 (m), 873 (m), 840 (m), 820 (m), 791 (s), 737 (s), 657 (m), 640 (m), 618 (s), 576 (s), 554 (s).

6.2.14 Synthesis of $[Ru_2L^a(NH_3)_8]Cl_4$

$[Ru(NH_3)_5(H_2O)](PF_6)_2$ (100 mg, 0.2 mmol) and L (38 mg, 0.1 mmol) were dissolved in an argon-purged acetone (15 mL) and the reaction mixture was stirred at room temperature under an argon atmosphere for 18h. The solution was filtered off, saturated solution of t-Bu_4NCl (5 mL) was added to the filtrate and the red precipitate was filtered off, washed with acetone (50 mL) and diethyl ether and dried *in vacuo*. Purification was performed on an alumina column with CH_3CN/H_2O 80/20 as an eluent. The compound was eluted as a third band. Yield (56 mg, 62 %)

Crystals suitable for X-Ray analysis (needles) were obtained by slow diffusion of Et_2O into a methanolic solution of the compound.

^1H NMR (300 MHz, MeOD) δ = 8.81 (d, J = 5.3 Hz, 1H, H_6), 8.53 (d, J = 7.7 Hz, 1H, H_3), 8.02 (ddd, J = 7.4, 5.8, 1.4, 1H, H_4), 7.76 (ddd, J = 7.3, 5.9, 1.3, 1H, H_5), 7.70 (d, J = 8.5 Hz, 2H, $H_{8/9}$), 7.62 (d, J = 8.5 Hz, 2H, $H_{8/9}$), 4.30 (s, 1H, H_{11})

MS ES+ (CH_3OH): *m/z* = 250.1 $[Ru_2L^a(NH_3)_8]Cl^{3+}$, 245.2 $[Ru_2L^a(NH_3)_7]Cl^{3+}$, 239.1 $[Ru_2L^a(NH_3)_6]Cl^{3+}$, 233.3 $[Ru_2L^a(NH_3)_5]Cl^{3+}$, 358.4 $[Ru_2L^a(NH_3)_8]^{2+}$

EA (%): Found: C: 31.9, H: 4.7, N: 22.8; Calc. for $Ru(C_{23}H_{18}N_4)(NH_3)_8Cl_4$, C: 32.2, H: 4.9, N: 22.8

UV-Vis (H_2O) λ max/nm, (ε/dm^3 mol^{-1} cm^{-1}): 227 (22900), 333 (20400), 478 (9000).

IR, ν (cm^{-1}): 3141 (s, br), 1623 (s), 1598 (m), 1455 (m), 1280 (s), 1244 (m), 1202 (m), 771 (s), 619 (s)

Crystal structure data for $C_{23}H_{42}N_{14}Ru_2$, 4(Cl), 2(CH_3OH), 0.7(H_2O): M = 935.34, Monoclinic, a = 21.6832 (6) Å, b = 7.4548 (2) Å, c = 25.3399 (7) Å,

β = 94.048 (1)°, *U* = 4085.8 (2) Å^3, *T* = 120 (2) K, space group *P2$_1$/c* (no. 14), *Z* = 4, 59791 reflections measured, 7188 unique (R_{int} = 0.1277) which were used in all calculations. Final *R*-indices (I>2σ(I)): *R1* = 0.0869, *wR2* = 0.1909

Crystal structure data for $C_{23}H_{42}N_{14}Ru_2$, 4(PF_6), 4(H_2O): *M* = 1368.79, Monoclinic, *a* = 16.9517 (9) Å, *b* = 14.4634 (7) Å, *c* = 38.9319 (18) Å, β = 91.194 (3)°, *U* = 9543.2(8) Å3, *T* = 120 (2) K, space group P2(1)/n, *Z* = 8, 73837 reflections measured, 16442 unique (R_{int} = 0.1377) which were used in all calculations. Final *R*-indices (I>2σ(I)): *R1* = 0.0872, *wR2* = 0.1983.

6.2.15 Synthesis of [RuL^a(NH$_3$)$_4$]Cl$_2$

[Ru(NH_3)$_5$(H_2O)](PF_6)$_2$ (100 mg, 0.2 mmol) and L (76 mg, 0.2 mmol) were dissolved in argon-purged acetone (20 mL) and the reaction mixture was stirred at room temperature under argon atmosphere for 18h. A saturated acetone solution of t-Bu_4NCl was added (5 mL) and the formed precipitate was filtered off, washed with acetone (50 mL) and dried *in vacuo*. Purification was performed on an alumina column with CH_3CN/H_2O 80/20 as an eluent. The compound was eluted as a second orange band. Yield (68 mg, 55 %)

Crystals suitable for X-ray analysis were obtained by slow diffusion of Et_2O into a methanolic solution of the compound (crystals of chloride salt) and by slow evaporation of CH_3CN from the mixture H_2O/CH_3CN (crystals of hexafluorophosphate salt).

^{1}H NMR (500 MHz, 300K, MeOD) δ = 8.80 (d, *J* = 5.6 Hz, 1H, H_6), 8.70 (dd, *J* = 4.7, 0.9 Hz, 1H, $H_{6'}$), 8.52 (d, *J* = 8.1 Hz, 1H, H_3), 8.10 (td, *J* = 7.9, 1.7 Hz, 1H, $H_{4'}$), 8.01 (m, 3H, $H_{Ph\&4}$), 7.89 (d, *J* = 8.1 Hz, 1H, $H_{3'}$), 7.75 (ddd, *J* = 6.5,

1.1 Hz, 1H, H_5), 7.67 (d, *J* = 8.4 Hz, 2H, H_{Ph}), 7.62 – 7.55 (m, 5H, $H_{5'\&Ph}$), 4.27 (s, 2H, H_{11});

^{13}C NMR (500 MHz, 300K, MeOD) δ = 171.00 (C_2), 164,00 ($C_{2'}$), 157.72 ($C_{7/7'}$), 152.40 ($C_{7/7'}$), 151.50 (C_6), 150.05 ($C_{6'}$), 147.42 ($C_{10/10'}$), 143.82 ($C_{10/10'}$), 140.71 ($C_{4'}$), 138.51 (C_4), 131.22 ($2C_{Ph}$), 131.11 ($2C_{Ph}$), 127.09 ($C_{5'}$), 124.86 ($2C_{Ph}$), 124.38 (C_5), 124.18 ($2C_{Ph}$), 123.88 (C_3), 115.74 ($C_{3'}$), 42.30 (C_{11})

MS ES^+ (MeOD) *m/z* = 273.8 $[RuL^a(NH_3)_4]^{2+}$, 256.5 $[RuL^a(NH_3)_4]^{2+}$, 240.1 $[RuL^a(NH_3)_2]^{2+}$

IR, ν (cm^{-1}): 2961 (w), 1725 (s), 1515 (m), 1438 (m), 1403 (m), 1300 (m), 1247 (m), 1231 (m), 1181 (m), 1110 (w), 1155 (w), 1030 (w), 971 (w), 829 (m), 800 (m), 787 (m), 775 (m), 716 (w)

Crystal structure data for $C_{23}H_{30}N_{10}O_3Ru$, 2(Cl), 0.25(C_2H_3N), 3(H_2O), *M* = 682.85, Orthorhombic, *a* = 11.6956(2) Å, *b* = 31.2498(8) Å, *c* = 8.4504(2) Å, β = 90°, *U* = 3088.50(12) $Å^3$, *T* = 120(2) K, space group *P cc2*, *Z* = 4, 18785 reflections measured, 4728 unique (R_{int} = 0.0588) which were used in all calculations. Final *R*-indices (I>2σ(I)): *R1* = 0.0577, *wR2* = 0.1541.

6.2.16 Synthesis of (E)-2-(phenyldiazenyl)pyridine, L^{azpy}

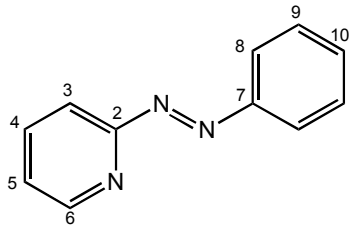

$C_{11}H_9N_3$

FW: 183.2

2-nitrosopyridine (0.216 g, 2 mmol), aniline (0.186 g, 2 mmol) and one drop of glacial acetic acid were stirred in dichloromethane (30 mL) for 12 h. The

solution was concentrated and the crude product was purified by column chromatography on silica gel with $CHCl_3$ as an eluent. The compound was eluted as a second intensive orange band. Yield (0.27 g, 73.8 %)

^{1}H NMR (400 MHz, $CDCl_3$) δ = 8.72 (ddd, J = 4.8, 1.8, 0.8, 1H, H_6), 8.05 (ddd, J = 5.2, 4.3, 1.9, 2H, $H_{8/9}$), 7.87 (ddd, J = 8.0, 7.3, 1.8, 1H, H_4), 7.81 (dt, J = 8.0, 1.0, 1H, H_3), 7.55 - 7.48 (m, 3H, $H_{10\&8/9}$), 7.37 (ddd, J = 7.2, 4.8, 1.2, 1H, H_5)

^{13}C NMR (400 MHz, MeOD) δ= 162.85 (C_2), 152.4 (C_7), 149.5 (C_6), 138.35 (C_4), 132.2 (C_{10}), 129.15 ($C_{8/9}$), 125.2 (C_5), 123.6 ($C_{8/9}$), 115.55 (C_3)

MS (ES+) *m/z* = 206.1 $[M + Na]^+$

EA (%): Found: C: 72.2, H: 4.9, N: 22.9; Calc. for $C_{11}H_9N_3$: C: 72.1, H: 4.95, N: 22.9.

IR, ν (cm^{-1}): 3061 (w), 1578 (s), 1492 (m), 1462 (m), 1416 (s), 1304 (w), 1261 (w), 1217 (w), 1182 (w), 1136 (m), 1090 (w), 989 (m), 920 (w), 787 (s), 735 (s), 681 (s), 621 (m), 577 (w), 552 (s)

6.2.17 Synthesis of $[RuL^{azpy}(NH_3)_4]Cl_2$

$[Ru(NH_3)_5(H_2O)](PF_6)_2$ (15 mg, 0.03 mmol) and L^{azpy} (11 mg, 0.03 mmol) were stirred in acetone (15 mL) under an argon atmosphere for 18h. The red solution was filtered off and the filtrate was concentrated under reduced pressure. Addition of diethyl ether afforded an orange/red precipitate, which was filtered off, washed with diethyl ether and dried in *vacuo.* The chloride salt of the compound was obtained by anion metathesis using t-Bu_4NCl.

Yield (11.3 mg, 29 %)

Red, needle-shaped crystals of hexafluorophosphate salt suitable for X-ray diffraction were obtained by slow diffusion of benzene into CH_3CN solution of the compound.

^{1}H NMR (300 MHz, MeOD) δ = 8.76 (ddd, J = 5.8, 1.3, 0.6 Hz, 1H, H_6), 8.53 (ddd, J = 8.2, 1.3, 0.7 Hz, 1H, H_3), 8.01 (ddd, J = 8.2, 7.4, 1.5 Hz, 1H, H_4), 7.75 (ddd, J = 7.3, 5.9, 1.4 Hz, 1H, H_5), 7.69 – 7.60 (m, 5H, $H_{8,9,10}$)

MS ES+ (CH_3OH) *m/z* = 320.1 $[RuL^{azpy}]Cl^+$, 354.1 $[RuL^{azpy}(NH_3)_2]Cl^+$, 371.1 $[RuL^{azpy}(NH_3)_3]Cl^+$, 388.2 $[RuL^{azpy}(NH_3)_4]Cl^+$

EA (%): Found: C: 31.3, H: 4.7, N: 23.1; Calc. for $Ru(C_{11}H_9N_3)(NH_3)_4Cl_2$: C: 31.2, H: 5.0, N: 23.1

UV-Vis (H_2O) λ max/nm, (ε/dm^3 mol^{-1} cm^{-1}): 223 (10 500), 323 (10 000), 477 (4 300)

IR, ν (cm^{-1}): 3100 (s, br), 1639 (m), 1463 (m), 1450 (m), 1278 (s), 1248 (m), 1198 (m), 771 (s), 706 (s)

Crystal structure data for $C_{11}H_{21}N_7Ru$, C_6H_6, 2(PF_6): M = 720.47, Monoclinic, a = 16.338(4) Å, b = 10.733(3) Å, c = 16.797(4) Å, b= 115.673(14)°, U = 2654.6(11) Å^3, T = 120 (2) K, space group P 2(1)/n, Z = 4, 22120 reflections measured, 4646 unique (R_{int} = 0.1395) which were used in all calculations. Final R-indices (I>2σ(I)): *R1* = 0.1359, *wR2* = 0.2959.

6.3 DNA binding studies

6.3.1 Materials and methods

Calf-thymus DNA (highly polymerized ct-DNA) was purchased from Sigma Aldrich and used as received. The stock solutions of DNA were prepared by dissolving the fibers in ultrapure water (1 mg per 1 mL of H_2O) and the aliquots were stored at -20 ^oC. Solutions with the required DNA concentrations were always freshly prepared from the stock samples on the day of the experiment and retained in ice until needed. The final concentration of DNA was determined by UV-Vis spectroscopy on the basis of the extinction coefficient of ε_{258} = 6600 mol^{-1} dm^3 cm^{-1} per DNA base.[9] Solutions of DNA gave an absorbance ratio at 260 nm and 280 nm, A_{260}/A_{280}, of ~1.8, implying that the DNA was satisfactorily free from proteins.

All DNA binding experiments were performed at 25^oC in buffer containing 20 mM NaCl and 1 mM sodium cacodylate. Ultrapure water (Sigma Aldrich) was used in all experiments.

Stock solutions of ruthenium(II) compounds (600 μM) were prepared by dissolving the chloride form of the complex in milli-Q water.

6.3.2 Circular and linear dichroism

Circular dichroism and linear dichroism measurements were conducted using a Jasco J-810 spectropolarimeter. Experiments were carried out at a constant DNA concentration (300 μM) in the buffer containing 20 mM sodium chloride and 1 mM sodium cacodylate, pH 6.8. During the titration the concentration of the complex in the sample was gradually increased from 5 μM to 50 μM, which corresponds to DNA base to complex ratios ranging from 60:1 to 6:1.

CD spectra were obtained using a 10 mm pathlength cuvette in the range of 700 to 300 nm and 2 or 1 mm pathlength cuvette for the 300 - 200 nm range.
Parameters: Sensitivity – standard (100 mdeg), Data pitch – 0.5 nm, Scanning mode – continuous, Scanning speed – 200 nm/min, Response – 1 sec, Band width – 1 nm, Accumulation - 12
Linear dichroism spectra were recorded using a flow Couette cell with a total pathlength of 1 mm.
Parameters: Sensitivity – Standard (0.1 dOD), Data Pitch: 0.5 nm, Scanning mode – continuous, Scanning speed – 500 nm/min, Response – 0.25 sec, Band width – 2 nm, Accumulation – 8
During both CD and LD titration experiments the HT value was kept below 600 V. [10]

6.3.3 Agarose gel experiments

Plasmid pBR322 was purchased from New England Biolabs, agarose powder was purchased from Bioline.

The samples were prepared as follows: Plasmid pBR322, 1 μL of 1 μg mL^{-1} stock solution, was mixed with varying amounts of complex and ultrapure water to give a final volume of 16 μL. The volume of the complex added (stock solution 60 μM) varied from 1.28 μL at the ratio of 20 base pairs to 1 complex to 12.83 μL at ratio 2 : 1. The prepared solutions were incubated for 1 h at 37^{o}C. After incubation the loading buffer (30% glycerol, 0.05% bromophenol blue and 0.025 % cyanol xylene in ultrapure water) was added (4 μL) and the solutions were vortex and gently centrifuged.

1 % agarose gel was prepared by melting 2 g of agarose in 200 mL of 1 x TAE buffer, poured into the tray and left to set for 30 min. 16 μL aliquots were loaded into wells (first and last well were control samples). The gel was run in a 1 x TAE buffer for 2.5 h at 5 V cm^{-1}. After electrophoresis the gel was stained in a TAE solution of ethidium bromide (0.5 μg mL^{-1}) for 30 min. Visualisation of the agarose gels was performed at 312 nm using a UVIPro Platinum system (UVIDoc, Cambridge, UK).

6.3.4 Thermal denaturation

ct-DNA thermal denaturation experiments were performed on Cary 5000 Varian spectrophotometer in a buffer containing 20 mM sodium chloride and 1 mM sodium cacodylate. The measurements were carried out in the range of temperatures 25 – 95 ^{o}C with heating speed 1 ^{o}C/min. The analysis of the DNA denaturation profiles was performed using the derivative method.

6.4 Cell tests

RPMI, DMEM, FBS, L-glutamine, HEPES, sodium pyruvate, and 10% trypsin-EDTA were purchased from Invitrogen. Antibiotic-actinomycin solution, 3-(4,5-Dimethylthiazol-2-yl)-2,5-diphenyltetrazolium bromide (MTT) and DMSO were obtained from Sigma Aldrich.

Cells were cultured in RPMI (T47D) or DMEM (MDA-MB-231) medium supplemented with 10 % FBS, 1 % L-glutamine, 1 % HEPES buffer, 1 % sodium pyruvate and 1 % antibiotic. Cells were harvested by trypsinisation at 80-90 % confluence.

The MTT assay was performed as follows: 8000 cells/well (MDA-MB-231, T47-D) were seeded in a 96-well microtiter plate (Costar) and incubated at 37^{o}C for 24h to adhere. The following day the cells were treated with a range of concentrations of tested compound prepared in an appropriate medium (the concentrations applied were individual for each Ru complex) and the cells were incubated at 37^{o}C (5 % CO_2 atmosphere) for 72 hours. This was followed by an addition of 20 µL of MTT solution in PBS (5 mg/mL) into each well (except for 4 control wells) and incubation of plates for a further 3 hours. The medium was removed and 100 µL of DMSO added. The plates were covered with aluminum foil and gently shaken for 30 min. Optical density was determined using a microplate reader (BioRad) operating at 590 nm.

The assay was repeated three or four times for each compound. The IC_{50} values were determined from concentration-response curves.

6.5 References

[1] I. P. Evans, A. Spencer, G. Wilkinson, *J. Chem. Soc.-Dalton Trans* **1973**, 204.

[2] C. Painting, *PhD Thesis, University of Warwick* **1997**.

[3] M. J. Hannon, C. L. Painting, A. Jackson, J. Hamblin, W. Errington, *Chem. Commun.* **1997**, 1807.

[4] G. I. Pascu, A. C. Hotze, C. Sanchez-Cano, B. M. Kariuki, M. J. Hannon, *Angew. Chem. Int. Ed.* **2007**, *46*, 4374.

[5] Y. Parajo, J. Malina, I. Meistermann, G. J. Clarkson, M. Pascu, A. Rodger, M. J. Hannon, P. Lincoln, *Dalton Trans.* **2009**, 4868.

[6] M. Pascu, *PhD Thesis, University of Birmingham* **2007**.

[7] F. Tuna, M. R. Lees, G. J. Clarkson, M. J. Hannon, *Chem. Eur. J.* **2004**, *10*, 5737.

[8] L. J. Childs, *PhD Thesis, University of Warwick* **2003**.

[9] R. D. Wells, J. E. Larson, R. C. Grant, B. E. Shortle, C. R. Cantor, *J. Mol. Biol.* **1970**, *54*, 465.

[10] S. M. Kelly, T. J. Jess, N. C. Price, *Biochim Biophys Acta* **2005**, *1751*, 119.

7

Conclusions and Future Perspectives

Supramolecular chemistry has proven to be a powerful tool in the design of novel DNA-binding therapeutic agents.

Supramolecular ruthenium triple-stranded helicates presented in chapter 2 have been shown to bind to DNA and alter its secondary structure by bending and unwinding the double helix. Although, as it has been shown previously, the DNA recognition properties of the cylinders can be 'tuned' by introducing modifications *e.g.* substituents in the cylinders building moieties, the work presented in chapter 2 showed that simply by changing the metal binding units in the helicates, while maintaining the overall size and shape of the cylinder, the binding properties of these compounds can change dramatically. Excitingly, these discrete changes in the structure of the helicate *i.e.* using imidazole instead of pyridine in the ligand, led to a considerable increase in the cytotoxicity of the helical drugs.

Chapters 3 and 4 are focused on chiral recognition between the supramolecular cylinders and biomolecules as well as within small molecule systems. It has been shown that the two optical isomers of ruthenium cylinder interact differently with DNA and with Δ-TRISPHAT. Indeed, the interaction of the cylinders within the two systems is driven by molecular shape 'compatibility' and the recognition of DNA by chiral helicates appears to be a function of multiple events, which all together lead to severe structural changes in the biomolecule. These are naturally distinctive and characteristic for each enantiomer.

Chapter 5 focuses on combining the moieties of supramolecular cylinders, ammine drugs and ruthenium azopyridine complexes in order to achieve

integrated effects of these drugs. The three complexes consisting of the above building units have been successfully prepared and characterised. Moreover, the DNA binding studies on the dinuclear tetracationic Ru complex and its mononuclear analogue showed that the dinuclear complex has a much greater potential to interact with the biomolecule. This could be due to a number of factors, such as the potential of the complex for electrostatic attractions or hydrophobic interactions.

Understanding molecular insights of the drug-DNA recognition processes is of crucial importance for rational drug design and future development of novel, superior therapeutics. In this context, in order to better understand the forces that drive the recognition processes and also to understand the cellular outcomes of our drugs binding to DNA, future work on the systems presented in this thesis should include exhaustive studies of the DNA recognition processes at the structural, electronic, thermodynamic and kinetic level.

Supplementary Information

S1. Lipophilicity of ruthenium triple-stranded helicates

Compound	P	log P
$[Ru_2L_3]Cl_4$	0.099	-0.96 ± 0.07
$[Ru_2L^{o}_3]Cl_4$	0.0150	-0.88 ± 0.12

Table S1 Octanol-water partition coefficients for Ru(II) triple-stranded helicates; (each value represents the average of the values obtained from three independent experiments, errors represent standard deviations)

The partition coefficient (P) of the complex between n-octanol and water was determined using shake-flask method.[1] All measurements were carried out at room temperature. N-octanol and water were saturated one with another and equilibrated for 24 h before experiment. The absorption spectra were recorded using a Cary 5000 Varian spectrophotometer.

Aliquots of working solutions of ruthenium complexes were added to equal volumes of n-octanol and shaken in a mechanical shaker (IKA Vibrax VXR basic) for 3h at 1000 1/min. The solutions were then left to equilibrate for one hour, the organic and aqueous layers were then carefully separated and the UV-Vis spectra of the aqueous layer before and after partition were recorded. Experiments were carried out in triplicate for two or three different concentrations of the compounds. The partition coefficients were calculated using the equation: $\log P_{oct} = \log[(A_1-A_2)/A_2]$, where A_1 and A_2 – UV-Vis absorption values of the compound at the aqueous phase before and after partition respectively.

[1] J. Sangster, *Octanol-Water Partition Coefficients: Fundamentals and Physical Chemistry, Vol. 2*, John Wiley & Sons, New York, **1997**.

S2. 2D NMR spectrum of $[RuL^a(NH_3)_4]Cl_2$

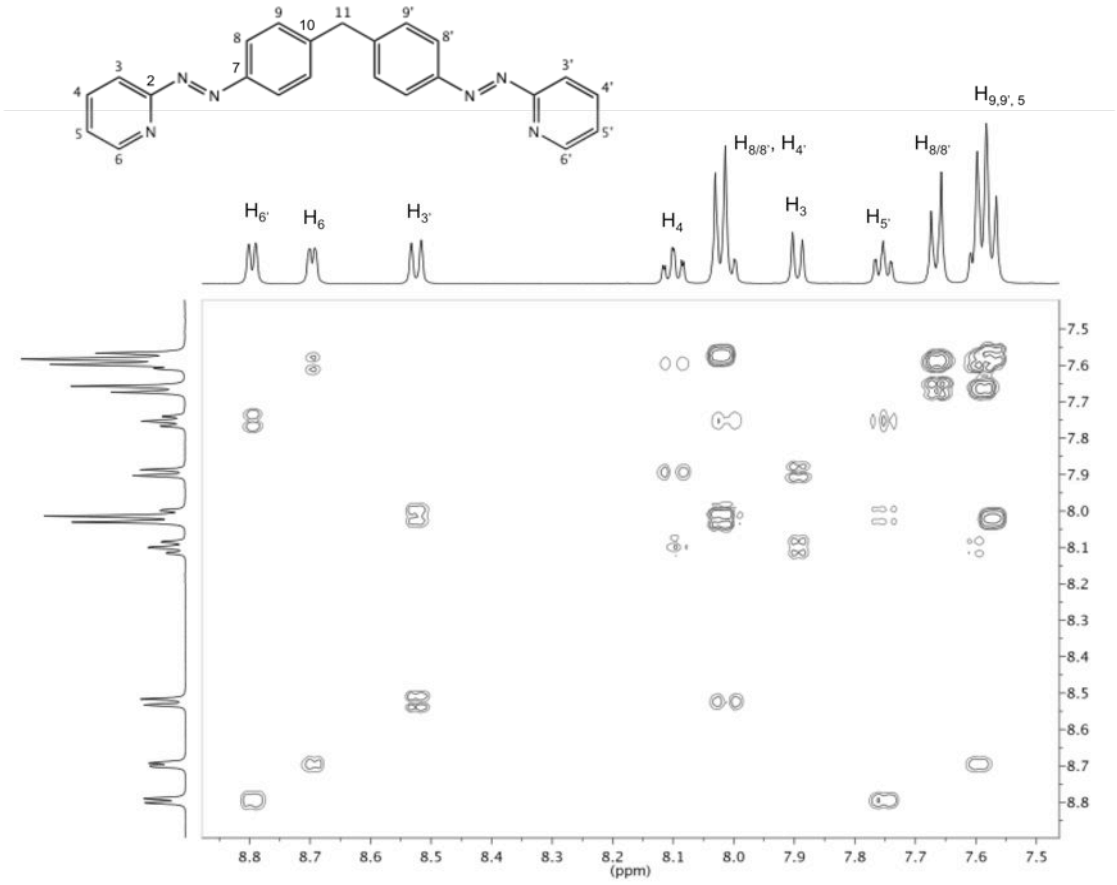

Fig. S1 ^1H-^1H COSY NMR spectrum of $[RuL^a(NH_3)_4]Cl_2$ in MeOD.

S3. UV-Vis spectra of $[Ru_2L^a(NH_3)_8]Cl_4$ and $[RuL^{azpy}(NH_3)_4]Cl_2$ in H_2O

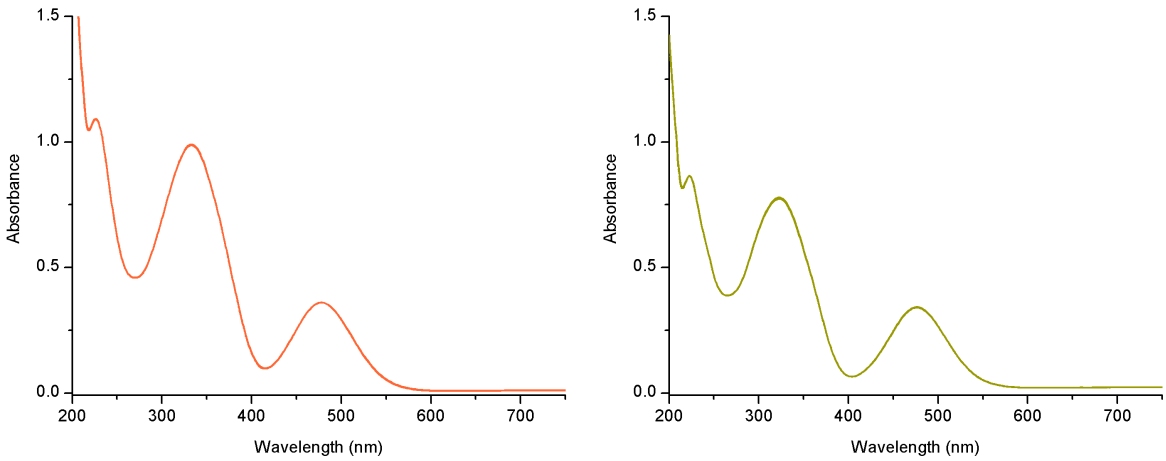

Fig. S2 UV-Vis absorption spectra of (left) $[Ru_2L^a(NH_3)_8]Cl_4$ and (right) $[RuL^{azpy}(NH_3)_4]Cl_2$ in aqueous solution recorded at room temperature.